Using Narrowband Pulse-shaping to Characterize Polymer Structure and Dynamics: Deathstar GHz Spectroscopy

by

Neal Arvind Vachhani

B.S. Ceramic and Materials Engineering
School of Engineering at Rutgers University, 2002

Submitted to the Department of Materials Science and Engineering
in partial fulfillment of the requirements for the degree of

MASTER OF SCIENCE IN MATERIALS SCIENCE AND ENGINEERING

at the

MASSACHUSETTS INSTITUTE OF TECHNOLOGY

February 2005

© Massachusetts Institute of Technology 2005. All rights reserved.

Author .....
Department of Materials Science and Engineering
January 14, 2005

Certified by .....
Edwin L. Thomas
Morris Cohen Professor of Materials Science and Engineering
Thesis Supervisor

Accepted by .....
Carl V. Thompson
Stavros Salapatas Professor of Materials Science and Engineering
Chairman, Department Committee on Graduate Students

Using Narrowband Pulse-shaping to Characterize Polymer Structure and Dynamics: Deathstar GHz Spectroscopy

by

Neal Arvind Vachhani

Submitted to the Department of Materials Science and Engineering
on January 14, 2005, in partial fulfillment of the
requirements for the degree of
MASTER OF SCIENCE IN MATERIALS SCIENCE AND ENGINEERING

Abstract

A narrowband pulse-shaper called the *Deathstar* has been used along with a picosecond acoustic technique to study amorphous polymers. The temperature dependence of the longitudinal acoustic velocity and the frequency dependence of the acoustic attenuation have been measured. The frequency range of longitudinal phonons studied is not directly accessible by other spectroscopies. Probing material response in this intermediate regime is valuable because it helps characterize secondary transitions and energy dissipation mechanisms in polymers.

Broadband experiments have been done to study the temperature dependence of the acoustic velocity for polystyrene and poly(methyl methacrylate) from 10 K to 300 K. The results are in line with literature values and the predictions of a model based on acoustic impedance mismatch theory.

Narrowband studies with the technique used were previously limited to amorphous silica. They are extended for the first time to amorphous polymers. The Deathstar GHz spectroscopy is used to determine the absolute acoustic attenuation coefficient as a function of frequency for PMMA. The values obtained are similar to those found in literature. However, the method used to measured attenuation here is more reliable. The frequency at which attenuation has been measured ranges from 55 GHz to 160 GHz. To explore additional dynamics, attenuation is also measured at temperatures above and below the polymer glass transition.

The details of the experimental technique are discussed, and the results are presented. The validation of this technique for probing amorphous polymer structure and dynamics lays the ground for further study of heterogeneous materials, such as nanocomposites and block copolymers.

Thesis Supervisor: Edwin L. Thomas
Title: Morris Cohen Professor of Materials Science and Engineering

Acknowledgments

This place is grueling. I arrive in August 2002 naïve, not knowing what to expect. Sure the classes are difficult, but more troubling is the nebulous world of research. In its initial phase, the process of research can leave a person just about as clueless as she'll ever be in her life. The project might be ill-defined, the approach unclear, and the equipment not cooperative. Any one of many factors is likely to be present to ensure that things won't go smoothly. Despite all of this, we draw for ourselves a path, from which we hopefully do not deviate too far. There are people that have helped define this path for me, and their contributions are greatly appreciated.

My thesis advisor, Professor Edwin L. Thomas, whom we call Ned, has been integral in the development of my scientific capacity. He shows incredible faith in his students, and he recognizes the value of independence. Ned single-handedly built my research self-confidence by trusting me to lead my own project. His vast research experience and scientific intuition have taught me to ask the right questions and to think more critically. One of the most important lessons I've learned is that if you cannot explain a concept in a few short sentences using run-of-the-mill words, then you don't understand it well enough. Hopefully, this thesis doesn't have too many convoluted sentences with multiple clauses and thesaurus-driven wording. Giving him an update one night, he says, "I'm here this late talking to you not because I don't have anything better to do, but because I know that you can do it."

Most of the experimental work that comprises this thesis was done in the laboratory of Professor Keith A. Nelson. I cannot express how welcome he and the members of his group have made me feel, even though I've greatly complicated their world by introducing these long-chained squishy things called polymers. His fundamental understanding of physical chemistry continues to serve as an excellent source of clarification and insight.

The sincerity with which the soon to be Dr. Jaime D. Choi has taken me under her wing throughout the course of this research cannot be justly explained in words. I was so pleasantly surprised at not only how accommodating she was in allowing me to share the experimental setup, but also with her relentless patience. I must have asked her the same question umpteen times and had her explain the most basic things over and over again. Not once did she hesitate. I was taken from zero to 60 in a matter of months, now claiming to be competent enough to take measurements by myself. I promise not to forget to change back the time constant! Check out her doctoral dissertation for answers to questions that I've only grazingly addressed [4].

Kenji Katayama, a postdoctoral associate in the Nelson Group, has also been incredible in helping to take and analyze data. His strong theoretical background and experimental finesse have helped to answer some puzzling questions, and have posed just as many new ones. Like Jaime, he has spent many weekends in the lab with me, laboring over alignment and dismal signal quality.

I would like to thank the U.S. Army Research Office for their generous and continued support of the Institute for Soldier Nanotechnologies at MIT. The Institute is not even two years old and it has already become home to so many students and

visiting scientists.

My loving parents, Ma and Dadu, continue to be my inspiration and source of endless support. While she'll always be my little sister, I know that for Resham there is no obstacle too formidable–no wall that she cannot tear through with her persuasion and perseverance.

To my bride Radha, who for putting up with more research-related frustration than anyone, is duly commended. She notes that even if I don't finish this thesis, she'll still love me. (See Ned, above).

Contents

List of Figures

List of Tables

Chapter 1

Introduction

This thesis is the beginning of a broader investigation that aims to better understand energy propagation and energy dissipation in polymeric materials at blast frequencies. The approach is to establish the compatibility of a picosecond acoustic technique known as *Deathstar GHz spectroscopy* with amorphous homopolymers that allows for probing of nanoscale structure and picosecond dynamics.

The characterization of energy dissipation mechanisms in polymeric materials is germane to the development of better engineering materials. Studying material response under high strain rates and at high loading frequencies is especially important for soldier armor and personnel protection. Besides armor, the response of human tissue, organs, biopolymers, and gels to blunt trauma forces and blast dynamics is a relatively unexplored area of huge importance. The molecular-level deformation of physiological materials during blast events and associated injuries is not well understood. Other applications might include assessment of bomb shelter or bunker materials for force protection.

The typical blast wave generates strain rates slightly greater than $10^4\,\mathrm{s}^{-1}$, while typical ballistic strain rates are on the order of $10^5\,\mathrm{s}^{-1}$. Current methods of high rate dynamic mechanical characterization such as the split-Hopkinson pressure bar can

barely reach strain rates of $10^4\ s^{-1}$. Beyond that, a gas gun can be used for penetration studies, but quantitative feedback is limited and most experiments are empirically-driven. The gas gun would be a great characterization tool if laser-based diagnostics were coupled to the system to allow researchers to evaluate ballistic deformation *in situ*. The first step in realizing this involves understanding material behavior when energy is delivered very quickly. It is the goal of this thesis to present a novel technique that can directly characterize the temperature-dependent acoustic velocity and the frequency-dependent acoustic attenuation of polymeric materials.

Using a nondestructive spectroscopic technique enables relevant mechanical properties to be determined without sacrificing large amounts of material. In fact, a modestly thorough characterization can be done with just a few milligrams of material. Many experiments can be performed using the same sample, too. This is not a major concern now since the materials initially investigated (PS and PMMA) are commercially available polymers. However for material synthesized in limited quantities, the Deathstar GHz spectroscopy can prove very valuable. A deeper understanding of material response would allow for feedback to chemists to improve material design at the molecular level.

Optically generated and optically detected acoustic waves are ideal for materials characterization since they couple directly to structure and density fluctuations. Fundamental physical responses are exploited in this investigation by using modern lasers, which probe higher wavevectors than the conventional acoustic techniques described in Section 2.4. As will be described in detail in Chapter Three, the modulation of the sample thickness is directly measured at GHz frequencies.

The acoustic frequency range probed is from 55 GHz to 160 GHz, at temperatures above and below polymer T_g. Although the imposed strains are small enough that the material remains elastic ($\approx 0.4\%$), strain rates are between $10^7\ s^{-1}$ and $10^8\ s^{-1}$. In terms of frequency, a strain rate of $10^7\ s^{-1}$ corresponds to about 10 GHz for the sam-

ples investigated. Lower frequency techniques include impulsive stimulated thermal scattering (ISTS) and Brillouin light scattering (BLS), which probe frequencies less than 1 GHz and 20 GHz, respectively. Whereas, inelastic neutron scattering (INS) observes behavior at frequencies in excess of 1 THz. Thus, there is presently no method that can access the entire intermediate frequency range from 20 GHz to 1 THz. The Deathstar GHz spectroscopy is able to probe precisely at these frequencies. In order to fully explore interesting structure and dynamics in complex materials, the technique must first be validated by studying simple materials. This will be done by investigating polystyrene (PS) and poly(methyl methacrylate) (PMMA), two glassy amorphous polymers.

Chapter Two provides a fundamental technical overview of sound theory and prior work done in relevant spectroscopies. Chapter Three describes the details of the Deathstar GHz spectroscopy, for the operational user. In Chapter Four, the results of the acoustic characterization and their interpretation are discussed. Chapter Five outlines the conclusions drawn and makes suggestions for future work.

Chapter 2

Background

2.1 Basic Concepts in Sound

Acoustics is the scientific study of sound, namely sound propagation through any medium. Sound can be considered to be a wave phenomenon. There are two types of sound waves, transverse and longitudinal. The general wave equation is:

$$u_t = u_0 e^{i(kx \pm \omega t)} \tag{2.1}$$

where $u(x,t)$ is the displacement in the x-direction at time t, u_0 is the wave amplitude, $k = \frac{2\pi}{\lambda}$ is the wavenumber[1], λ is the wavelength, and ω is the oscillation frequency. The energy of a wave moves in the direction of wave propagation.

[1]The wavenumber (k) is the magnitude of the wavevector ($\overrightarrow{k}$). Wavenumber can also be denoted by q).

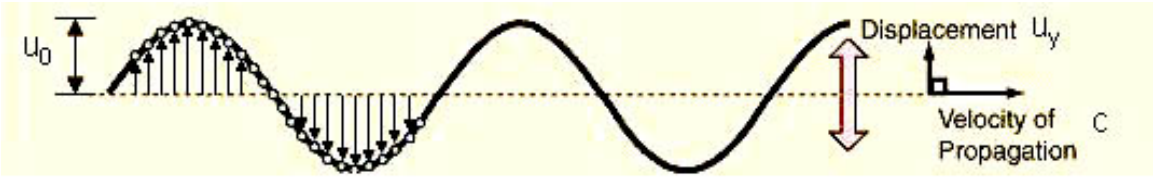

Figure 2-1: Diagram of transverse wave propagation, showing particle displacement perpendicular (u_y) to the direction of wave propagation (x).

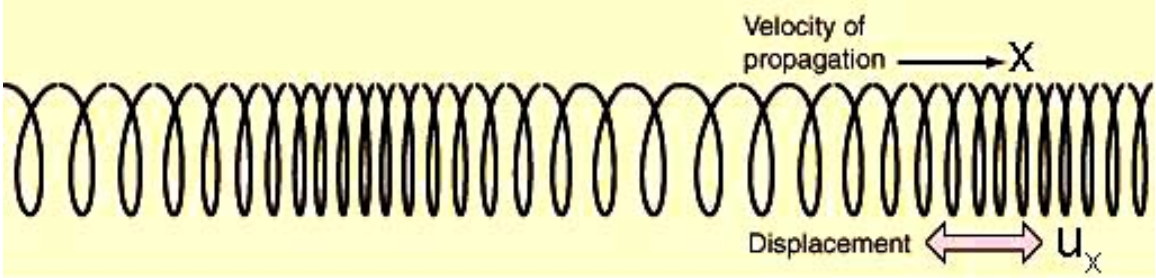

Figure 2-2: Diagram of longitudinal wave propagation, showing particle displacement parallel (u_x) to the direction of wave propagation (x).

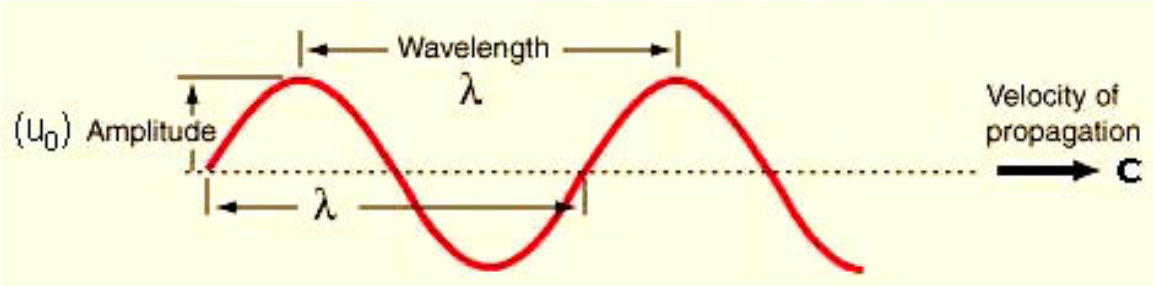

Figure 2-3: A snapshot of a wave in time, showing how wavelength and amplitude are defined.

In a transverse wave, the particles do not move along with the wave from left to right Figure 2-1. Rather, they oscillate up and down as the wave passes by. The particles of the medium are displaced *perpendicular* (u_y) to the direction of wave propagation (x). Whereas in a longitudinal wave, the particles are temporarily displaced in a direction *parallel* to energy transport before returning to their original position. This can be depicted by a Slinky®, as shown in Figure 2-2. As the longitudinal wave propagates, local regions of compression and tension are created as the "particles" of the Slinky® move closer together and then further apart. These expansions and contractions are what give rise to local density fluctuations. This is essentially a strain pulse (Figure 3-7 depicts a typical strain profile). The displacement of a single particle is plotted as a function of time. The strain profile is equivalent if the displacement of many particles is observed as a function of position at a given instant in time. The sign of the strain pulse indicates whether it is compressive strain (negative) or tensile strain (positive). For this investigation, only longitudinal sound waves are

considered. Hence, references to *sound wave*, *acoustic wave*, and *phonon* in this thesis all imply *longitudinal* sound waves. A phonon is a quantum of energy that describes a lattice vibration. In an amorphous material, phonons can be thought of as vibrations between any structural features, e.g. entanglements, bonds, or R-groups. Analogous to a photon propagating the energy of an electromagnetic wave, a phonon propagates the energy of an elastic wave.

The frequency of a wave is the number of complete back-and-forth vibration cycles per unit of time. The time in seconds it takes for one complete cycle is the *period*. Frequency is measured in Hertz (Hz) and is dimensionally equivalent to s^{-1}. Frequency may also be noted by f and ν and be referred to as the *acoustic frequency* or *phonon frequency* in the case of a sound wave. The acoustic wavelength is the distance traveled within the medium by the wave in one period. The wavelength is defined by the peak-to-peak distance, as shown in Figure 2-3. As with any wavespeed, the speed of sound ($c_{acoustic}$) refers to how fast the disturbance travels within the medium. The speed of sound can also be referred to as the *acoustic velocity* and may be represented as $v_{acoustic}$ or c_L (L is for longitudinal). The acoustic velocity is related to the acoustic wavelength and the acoustic frequency as follows:

$$c_{acoustic} = \lambda\omega \tag{2.2}$$

The acoustic dispersion describes $\omega(\mathbf{K})$, which is the phonon frequency as a function of the incident wavevector. The slope of the dispersion relation gives the acoustic group velocity[2]:

$$v_g = \frac{d\omega}{dK} \tag{2.3}$$

Thus, phonon velocities have varying degrees of sensitivity to phonon frequency, depending on the incident wavevector.

[2]The group velocity (v_g) is the same as $c_{acoustic}$.

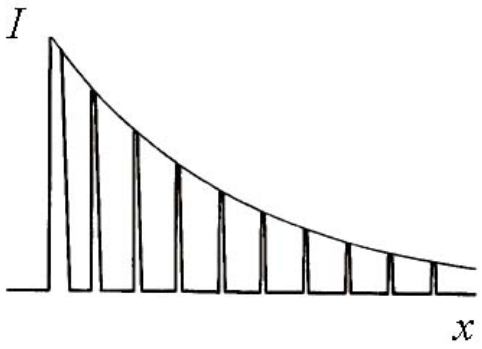

Figure 2-4: Acoustic energy diminishes as it travels within any medium. The relationship between the amount of decrease in intensity and distance traveled is described by the attenuation coefficient.

The amount of acoustic energy that is transmitted through a given area of the medium per unit time is known as the sound intensity (I). The greater the amplitude of vibrations of the particles in the medium, the more intense the sound waves. Intensity is given by:

$$I = \frac{\text{energy}}{\text{time} \times \text{area}} = \frac{\text{power}}{\text{area}} \tag{2.4}$$

A standard unit of intensity is W/m^2 (W is for Watt). The ratio of intensity entering a system to the intensity leaving a system is what allows for the calculation of attenuation. Acoustic waves experience frequency-dependent attenuation, or loss of intensity, when propagating through any medium (except for a vacuum, through which sound waves cannot travel). Attenuation combines all types of losses into the material, including absorption (i.e. conversion to heat) and scattering. For a sound wave that travels a distance x within a material, the transmitted intensity (I) is related to the original or incident intensity (I_0) via the *acoustic attenuation coefficient* or *damping coefficient* (α) as:

$$I = I_0 e^{-\alpha x} \tag{2.5}$$

Accordingly, the attenuation coefficient is a measure of the length scale over which intensity diminishes (see Figure 2-4). A higher attenuation coefficient implies that

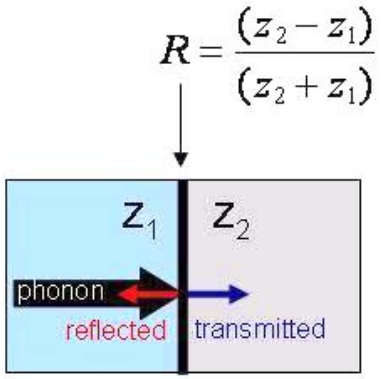

Figure 2-5: When a phonon is incident normal to an interface between two media of different impedance, part of the acoustic energy is reflected and part of the acoustic energy is transmitted.

more intensity is lost over a shorter length scale. It is a goal of this thesis to accurately measure α as a function of acoustic frequency and at a particular temperature. Interestingly, α is very dependent upon the particular material and the particular frequency.

In a homogeneous and isotropic material, the acoustic velocity is also directly related to the Young's modulus (E) and the bulk density (ρ) as follows:

$$c_{acoustic} = \sqrt{\frac{E}{\rho}} \tag{2.6}$$

The acoustic velocity can therefore be regarded as an indication of specific material stiffness. Variations in $c_{acoustic}$ with frequency or temperature suggest changes in the mechanical behavior of the material.

Sound can be reflected, transmitted, absorbed, or scattered. Acoustic impedance mismatch theory explains what happens to sound traveling through an interface between two materials. In comparison to reflection and transmission, scattering and absorption at the boundary are presumed negligible. The acoustic impedance of a material (z) is given by:

$$z = c_{acoustic} \times \rho = \sqrt{E\rho} \tag{2.7}$$

Acoustic impedance can be regarded as a material's stiffness as experienced by sound. Thus, highly rigid materials have high values of z. Assume that sound is traveling from medium 1 with impedance z_1 to medium 2 with impedance z_2. So long as $z_1 \neq z_2$, the sound wave encounters an *impedance mismatch*. Impedance mismatch can also exists within a given material, resulting from heterogeneities that are of a lengthscale greater than or equal to the wavelength of the propagating wave. Any change in local density or stiffness results in a local change in the impedance. The reflection coefficient (R) quantifies the amount of the acoustic wave that is reflected at the interface and is given by:

$$R = \frac{(z_2 - z_1)}{(z_2 + z_1)} \tag{2.8}$$

If $z_2 \gg z_1$, then $R \approx 1$ and the boundary is said to be rigid and reflects most of the incident acoustic energy without a change in phase. This means that the sign of the propagating pulse remains the same. Whereas, if $z_2 \ll z_1$, then $R \approx -1$ and the boundary is soft or lossy. While most of the pulse is still reflected, there is a π phase shift. This means that an originally compressive strain pulse is reflected as a tensile strain pulse and vice versa. It is also possible to impedance match two materials so well ($z_1 \approx z_2$) that $R \approx 0$ and most of the signal is transmitted across the boundary. In general, strong acoustic reflection will be evident wherever there is a strong spatial gradient in impedance. The properties of the materials relevant to this investigation are shown in Table 2.1.

2.2 Advanced Treatment of Phonon Propagation

The propagation of acoustic waves through polymers can be described using the theory of elasticity and the thermodynamics of an irreversible process. Assume that a plane sound wave is propagating through a heat-conducting viscoelastic medium. A

Table 2.1: Room temperature acoustic properties of materials employed in the current investigation[7].

Material	$c_{acoustic}$ $[\frac{cm}{s}]$	ρ $[\frac{\text{g}}{\text{cm}^3}]$	z $[\frac{\text{g}}{\text{cm}^2\times\text{s}}]$
Air	3.44×10^4	1.29×10^{-3}	0.00044×10^5
Sapphire	1.12×10^6	3.98	44.6×10^5
Al	6.42×10^5	2.70	17.3×10^5
a-PS	2.31×10^5	1.06	2.53×10^5
a-PMMA	2.68×10^5	1.19	3.37×10^5

plane wave is the simplest type of wave motion, very similar to the longitudinal wave described in Section 2.1. The characteristic property is that the particle displacements and density changes have common phases and amplitudes at all points on any given plane perpendicular to the direction of wave propagation [27]. Although thermal conductivity is usually ignored, it is relevant when discussing low temperature acoustic properties of polymers. This is because thermal conductivity drops significantly at low temperatures, increasingly the polymer's sensitivity to temperature changes. The governing equations in one dimension are the conservation laws of mass, momentum, and energy, respectively, as shown:

$$\frac{\partial \rho}{\partial t} = -\rho \frac{\partial c_{acoustic}}{\partial t} \tag{2.9}$$

$$\rho \frac{\partial^2 u_x}{\partial t^2} = \frac{\partial \sigma_{xx}}{\partial x} \tag{2.10}$$

$$\rho C_v \frac{\partial T}{\partial t} - \frac{T\beta K_T}{\rho} \cdot \frac{\partial \rho}{\partial t} = -\frac{\partial q_x}{\partial x} \tag{2.11}$$

The velocity in the x direction is given by $c_{acoustic} = \dot{u}_x$, where u represents the displacement of particles in the medium upon deformation. σ_{xx} is the stress arising from a force applied in the x direction on a plane whose normal is along $\widehat{x}$, T is

the temperature, ρ is the density, and C_v is the specific heat at constant volume. The thermal expansion coefficient is $\beta = (\frac{1}{V})(\frac{\partial V}{\partial T})_{\mathrm{P}}$, where V is the specific volume. $K_T = -V(\frac{dp}{dV})_{\mathrm{T}}$ is the isothermal bulk modulus and q_x is the x component of the heat flux density vector, $\overrightarrow{q} = -\kappa\nabla T$. To unify Equations 2.10 and 2.11, there must be a relationship between the stress tensor σ_{ij} and the heat flux density vector $\overrightarrow{q}$[3]. The stress tensor for a viscoelastic medium such as a polymer is a given by:

$$\overline{\sigma}_{ij} = \sigma_{ij} + \sigma'_{ij} \tag{2.12}$$

where σ_{ij} is the stress tensor for an elastic solid and σ'_{ij} is the stress tensor for a viscous dissipative material. In an elastically deformed solid, the following relationship between the Helmholtz free energy (F) and the strain tensor (ϵ_{ij}), holds:

$$\sigma_{ij} = \left(\frac{\partial F}{\partial \epsilon_{ij}}\right)_{\mathrm{T}} \tag{2.13}$$

The Helmholtz free energy is a measure of the amount of energy required to create a system after accounting for spontaneous energy transfer to the system from the environment. More on this topic can be read in a Thermodynamics textbook. Since σ'_{ij} has the same form for a liquid as it does for a solid, it can be substituted into Equation 2.12, resulting in:

$$\begin{aligned} \overline{\sigma}_{ij} &= -K_T\beta(T - T_0)\delta_{ij} + 2G\left(u_{ij} - \frac{1}{3}\delta_{ij}u_{kk}\right) \\ &+ K_T u_{ll}\delta_{ij} + 2\eta\left(\dot{u}_{ij} - \frac{1}{3}\delta_{ij}\dot{u}_{kk}\right) + \eta'\dot{u}_{kk}\delta_{ij} \end{aligned}$$

where G is the shear modulus, $\eta = G\tau_1$ is the shear viscosity coefficient (τ_1 is the relaxation time), and $\eta' = K_T\tau_2$ is the bulk viscosity coefficient (τ_2 is the relaxation

[3]This is not the same $\overrightarrow{q}$ used to represent the phonon wavevector

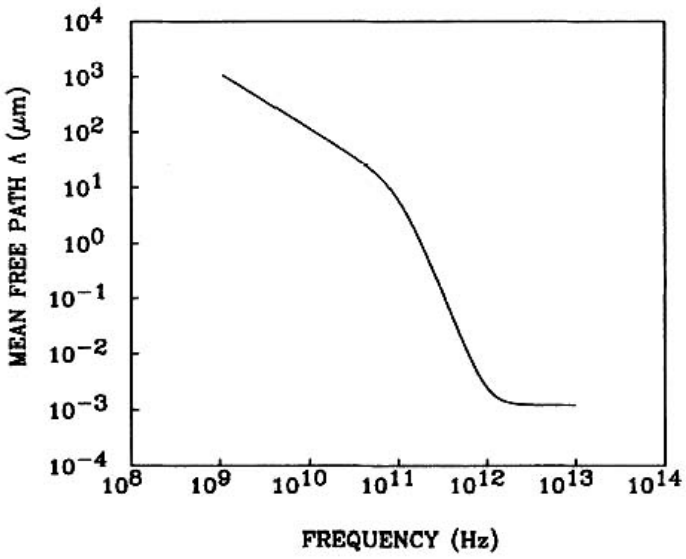

Figure 2-6: The phonon mean free path for a typical amorphous material, shown here for SiO_2. MFP decreases for higher phonon frequencies [48].

time). The propagation of a sound wave will result in rapidly changing gradients. This causes deviations of the terms in the expression for $\overline{\sigma}_{ij}$ from their steady-state values. After a series of substitutions and solving a system of equations, expressions for longitudinal sound wave velocity and acoustic attenuation are obtained. When extended to the continuous spectrum, the following two relationships that include $c_{acoustic}$ and $\alpha(\omega)$ result:

$$\rho c^2_{acoustic} = \rho c_0^2 + \int_0^\infty \frac{H(\tau)\omega^2\tau^2}{1+\omega^2\tau^2} d\tau \tag{2.14}$$

$$\frac{\alpha(\omega)\lambda}{2\pi} = \frac{1}{2\rho c^2}\int_0^\infty \frac{H(\tau)\omega\tau}{1+\omega^2\tau^2} d\tau \tag{2.15}$$

H(τ) represents the relaxation time spectrum density and is a linear combination of terms that describe individual relaxation processes. It is thus shown that by using basic conservation laws, expressions can be found for acoustic velocity and absorption in polymers. A more detailed derivation is found in Perepechko [35] or Kinsler [27].

The relationship between λ and the phonon mean free path (MFP or Λ) determines

the propagation and absorption of sound energy in materials. The MFP is the distance a phonon travels before encountering either a $\Delta\rho$ or ΔE (or both), causing the phonon to lose intensity or scatter and change momentum[4]. As shown in Figure 2-6, the MFP decreases with increasing frequency. This is because high frequency phonons couple into the high frequency modes of the material. These modes correspond to shorter lengthscale structure and dynamics, resulting in a reduced Λ. The dependence of MFP upon frequency is not linear, implying also that there are different mechanisms responsible for the variation in the frequency dependence of attenuation. That is, $\alpha(\omega) \sim \omega^p$ where p takes on different values.

A coherent phonon is the directional longitudinal sound wave that is referred to throughout this thesis. It is called coherent because the acoustic energy is launched in a spatially and temporally controlled manner. Whereas, an incoherent (or thermal) phonon describes the relatively smaller lattice vibrations that result from available thermal energy in the material. The phonon wavevectors of thermal phonons are randomly directed within the material. When the acoustic wavelength is smaller than the phonon MFP ($\lambda < \Lambda$), the damping of acoustic energy caused by collisions between coherent phonons and incoherent phonons is significant. Each collision between coherent and incoherent phonon generates a third phonon. This is called the *normal process*, where momentum is conserved.

However, Λ is so small for amorphous polymers ($\Lambda \approx 100\,\text{nm}$) that it is dwarfed by the acoustic wavelength, even when high frequency phonons on the order of 10^6 to 10^9 Hz are used. For example, if $\omega = 10^9\,\text{Hz}$, then λ is O(μm). This is still much longer than the typical phonon MFP in a polymer. When $\lambda > \Lambda$, there is no direct interaction between coherent phonons and incoherent phonons. As is generally the

[4]The presence of one phonon causes periodic elastic strain which modulates the density of the material in space and time. A second phonon senses the density modulation and is scattered to produce a third phonon. Elastic scattering occurs when the scattered phonon is of the same energy as the incident phonon. Whereas, inelastic scattering results in a change in the energy of this third phonon because of interactions between the incident wave and the sample. Kittel describes scattering in noncrystalline solids in further detail [28].

case, a wave can only "see" features of size greater than or equal to its wavelength. When there is no acoustic wave present, the number of Debye (i.e. thermal) phonons in a particular state is determined by the Planck distribution function [1]. When there is an acoustic wave, this distribution no longer applies. This is because the acoustic wave excites the thermal phonons, thereby changing their distribution. The thermal phonons eventually return back to their equilibrium state after the temperature rise is dissipated. Thus, the absorption of sound results from nonlinear coupling with thermal phonons. This translates to a dissipation of acoustic energy into heat.

Woodruff and Friedreich also consider sound absorption. They discuss the condition $\omega\tau_c < 1$, where τ_c is the characteristic relaxation time of a dynamic process. This condition implies that the frequency at which the experiment probes is too slow to observe the relaxation process. They too agree that the acoustic wave lifts thermal phonons from equilibrium briefly, only to resettle after a series of collisions [46]. This transient phenomenon causes modulation of thermal phonon frequency by sound. This knowledge leads to the solution of the linearized Boltzmann equation, which provides another expression for $\alpha(\omega)$ with a quadratic frequency dependence, given by:

$$\alpha(\omega) = \frac{C_v T \bar{\gamma}^2 \omega^2 \tau}{3\rho c_{acoustic}^3} \tag{2.16}$$

where C_v is the specific heat at constant volume, T is the temperature, $\bar{\gamma}$ is the averaged Grüneisen constant[5], ρ is the density, and $c_{acoustic}$ is the acoustic velocity [35].

If probing frequency is steadily varied while observing a loss parameter such as $\alpha(\omega)$, then when $\omega\tau_c \approx 1$, a peak in the loss parameter (i.e. dissipation) will develop. Equivalently, the temperature could be systematically lowered to slow down the dynamic process responsible for the loss. Either way, the same result is observed (Figure

[5]The Grüneisen constant is defined as an average value of the change of vibration frequency per unit dilation. It describes the anharmonicity in the shape of the potential well in a plot of potential energy vs. interatomic distance.

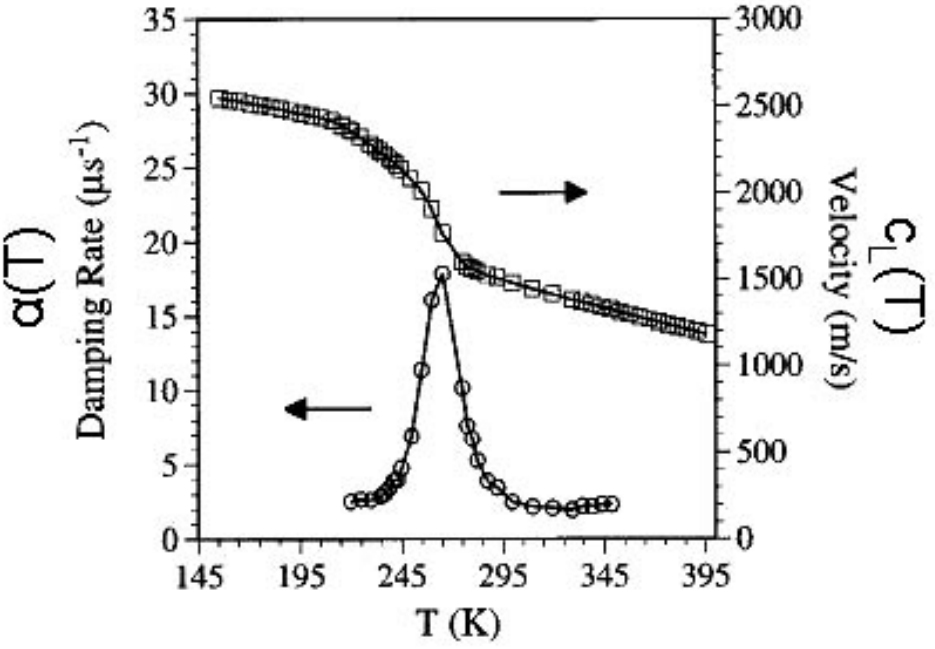

Figure 2-7: Temperature dependence of the acoustic velocity (□) and damping rate (∘) in salol from fits to ISTS data at $q = 0.1352\,\mu\mathrm{m}^{-1}$. As the temperature is lowered, the sound velocity increases from the room temperature value of $c_{acoustic}$. This is because of relatively slower structural relaxation dynamics. The sound velocity increases as the temperature is lowered further and the structural relaxation dynamics become very slow compared to the acoustic oscillation period. The damping rate shows a maximum at about 265 K, when the relaxation time corresponds to the acoustic frequency [47].

2-7). The location of the damping peak corresponds to the temperature ($T_{transition}$) at which the relaxation time of the dissipation process in the material is on the order of the period of the imposed stimulus (left axis). Below $T_{transition}$, the sample shows increased resistance to deformation. A rise in the acoustic velocity results at $T_{transition}$, which is an indication of increased stiffness (right axis). Compare the temperature dependence of the acoustic velocity shown here for the glass-forming liquid Salol to the temperature dependence of the modulus shown in Figure 2-10 for a typical polymer. The similarity in the curves and the fundamental relationship between $c_{acoustic}$ and ρ implies that a change in acoustic velocity with temperature may coincide with a phase transition or a dynamic process. Examples of such processes are given in Section 2.3.

While the condition $\omega\tau_c \approx 1$ is typically discussed in the context of dynamics, $qd \approx 1$ is the appropriate condition to consider when characterizing structural features. When the condition holds, the wavevector ($\overrightarrow{q}$ or $\mathbf{K}$) corresponds to the size of the structural feature (d) as follows:

$$q = \frac{2\pi}{d} \tag{2.17}$$

When $qd \approx 1$, acoustic wave energy is coupled to a density fluctuation [48] and strong damping is observed [47]. This is the case for amorphous materials since no other structural irregularities exist. Otherwise, the acoustic energy would couple into structural heterogeneities such as nanoparticles as well. The damping rate shown by the authors ($\dot{\alpha} = \alpha c_{acoustic}$) is a measure of the timescale over which energy is lost into the modes of the material.

2.3 Dynamic Processes in Polymers

There is another component of polymer characterization beyond measuring elastic constants and attenuation coefficients, and that is mapping out dynamic processes

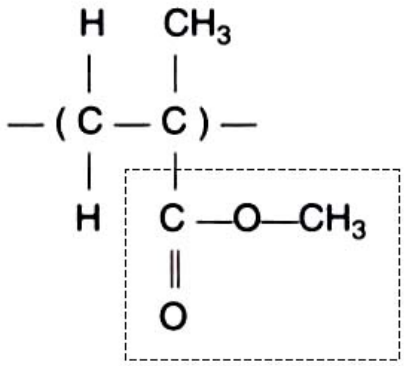

Figure 2-8: Chemical structure of the monomer repeat unit in poly(methyl methacrylate). The ester group is pendant from the main chain [7].

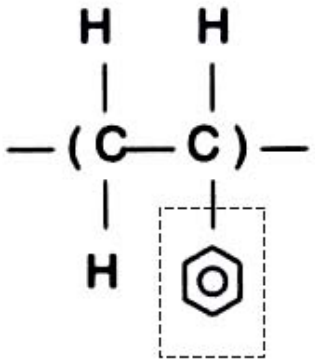

Figure 2-9: Chemical structure of the monomer repeat unit in polystyrene. The phenyl ring is pendant from the main chain [7].

as temperature and frequency are varied. In polymers, acoustic attenuation can be thought of as indicative of a lossy dynamic process. This section outlines some of the mechanisms responsible for this energy loss.

Viscoelastic processes in polymers are absorption modes by which energy can be coupled into a material. The individual processes are labeled α, β, γ, δ, etc. in the order in which they occur as the observation temperature is lowered. It is widely agreed upon that the α process corresponds to the cooperative segmental motion of approximately 20 to 40 monomers. This implies a lengthscale of $\approx 10\,\text{nm}$, which allows for movement of the main chain. When probed at quasi-static frequencies, the α-process temperature corresponds to the point at which the polymer begins to flow.

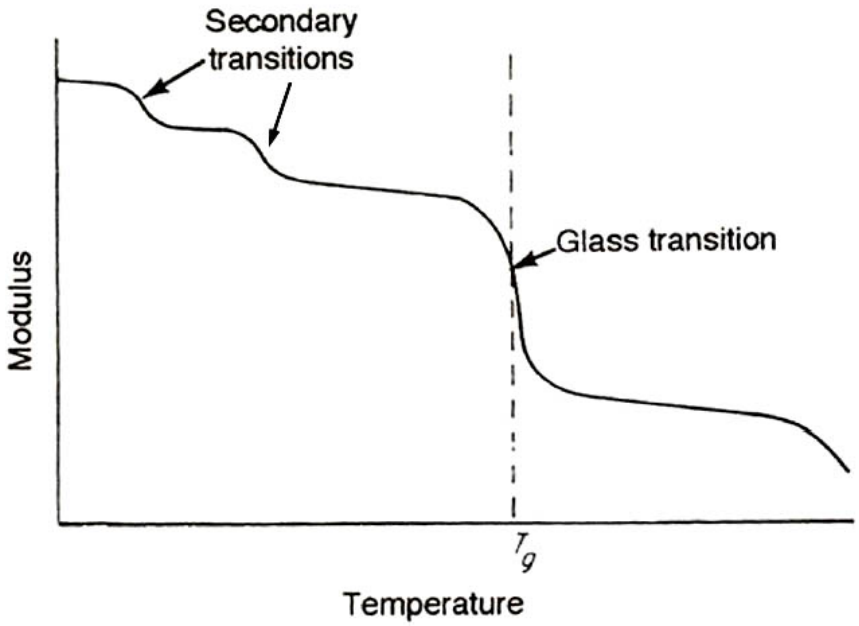

Figure 2-10: The variation of modulus with temperature shown here depicts both the secondary transitions that occur at lower temperatures, along with the α relaxation, which corresponds to the glass transition temperature of the polymer [45].

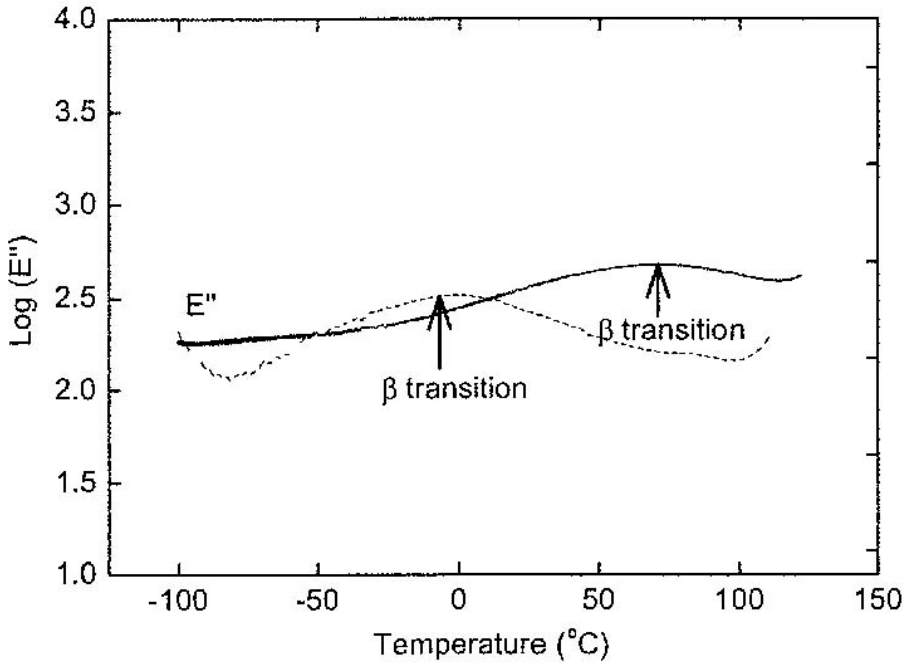

Figure 2-11: The temperature dependence of the loss modulus (E'') for PMMA, as measured by DMTA for two frequencies. Data is shown for 0.1 Hz (dashed line) and 100 Hz (solid line) [43].

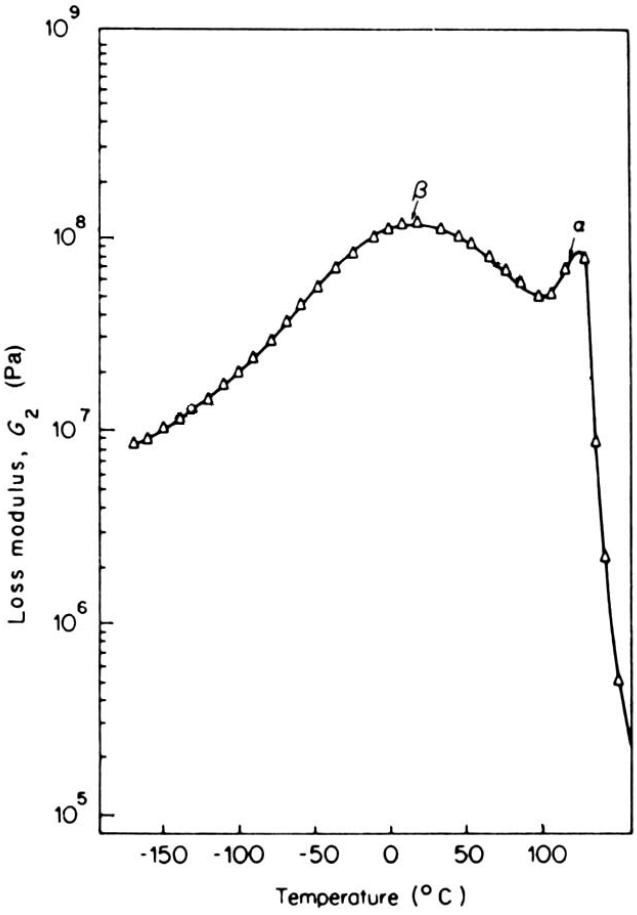

Figure 2-12: The loss modulus (G_2) as a function of temperature for PMMA measured by a low frequency torsional pendulum shows the α and β peaks [45].

For this reason, it is also known as the glass-rubber transition temperature or simply the glass transition (T_g). As seen in Figure 2-10, the glass transition corresponds to a sudden drop in Young's modulus with increasing temperature. Compared to the drastic change in modulus observed during the α process, the lower temperature transitions result in less change and are accordingly labeled "secondary." The actual polymer physics behind each of these lower temperature processes is often complex.

The α and β processes in PMMA are depicted in Figure 2-12. The β process in amorphous polymers often corresponds to the local motion of side groups stemming from the main chain. The rotation of the entire side group about the main chain will normally take place at a higher temperature and at a slower rate than the rotation of

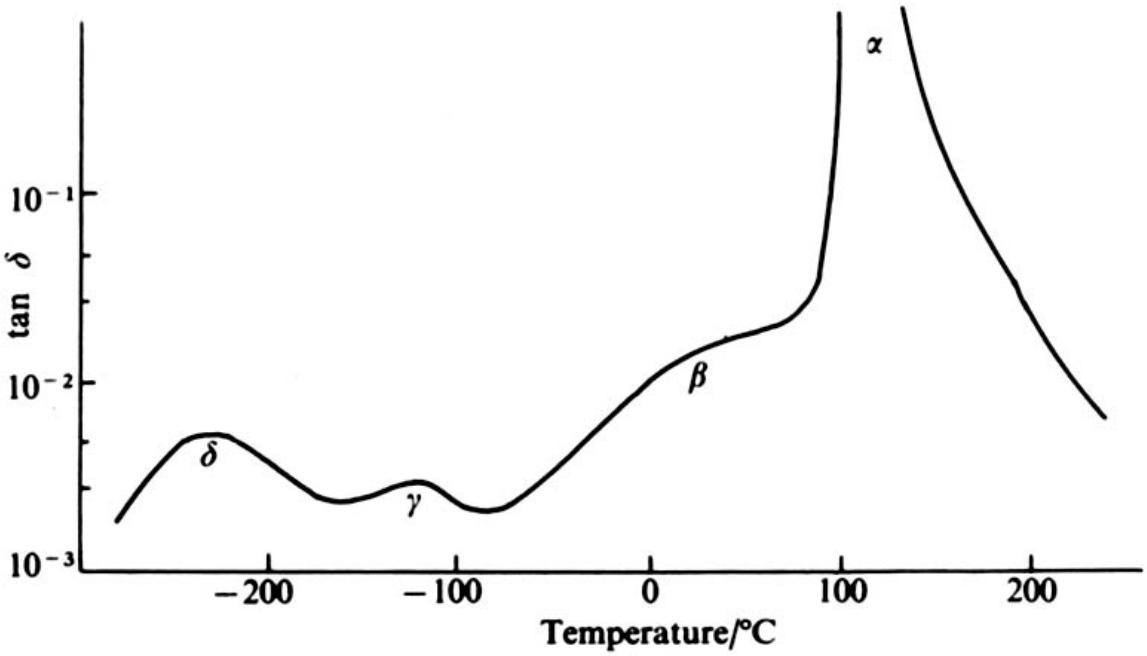

Figure 2-13: The loss parameter $\tan\delta$ as a function of temperature for PS at 0.5 Hz shows the α, β, γ, and δ peaks [2].

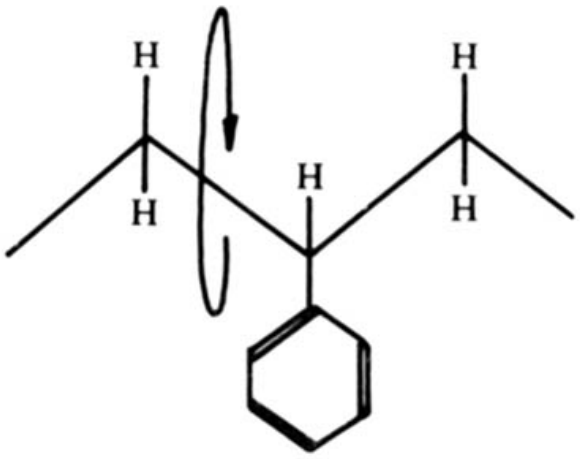

Figure 2-14: The crankshaft rotation in PS may be responsible for the β peak. Here the phenyl group does not rotate independently of the main chain; rather the chain itself rotates about its own axis just as a crankshaft does [2].

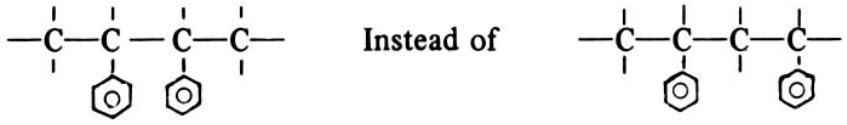

Figure 2-15: The γ process is possibly caused by inconsistent polymerization, when head-to-head groups form instead of head-to-tail groups [2].

a small side group or a portion of the group. In PMMA, the β process is associated with the rotation of the pendant ester group about the main chain (see Figure 2-8). The γ and δ (not shown) processes involve motions of the methyl groups attached to the main chain and side-chain, respectively [45].

The α process along with secondary relaxations β, γ, and δ are shown for PS in Figure 2-13. The suggested origins of the β relaxation are the rotation of the phenyl group around the main chain, twisting of the main chain, or perhaps a crankshaft rotation (see Figures 2-9 and 2-14). The γ peak may be caused by head-to-head polymerization instead of head-to-tail polymerization (see Figure 2-15) [2].

The temperature dependence of the loss modulus for PMMA as obtained by dynamic mechanical thermal analysis (DMTA) is shown in Figure 2-11. The loss modulus (E'') is simply another parameter that indicates energy dissipation within a material. The shift in the peak position indicates the dependence of the β transition on frequency. The peak goes from -5°C at 0.1 Hz to 75°C at 100 Hz or an increase of about 25°C per decade increase in frequency. The higher the frequency, the higher the temperature at which the β process is observed. When oscillations of a higher frequency are imposed on a material at a given temperature, the relevant part of the structure (e.g. the pendant ester group) may not have sufficient time to respond to the stimulus. This means that the particular molecular motion is restricted. Therefore, no energy is absorbed, and the particular molecular motion is said to be "frozen out." When the temperature is increased, there is enough thermal energy for the molecular motion to happen once again and energy is absorbed. Both dynamic

mechanical experiments and various types of spectroscopies are capable of observing these transitions. The Deathstar GHz spectroscopy used in this thesis will be another characterization tool to add to the portfolio.

2.4 Related Studies

Despite most of what has been done in the area, the acoustic properties of amorphous polymers remain to be fully understood. Presented below are overviews of other techniques commonly used to study polymer behavior at frequencies comparable to those probed in this thesis. While each of the techniques directly observes different material responses, the underlying phenomena that they strive to understand are often times similar. Specifically, the frequency dependence of acoustic attenuation $\alpha(\omega)$ is explored in two narrowband acoustic techniques. Dynamic processes in polymers are probed by two broadband techniques, Brillouin light scattering and dielectric relaxation spectroscopy. Along with a summary of recent developments with each technique is included brief commentary on its shortfalls. It is shown that there are questions which remain unsatisfactorily answered. Deathstar GHz spectroscopy presents a clear and direct method to quantitatively measure $\alpha(\omega)$ and $c_{acoustic}(T)$, thus characterizing energy loss and energy propagation in polymers.

2.4.1 Picosecond Ultrasonics

We begin by first reviewing the work of Morath and Maris, who study the attenuation of longitudinal phonons in amorphous solids [31, 32, 48]. They find a universal $\alpha \sim \omega^2$ behavior for frequencies up to 320 GHz and temperatures between 80 and 300 K. These researchers use a picosecond ultrasonic technique, which is similar in function, but not form, to the Deathstar picosecond acoustic technique used in the current study. Their results will constantly be referred to in this thesis as a point of close comparison.

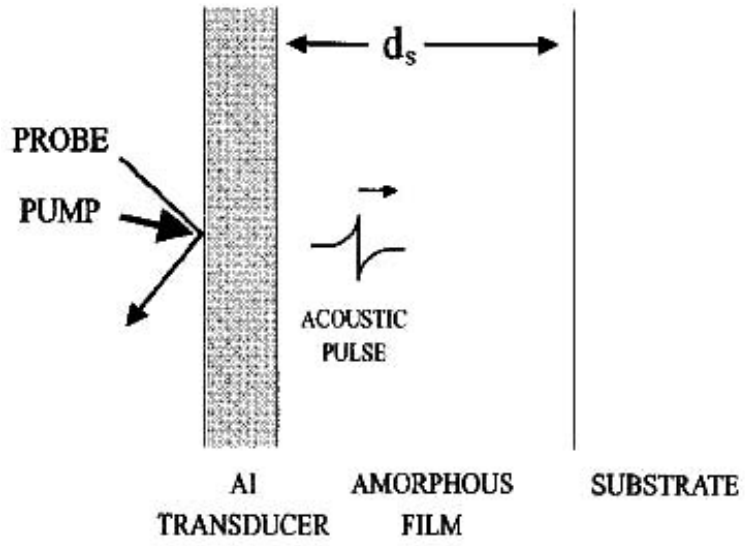

Figure 2-16: Schematic diagram of reflection mode experiment and sample structure used by Morath and Maris. The Al transducer is 18 nm thick, the amorphous film is 62 nm thick PMMA, and the substrate is sapphire. This technique employs *frontside excitation* and *frontside detection* [31].

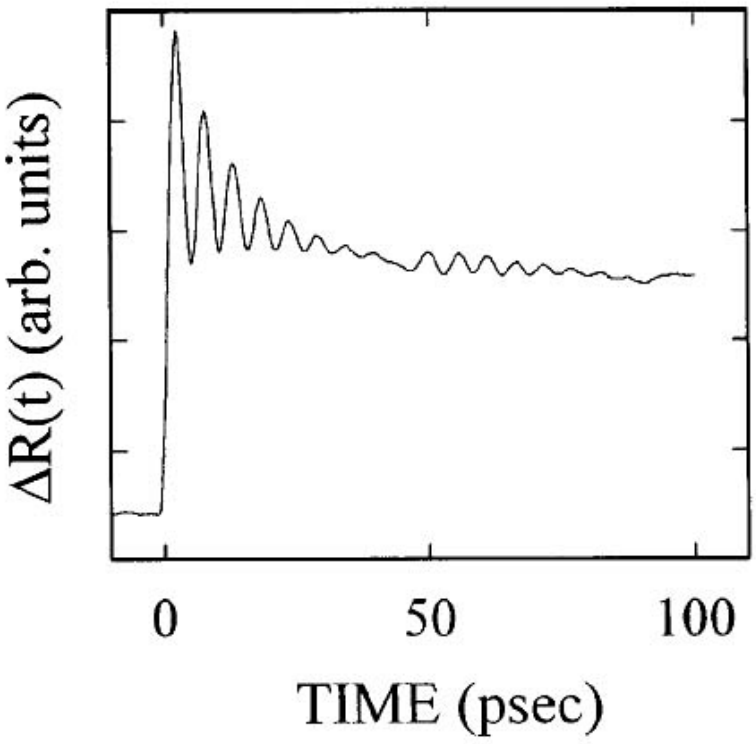

Figure 2-17: Change in optical reflectivity of Al versus time ($\Delta R(t)$) for the structure shown in Figure 2-16 (Morath and Maris) [31].

Their sample films are prepared by spin-coating a polymer solution onto a substrate, which is either sapphire, Si, of GaAs. The polymer is then coated with an aluminum film via electron beam deposition. The multilayer stack is shown in Figure 2-16. When the picosecond pump light is absorbed by the thin Al film, the Al film rapidly expands and an acoustic pulse (i.e. a purely longitudinal phonon) is launched into the polymer film. In this sense, the metal film serves as a photo-acoustic transducer. The shape of the pulse (traveling from left to right in the figure) depicts a compressive front (negative), immediately followed by tensile expansion (positive). This pulse gets reflected at the rigid polymer-substrate interface. The substrate is assumed to be thick enough that its own ringing does not complicate the observed signal.

The returning pulse strains the Al transducer, thereby changing its optical reflectivity (ΔR). This ΔR is detected by a time delayed probe pulse, which observes the time-dependent reflectivity of the Al, as indicated in Figure 2-17. Optical reflectivity in metals is known to be a sensitive indicator of structural changes at the surface. Thus, the local displacements that occur as the transducer is strained may result is misleading values of ΔR. The measured ΔR also tends to be relatively small, decreasing the signal-to-noise ratio (SNR). Furthermore, R_{Al} is temperature-dependent, so any temperature rise must be taken into account. The bandwidth, i.e. the accessible frequency range, is dictated by the thickness of the Al transducer layer. Thinner layers generate higher frequency phonons. This implies that transducers of different thicknesses be deposited for each frequency studied–a time-consuming process.

The results of the acoustic attenuation measurements conducted by Morath and Maris are presented. Part of this thesis aims to compare results with the values they obtain for the frequency and temperature dependence of attenuation for atac-

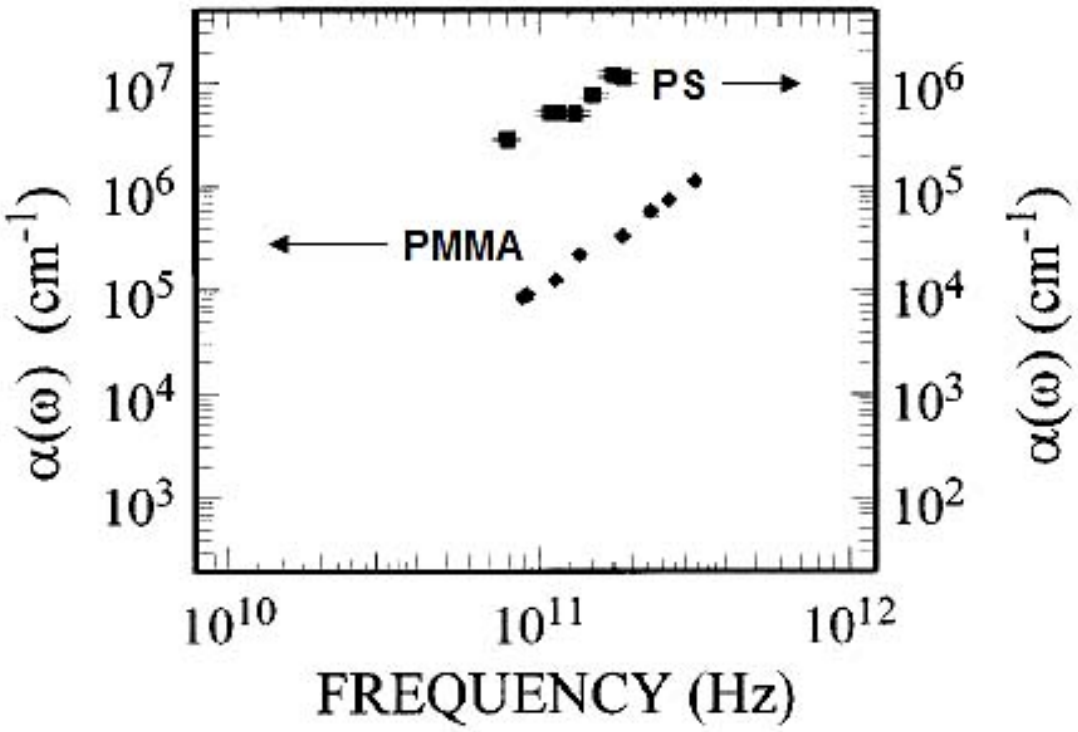

Figure 2-18: Phonon attenuation as a function of frequency at 300 K for PMMA (left axis) and PS (right axis) (Morath and Maris) [31].

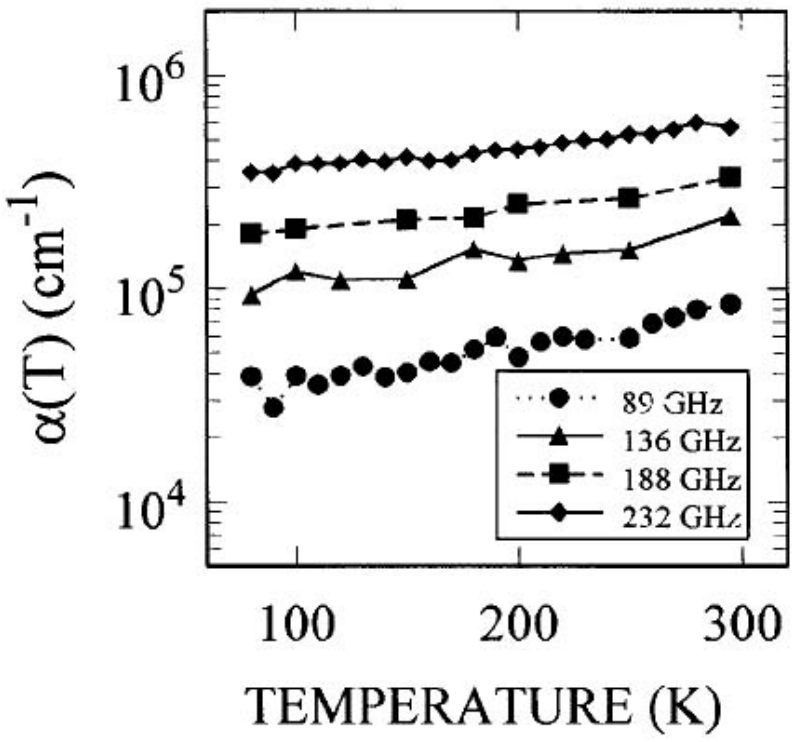

Figure 2-19: Acoustic attenuation ($\alpha(T)$) in PMMA as a function of temperature. The data at phonon frequencies of 89, 136, 188, and 232 GHz are from samples 145, 62, 62, and 35 nm thick, respectively (Morath and Maris) [31].

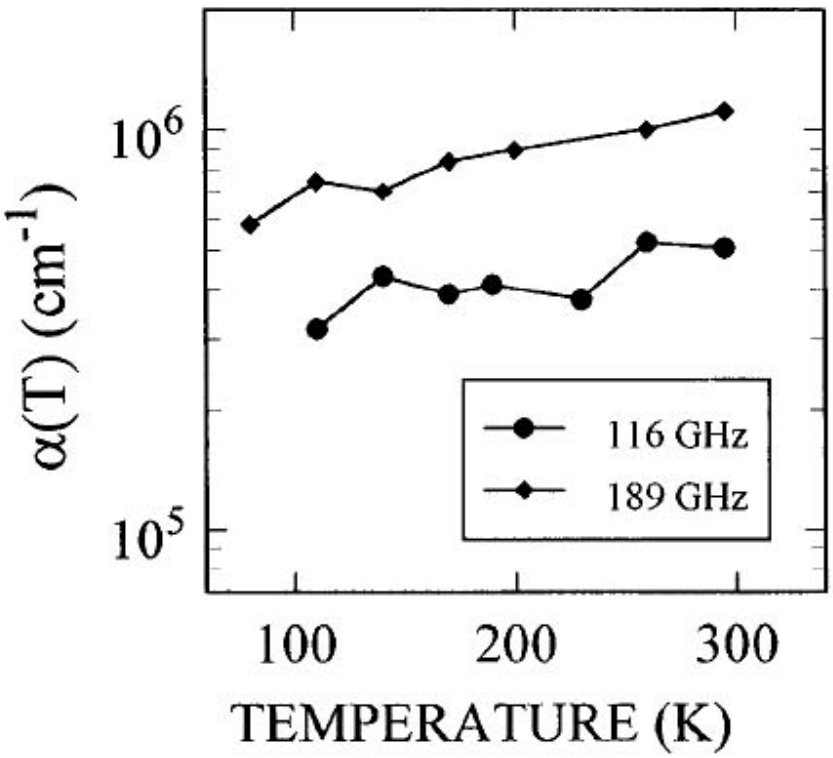

Figure 2-20: Acoustic attenuation ($\alpha(T)$) in PS as a function of temperature. The data at phonon frequencies of 116 GHz and 189 GHz are from a sample 30.5 nm thick (Morath and Maris) [31].

tic PMMA[6]. Obtaining similar values will validate the Deathstar GHz spectroscopy. Figure 2-18 shows the attenuation as a function of frequency for PS and PMMA at 300 K. Morath and Maris find a quadratic dependence of the attenuation upon frequency for all the amorphous materials they study. However, others do not always find this $\alpha \sim \omega^2$ relationship [24, 39, 17, 38]. Additional data is needed to see what the Deathstar GHz spectroscopy suggests. Importantly, the Deathstar extends the measurable range to lower frequencies. The temperature dependence for two frequencies obtained by Morath and Maris is shown in Figures 2-19 and 2-20 for a-PMMA and a-PS, respectively. The attenuation increases by a factor of two with increase of temperature from 80 K to 300 K for both polymers. The authors note that the temperature variation of the attenuation is independent of frequency, within experimental error [31].

The actual method by which Morath and Maris determine attenuation is not straightforward. By comparison, the Deathstar GHz spectroscopy is able to measure absolute acoustic attenuation, without having to make assumptions about material behavior. Section 4.4 compares the two approaches in detail.

The second part of experiments conducted by Morath and Maris involves determining how acoustic velocity dispersion is influenced by temperature and frequency. The approach taken is to generate two different phonon frequencies through a single PMMA sample 60 nm thick. By comparing the round trip transit times, $\tau(T)$, as a function of temperature for the two frequencies, the authors conclude that there is no velocity dispersion in this frequency and temperature range. This is indicated graphically in Figure 2-21, where the authors claim that the separation between the two curves remains constant within experimental error and is independent of temperature.

[6]An atactic polymer, denoted by the prefix *a*, is one where the side groups extending from the main chain take on a random configuration above and below the planar zigzag created by the backbone. An atactic polymer has no regularity from chiral center to chiral center. Polymers that are formed by free-radical polymerization are usually atactic. The regularity of the polymer's structure influences the degree to which it has rigid, crystalline long range order or flexible, amorphous long range disorder.

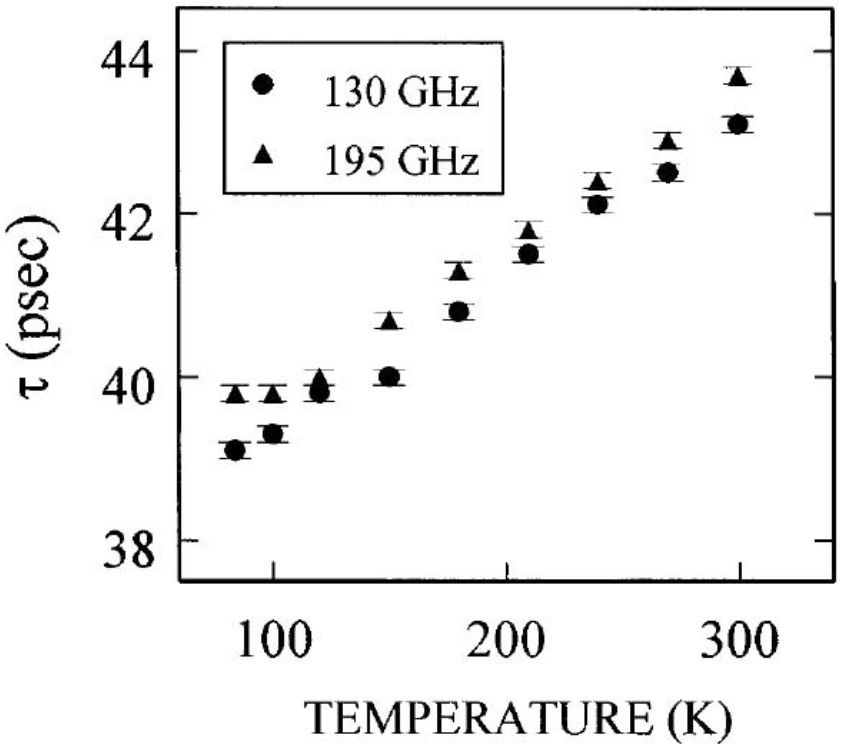

Figure 2-21: Round-trip acoustic transit time $\tau(T)$ for a 60 nm thick PMMA film on a sapphire substrate at 130 GHz and 195 GHz (Morath and Maris) [31].

In general, the temperature dependence of the velocity can be described by the temperature derivative $\beta(T)$[†],

$$\beta(T) \equiv \frac{1}{v_s}\frac{dv_s}{dT} \tag{2.18}$$

which equals $-5 \times 10^{-4}\,\mathrm{K}^{-1}$ over the range from 80 K to 300 K for PMMA and $-7 \times 10^{-4}\,\mathrm{K}^{-1}$ for PS. Because the thermal expansion coefficient of PMMA at these temperatures is only $5 \times 10^{-5}\,\mathrm{K}^{-1}$ [19], change in the film thickness is assumed to be negligible. The calculated value of $\beta_{\mathrm{PMMA}}(T)$ agrees with the results of Brillouin scattering [26] at about 10 GHz. More precise experiments in the MHz range show agreement above 120 K. At lower temperatures, $\beta_{\mathrm{PMMA}}(T)$ drops to $-2.8 \times 10^{-5}\,\mathrm{K}^{-1}$ and remains constant down to 4 K [34]. Upon heating, there is another abrupt change in $\beta_{\mathrm{PMMA}}(T)$ at 380 K, which corresponds to the T_g of PMMA [44].

The frequency dependence of the acoustic attenuation measured at 300 K by Morath and Maris is also of interest. The results for PS and PMMA in Figure 2-22 from 10^6 GHz to 10^9 GHz were measured by Morath and Maris using picosecond ultrasonics, and results from Brillouin-scattering [24] and an ultrasonic technique [44] are shown for comparison. They indicate a linear dependence of attenuation with frequency from the 10 GHz to 50 GHz range. This changes to a universally quadratic dependence at frequencies above 100 GHz.

The variations of the acoustic attenuation with frequency in PMMA as measured by picosecond ultrasonics, BLS, and thermal conductivity approximations are shown in Figure 2-23. The results summarized in the figure all indicate that attenuation increases with temperature; however, they do not agree on the rate of this change. The results of tunnel junction measurements (not shown) indicate a dependence of $\alpha \sim \omega^{4.5}$, which is in agreement with thermal conductivity results around 10^{12} Hz.

Recent work in picosecond acoustics in the GHz range by Lee *et al.* proposes

[†]This β represents the temperature derivative of the velocity and is not related to the dynamic β relaxation process described in Section 2.3.

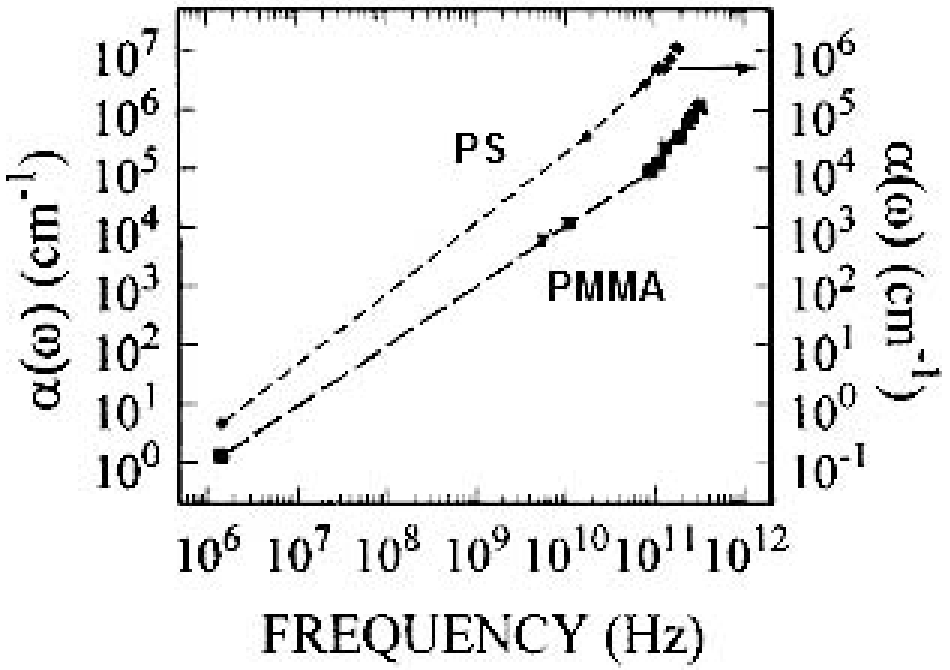

Figure 2-22: Acoustic attenuation versus phonon frequency in PS and PMMA over a broad frequency range at 300 K [31]. Low frequency results are from Brillouin-scattering measurements [24] and ultrasonic measurements [44].

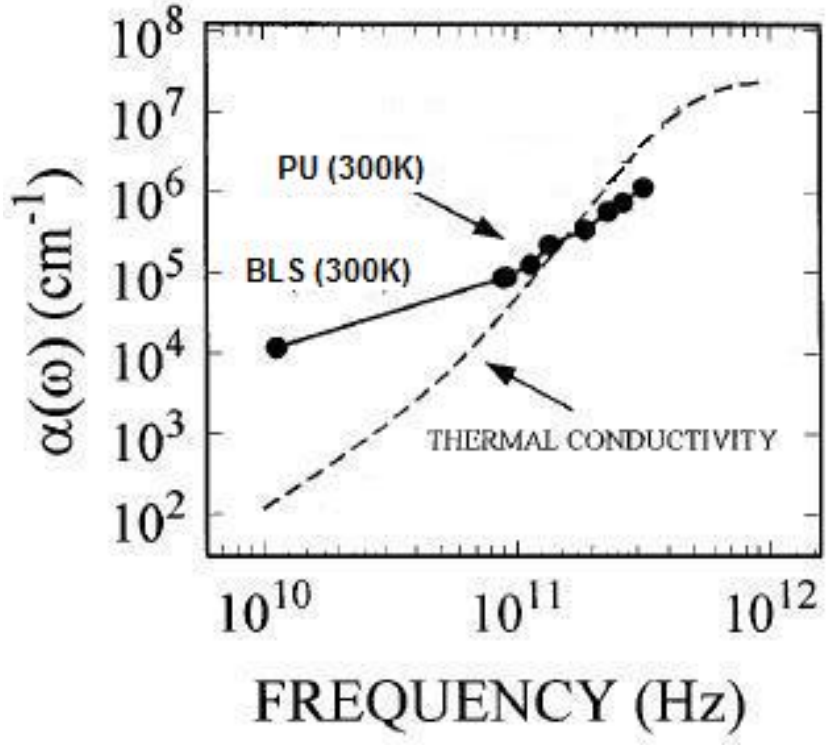

Figure 2-23: Attenuation results for PMMA from three different techniques. The dashed line is the estimate of the attenuation from a fit to the thermal conductivity of PMMA [17]. The picosecond ultrasonic (PU) measurements of the Maris Group and the Brillouin light scattering (BLS) measurements [24] are taken at a temperature of 300 K [31].

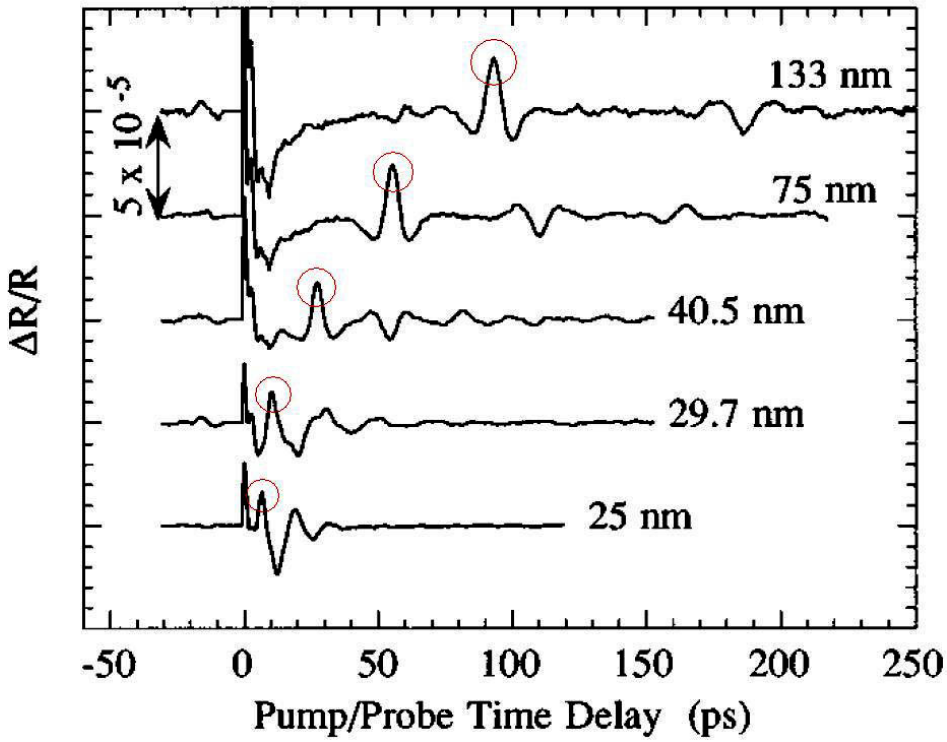

Figure 2-24: The acoustic signals observed by Lee, studying PMMA|Al|Si multilayers using picosecond acoustics. Even after a thermoreflectance background subtraction, there is a complicated overlap of incident and reflected pulses. Studying thinner films is limited in this method since the acoustic echo (circled) steadily becomes closer to the original pulse. Eventually, there comes a point where the two are inseparably merged (Lee) [29].

that longitudinal sound velocity increases three-fold for PMMA and PS thin films less than 40 nm on Al-coated Si substrates (i.e. polymer|Al|Si) as compared to bulk values [29]. This corresponds to a ten-fold increase in the modulus. The acoustic velocity measured using the Deathstar GHz spectroscopy do not show this trend. The dramatic changes observed by Lee are based on the so called time-of-flight principle. This approach becomes very difficult to use for films thinner than about 25 nm. This is indicated in Figure 2-24, where the problem of separating the spectral contribution from incident and reflected signals becomes increasingly difficult for thinner films. Incorrectly measured thickness values can also result in gross errors in time-of-flight velocity calculations (rate $= \frac{\text{distance}}{\text{time}}$).

Entirely conflicting conclusions are drawn by Morath and Maris. The mere 10-20% increase in phonon velocity they uncover for thin films over bulk values (compared to the 300% found by Lee) is attributed to unreliable film thickness measurements. They find ellipsometry to be an unreliable method of thickness determination for polymer films below 40 nm, reporting an overestimation of approximately 20% [31]. Thus, no inherent acoustic velocity difference for the substrate-supported thin film geometry is found as compared to the bulk. This is in agreement with the results of the broadband investigation conducted using the Deathstar GHz spectroscopy (Section 4.3).

Clearly, there is need for resolution regarding by how much longitudinal phonon velocity changes with parameters such as polymer film thickness and temperature. Part of this thesis will present relevant data and draw conclusions regarding this issue.

2.4.2 Brillouin Light Scattering

Brillouin light scattering (BLS) measures vibrational energies and intensities along with dipole polarizations via acousto-optical interactions in a scattering medium. This allows for determination of the sound velocity, acoustic dispersion, molecular relaxations, and elastic moduli [40].

In Brillouin scattering, a propagating sound wave creates modulations in the dielectric constant (ε). These modulations are detectable optically since they scatter light. Even small changes from bulk values of density significantly affect the speed of sound in a material (a small $\Delta\rho$ will result in a large $\Delta c_{acoustic}$ since $c_{acoustic} \sim \rho^{-1/2}$). By measuring the intensity of light as a function of scattering angle, a simple relationship can be developed between the phonon wave vector and the scattering angle. While this is useful for probing whether certain acoustic frequencies can be propagated through the medium (i.e. defining phononic band gaps), absolute acoustic attenuation cannot be obtained.

Included in Figure 2-23 are values of attenuation for PMMA from 1 K to 300 K derived from Brillouin light scattering (BLS) measurements. BLS experiments involve inherently different acoustic physics. Forrest notes that the film-guided modes propagated are hybridized longitudinal-transverse waves, as compared to the more straightforward pure longitudinal mode [9]. Since the mode velocity is a function of both the longitudinal and transverse acoustic velocities, additional work is required to separate the individual contributions.

BLS is used by Forrest *et al.* to measure the high frequency mechanical properties of free-standing PS films at room temperature [9]. The results of their investigation are similar for PMMA as well. However, there are discrepancies with results of picosecond ultrasonic measurements found in the literature. The BLS studies conclude that the thin film mechanical properties are consistent with bulk values and independent of film thickness; whereas, some acoustic techniques indicate otherwise.

2.4.3 Dielectric Spectroscopy

Dielectric relaxation spectroscopy (DRS) probes the interaction of a macroscopic sample with a time-dependent electric field ($\overrightarrow{E(t)}$). The resulting polarization ($\overrightarrow{p}$) can be expressed either by the frequency-dependent complex permittivity and conduc-

tivity or as an impedance spectrum. Both of these characterize the amplitude and timescale (via the relaxation time) of the charge-density fluctuations within the sample. Such fluctuations generally arise from the reorientation of the permanent dipole moments of individual molecules or from the rotation of dipolar moieties in flexible molecules, like polymers. Other possible mechanisms include the transport of ions or the appearance of interfacial charges in heterogeneous systems.

The timescales of these fluctuations depend upon the sample and the relevant relaxation mechanism. Relaxation times range from several picoseconds in low-viscosity liquids to hours in glasses, marking DRS as a technique with extensive coverage of dynamical processes. The corresponding measurement frequencies range from 10^{-4} Hz to 10^{12} Hz. In contrast to conventional spectroscopic methods, like NMR or vibrational spectroscopy, DRS is especially sensitive to intermolecular interactions. DRS is able to monitor cooperative processes. This provides a link between molecular spectroscopies that probe the properties of individual constituents, and bulk characterization techniques that probe viscoelastic and rheological behavior. The deconvolution of the dielectric spectrum into its individual relaxation processes gives the relative amplitudes and characteristic times of the underlying molecular motions.

The equivalent frequency range of dielectric spectroscopy has been expanded by various experimental techniques so that dielectric relaxation processes of characteristic times from 10^{5} s to 10^{-12} s can be measured. As a result, these techniques now occupy a special place among numerous modern methods used in physical and chemical analyses of materials. Dielectric spectroscopy provides a link between the dynamics of molecular motion of the individual constituents in complex materials and the characterization of their bulk properties. The recent successful developments of the time domain dielectric spectroscopy and broadband dielectric spectroscopy have radically changed the role of dielectric spectroscopy, making it an effective tool for structural investigation in solids and liquids on macroscopic, microscopic and mesoscopic levels

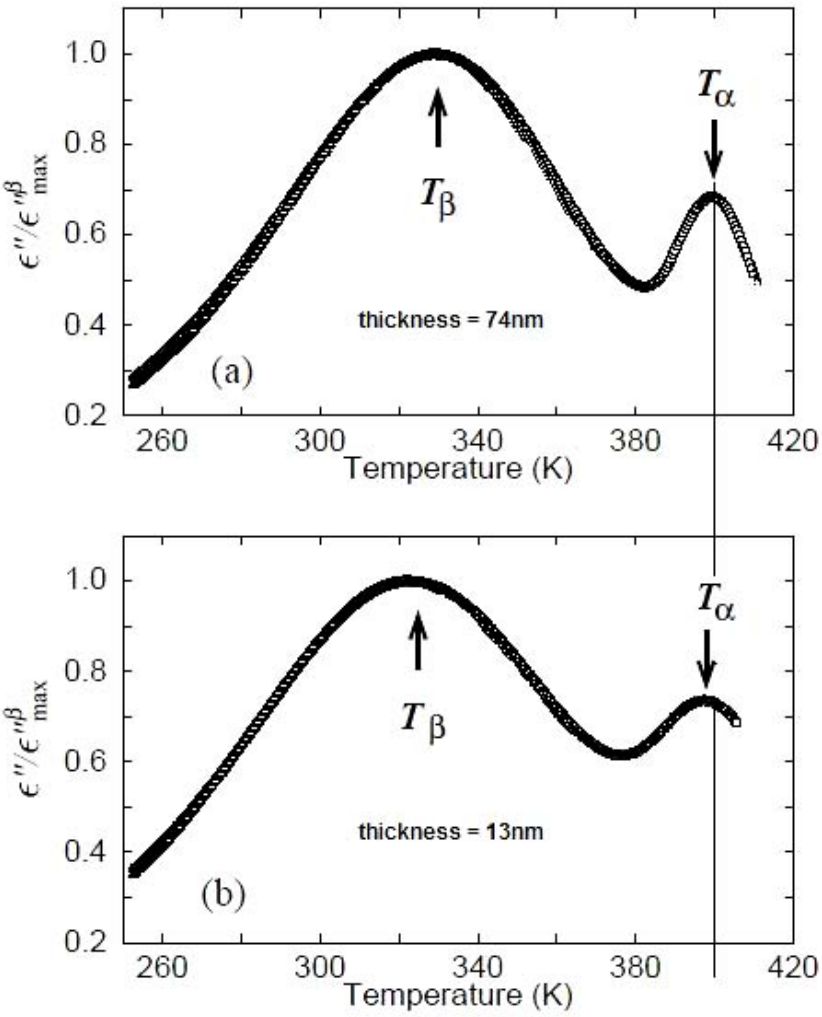

Figure 2-25: Temperature dependence of the normalized dielectric loss ($\epsilon/\epsilon''^{\beta}_{max}$) at 100 Hz for thin films of a-PMMA. The thicknesses of a-PMMA are d=74 nm and d=13 nm for the top and bottom graph, respectively (Fukao) [10].

[37].

Fukao reviews recent progress in dielectric studies of polymeric materials, specifically PMMA and PS [10]. DRS has been used to probe the α process in PS [11, 13, 12, 14] and both the α and β processes in PMMA [15]. The technique is well-suited to probe the shift in the positions of these relaxation processes as experimental parameters such as temperature and frequency are changed. The influence of sample variables such as thickness and molecular weight can also be investigated. Fukao studies the temperature of the α peak (T_α) for a-PMMA films of varying thick-

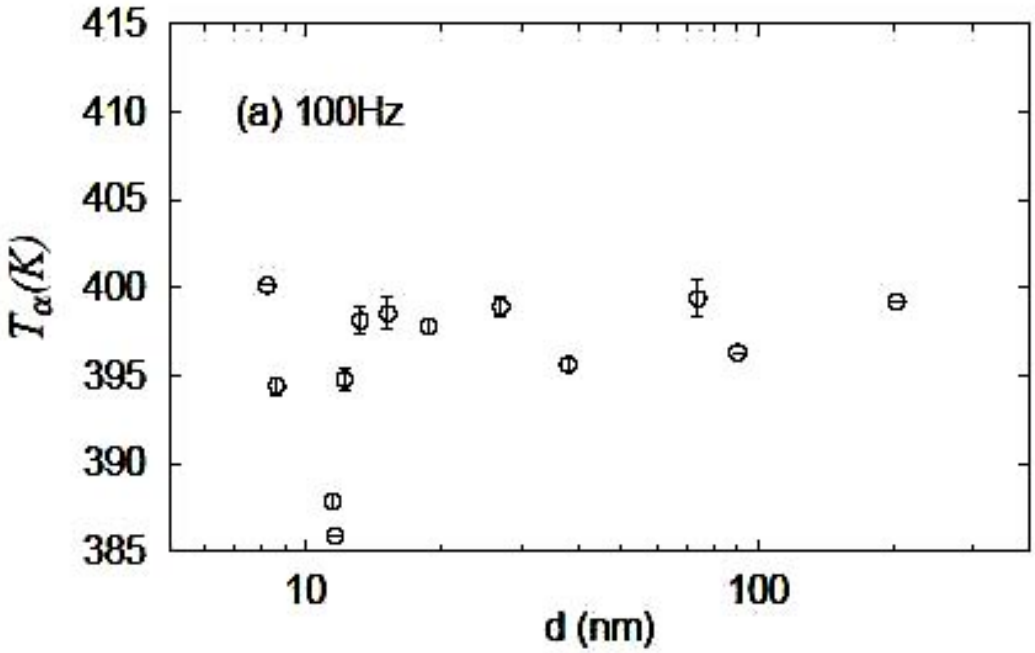

Figure 2-26: Thickness dependence of T_α for thin films of a-PMMA at 100 Hz (Fukao) [10].

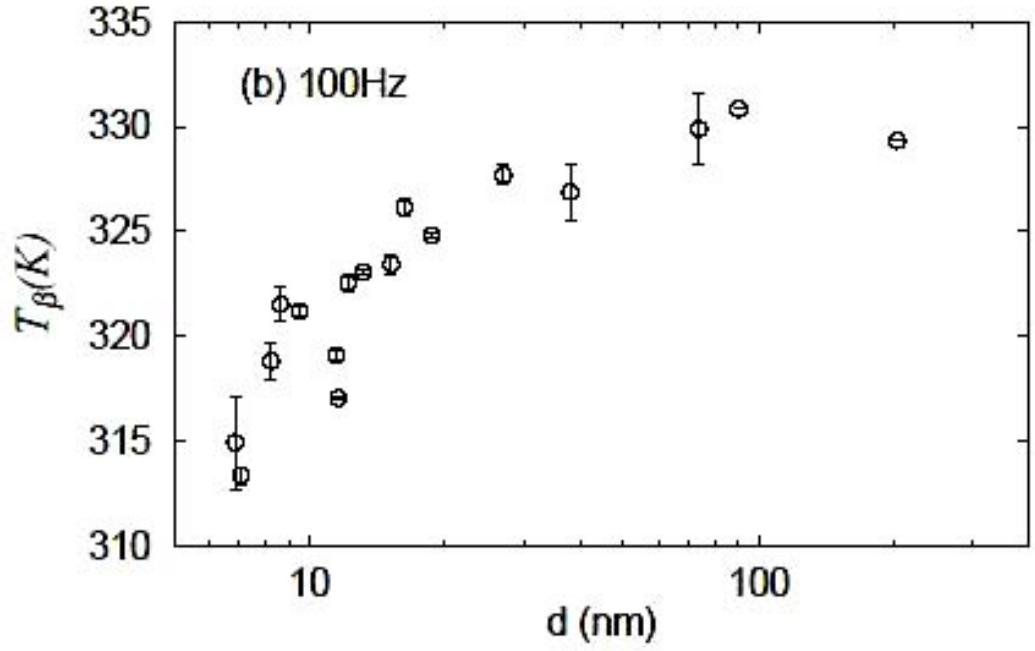

Figure 2-27: Thickness dependence of T_β for thin films of a-PMMA at 100 Hz (Fukao) [10].

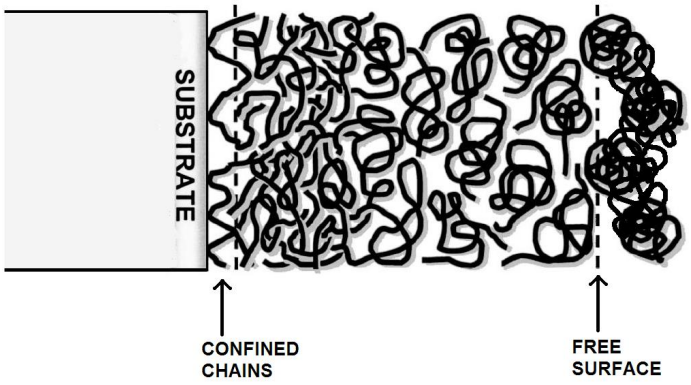

Figure 2-28: It is suggested that there are regions of varying polymer density or compactness. This influences the temperature at which dynamic processes occur due to the restricted mobility at a substrate interface as compared to the free surface.

nesses. This is also shown is Figure 2-25, where the α process appears around 400 K for both film thicknesses. This insight is valuable because it allows T_g to be assumed independent of film thickness, even for film thicknesses at or below the radius of gyration of the polymer ($R_g \approx 20\,nm$). When the experiment is repeated for several different film thicknesses, a plot of T_α as a function of film thickness results (Figure 2-26). This confirms that the α process in a-PMMA varies negligibly with film thickness for films less than about 20 nm thick. A similar plot for the β process shows that the T_β shifts evenly to lower temperatures with decreasing film thickness (Figure 2-27). A reason for this is not provided by the authors, and it seems counterintuitive. There is a troubling contradiction presented by these DRS results because the α peak should be *more* sensitive to film thickness since it corresponds to the large scale segmental motions of ≈ 20 monomers. The β process is caused by the very local motions of side chains. The explanation proposed by Fukao is based upon a variation of the layer model depicted in Figure 2-28[13, 15]. His explanation describes two competing effects within different sections of the thin film. The first effect enhances α and β process dynamics because the mobile layer that exists near surfaces has a higher density of chain ends (i.e. more free volume for molecular motion). Countering this is an increased attractive force between the polymer and the underlying substrate, which

hinders chain mobility and effectively raises the T_g. It does make sense that the T_g is effectively increased at the substrate|polymer interface and effectively reduced at the polymer|air interface. However, the T_g measured depends on the relative contributions of these interfacial layers. The majority of the polymer molecules in the thin film are surrounded by like polymer molecules. Accordingly, the thin film T_g should agree with the bulk T_g value.

Chapter 3

Spectroscopic Technique Overview: Deathstar GHz Spectroscopy

3.1 Introduction

Many techniques seek to probe the same underlying physical phenomena, but the directly observed parameters that they measure often vary. The details of such technique are described in Chapter Two. Our motivation for using a new technique is to study faster material dynamics and smaller material structures. The experimental details of the Deathstar GHz spectroscopy are presented. The differences between narrowband and broadband inputs are described in this chapter also.

3.1.1 Narrowband Spectroscopies

Existing narrowband spectroscopies have their limitations and setbacks. For example, impulsive stimulated thermal scattering (ISTS) can only probe frequencies up to a few GHz [36]. In ISTS, two picosecond pulses are crossed in the material. The resulting optical fringe interference pattern causes more light to be absorbed in regions of constructive interference. This absorption rapidly heats the material. The resulting

thermal expansion in the material launches a counter-propagating acoustic wave. The wavelength of this acoustic wave is determined by the crossing angle between incident beams. A third light beam is used as a time-dependent refractive index probe. These measurements are now performed routinely enough that the acoustic wavelength can readily be tuned by changing the pulse angle.

The picosecond ultrasonic technique used by Morath and Maris (Section 2.4.1) allows access to frequencies as high as 440 GHz [48]. As mentioned, a thin aluminum film absorbs pump light and heats up. The heating causes rapid thermal expansion. The strain induced by the thermal expansion launches a longitudinal phonon (see Figure 2-16). The phonon propagates through the polymer film and is reflected by the sapphire substrate back towards the aluminum film. When the phonon propagates into the aluminum film, there is a strain-induced change in the optical reflectivity of the aluminum film. The reflectivity is probed as a series of time-dependent echoes propagate through the structure.

A weakness of the described picosecond ultrasonic technique is the manner in which narrowband signals of different frequencies (50 GHz to 400 GHz) are generated. Upon excitation by the pump light, acoustic echoes in the aluminum film leak energy into the adjacent polymer layer with each oscillation. The intensity of the energy leaked depends upon the interface reflection coefficient, as described by Equation 2.8. It is this periodic acoustic energy that leaves the aluminum transducer each round-trip that comprises the high frequency wavepacket that propagates through the material[1]. To change the frequency of the narrowband input a transducer of different thickness must be used. This will change the timing between the pulses since they will have to travel through more or less aluminum. There is also a limitation to the envelop size in terms of number of pulses, depending on the impedance matching between the transducer and the sample. If the strain pulse is traveling from medium 1 to medium

[1]For clarification, *wavepacket*, *envelope*, and *pulse train* are all equivalent and are used to describe a group of the individual *pulses*. The pulse frequency is the inverse of the time between the pulses.

2, then good impedance matching at the boundary implies that $z_1 \approx z_2$. This means that $R \approx 0$ and most of the energy is transmitted into medium 2 during the first echo. The implication is that not much of the original energy is available for later echoes. The number of detectable echoes is thus less, decreasing the number of pulses in the envelope (since each echo corresponds to a pulse). Although this is not so much an issue for the Al transducers and polymer films studied (since impedance mismatch is high), it does limit potential sample candidates.

3.1.2 Deathstar GHz Spectroscopy

The Deathstar GHz spectroscopy enables both optical generation and optical detection of broadband and of tunable narrowband acoustic signals. When operating in broadband mode, it allows the time-of-flight experimental determination of the velocity of a propagating phonon. The velocity is modulated by the coupling of acoustic energy with transient density fluctuations and is related to the acoustic modulus as prescribed by Equation 2.6. In narrowband mode, the technique gives direct feedback regarding the dynamic processes and correlation lengths that exist within a material. Specifically, it allows for the determination of the absolute acoustic attenuation coefficient, $\alpha(\omega)$. The narrowband measurement can be methodically repeated at various chosen frequencies (from tens to hundreds of GHz) to map out the frequency-dependent attenuation of the material. The frequency interval was arbitrarily chosen to be 15 GHz, although 1 MHz steps can be achieved.

The advantage of a narrowband acoustic wave is that all of the spectral intensity is focused into a small range of frequencies, which improves the SNR. More importantly, the analysis of the observed signal is more straightforward since there is no superimposed contribution from secondary echoes and ringing within the sample structure, as can happen with broadband measurements. Conventional narrowband spectroscopies, such as the method employed by Morath and Maris, detect at the same transducer

that is originally excited. This results in a convolution of electronic and thermal responses from within the metal. Whereas, the experiments done here use a different sample structure, as will be described in Section 3.3. Excitation occurs at the *frontside* and detection occurs at the *backside*. This allows for confinement of variable excitation effects to the front, ensuring that a purely acoustic signal is observed at the back. Finally, the accessible frequency range of the technique is the most compelling reason for its development, since it fills the low-frequency void left by femtosecond pulse-shaping methods that probe from 1 to 100 THz. This thesis describes the use of the versatile Deathstar GHz technique, which is capable of probing narrowband response at frequencies ranging from the GHz to the THz regime. Note that a smaller subset of frequencies (25 GHz to 175 GHz) is used to study polymer dynamics. Table 3.1 compares the Deathstar GHz spectroscopy to other characterization methods.

3.2 Experimental Design

Following is a description of the technique used, in sufficient depth for the operational user. The various optical components are outlined, along with optimization techniques and experimental conditions found to produce the highest quality measurements. The intricacies of the physics behind the selection of each of the experimental parameters are discussed in further detail by Choi [4].

3.2.1 Deathstar Pulse Shaper

As shown in Figure 3-1, the heart of the experimental setup lies an ultra-fast pulse-shaper known as the *Deathstar* (top left). The Deathstar generates the desired optical pulse train using a multiple reflection technique. Exploiting the same physics as does the picosecond ultrasonic technique discussed earlier, the optical signal is converted into a series of longitudinal phonons by a transducer.

Table 3.1: The strain rates of mechanical characterization tools and accessible frequency ranges of various spectroscopies.

Mechanical Characterization Technique	**Strain Rate** [s^{-1}]	**Strain (Compressive)**	**Accessible Frequency Range**	**Spectroscopic Technique**
Creep [22]	10^{-8} to 10^{-5}			
Quasi-static [22]	10^{-5} to 10^{-1}			
Dynamic Mechanical Analysis [45]	10^{-3} to 10^{-1}	0.001		
Split-Hopkinson Pressure Bar [5]	10^{2} to 10^{4}	0.2→failure		
Gas Gun [23]	10^{5} to 10^{6}	0.1→failure		
	10^{7} **to** 10^{8}	**0.01**	**2 GHz to 1 THz**	**DEATHSTAR**
			<1 GHz	Impulse Stimulated Thermal Scattering [36] (ISTS)
			300 MHz to 30 GHz	Brillouin Light Scattering [9] (BLS)
		0.0001	89 to 320 GHz	Picosecond Ultrasonics (PU) [31]
			>1 THz	Inelastic Neutron Scattering (INS) [3]

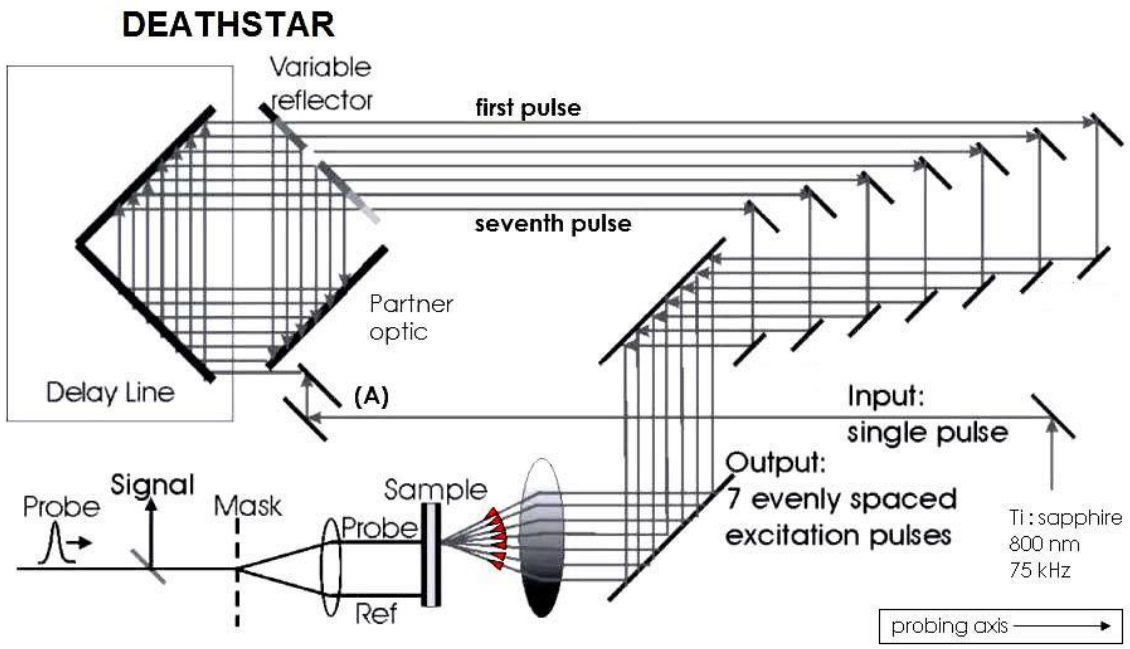

Figure 3-1: Layout of optical benchtop indicating relative positioning of pulse-shaper, sample, and detector. The sample area is shown in more detail in Figure 3-1.

The entire process originates with an amplified Ti:sapphire laser, which outputs 800 nm pulse envelopes at a 75 kHz repetition rate. A laser beam (*Input: single pulse* in Figure 3-1) enters the Deathstar pulse-shaper at (A), subsequently undergoing a series of reflections off the four mirrors shown. One of the mirrors is the *Variable reflector*, which is comprised of a series of seven sections, each with a different transmittance. Thus, with each pass a new pulse is created, as part of the original beam is transmitted through the reflector. The remainder of the beam is reflected back into the pulse-shaper. The transmittances of the individual sections are chosen such that the seven resulting pulses collectively form a Gaussian intensity profile as shown in Figure 3-2. The relative intensities of the seven pulses from left to right are 0.27|0.56|0.85|1.0|0.85|0.56|0.27. Thus, the first pulse has very low intensity (27% of the maximum), which is equal to that of the seventh pulse. Having accumulated power from the previous three reflections and passing through the least absorbing part of the variable reflector, the fourth pulse has the highest optical power (i.e. a

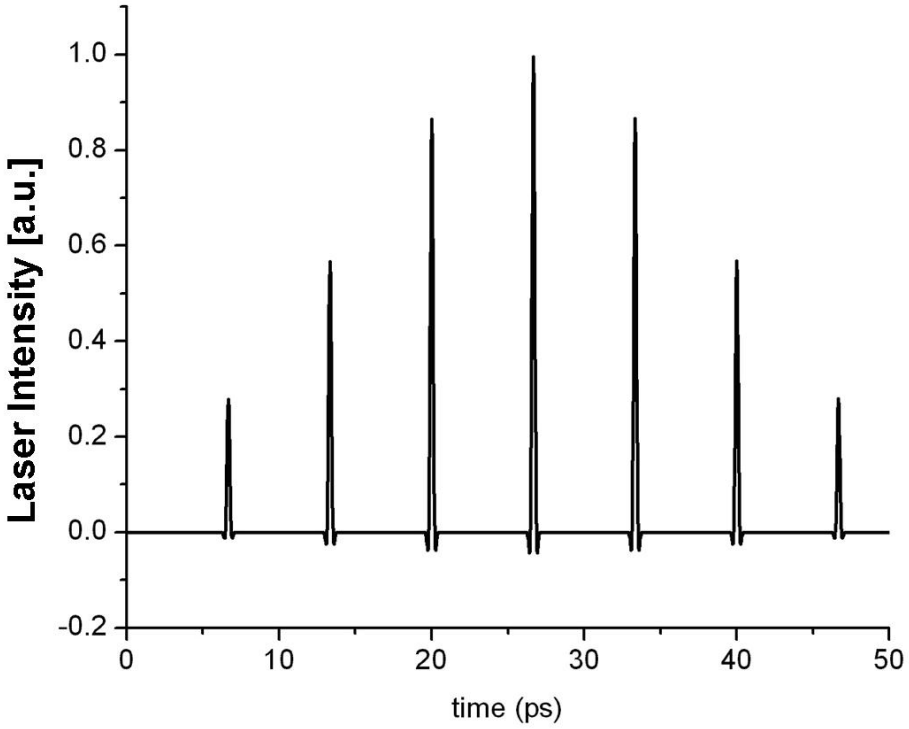

Figure 3-2: This is the theoretical Gaussian output of the pulse shaper. The pulses are 6.67 ps apart, corresponding to a pulse train frequency of 150 GHz. The pulse width is 200 fs (The pulse width refers to the full width at half-maximum of the peak. In this case, pulse width is measured in units of picoseconds because the signal is in the time domain.). The total envelope width is 40 ps. The relative intensities of the seven pulses are: 0.27|0.56|0.85|1.0|0.85|0.56|0.27.

relative intensity of 1.0). The *Partner optic* shown is adjusted to ensure that only one pulse is directed through each of the seven sections.

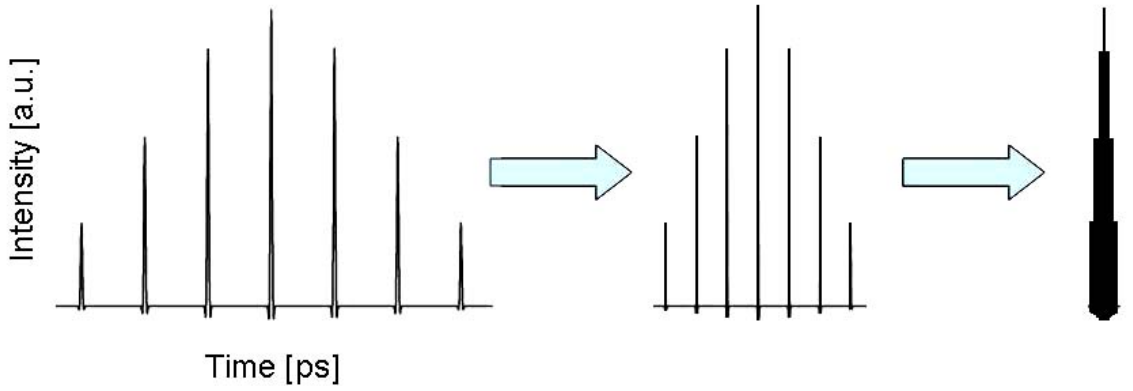

Figure 3-3: The *narrowband* input is a train of seven distinguishable pulses (left). As the frequency of the pulse train is increased, the pulses move closer together (center). The frequency limit is when the finite width of the pulses causes them to merge together. The result is effectively a single pulse, which is a *broadband* input (right).

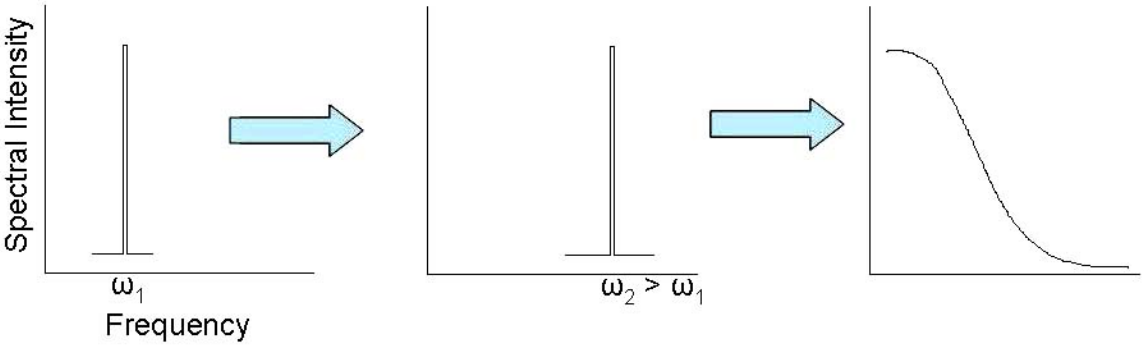

Figure 3-4: The FFT gives the spectral intensity as a function of frequency for the narrowband and broadband inputs. For the narrowband signal, the distribution of resolved frequency components is *narrow*. Whereas, the broadband signal includes a *broad* distribution of Fourier components.

For alignment purposes, the series of seven pulses are individually delayed by increasing their path length. It is easy to see that the pair of mirrors reflecting the first pulse is farthest to the right. The positions of each pair of mirrors is set such that each pulse arrives at the sample at the same time, generating a broadband wavepacket. In other words, the seven pulses are so close together that they appear as one (see Figure 3-3). This mirror placement is done with the *Delay Line* at the

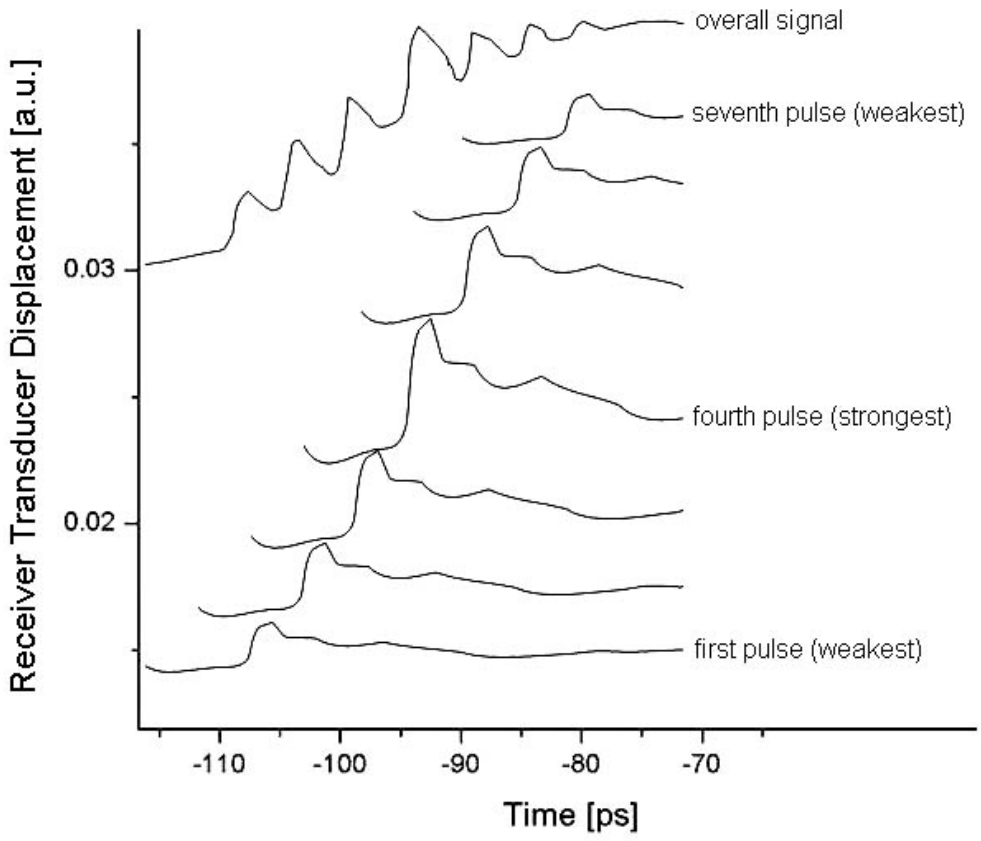

Figure 3-5: This schematic shows the contributions of each of the seven pulses to the overall displacement. One pulse is allowed to hit the sample, while the other six are blocked. The relative displacements induced are indicative of the input pulse amplitudes. The expected Gaussian distribution is seen in the overall signal.

rightmost position of its travel. The delay line is a motorized stage that translates along the figure horizontal. When the delay line is all the way to the right, the seven pulses are closest together. In this case, the pulse train frequency is at its maximum. To optimize the setup, the contribution of each individual pulse to the total signal is maximized sequentially by blocking the remaining six pulses. The contributions of each of the seven pulses to the overall narrowband response is shown in Figure 3-5. The arrival of each pulse is delayed in time, corresponding to its exit from the pulse shaper. Translating the delay line leftward evenly increases the time delay between each of the seven pulses. This spatial distribution determines the pulse train frequency. The maximum frequency of roughly 2 THz occurs when the stage is most right. The frequency limit is when the finite width of the pulses (each 200 fs wide) causes them to merge together. The result is effectively a single pulse, which is a broadband input. The minimum of 2 GHz, occurs when the stage is most left. If a longer delay line were used, then an even lower limit could be achieved. This was deemed unnecessary since the accessible frequencies are sufficiently overlapped with lower frequency spectroscopies.

3.2.2 Phonon Generation and Detection

Once the pulses are separated spatially as desired, they are collimated to a spot size of 120 μm and focused through the sapphire and onto the excitation transducer of the sample assembly. The generation of the acoustic wave occurs at the interface between the sapphire and the aluminum film (see Figure 3-6). The rigorous detail of the physical chemistry implicit within the photoacoustic transduction are beyond the scope of this thesis, but a few points are noted.

The two-temperature model (TTM) describes the dynamic processes that determine the actual profile of the acoustic strain pulse. Through the cascade of events depicted in Figure 3-7, a phonon is created. First, there is optical absorption of the

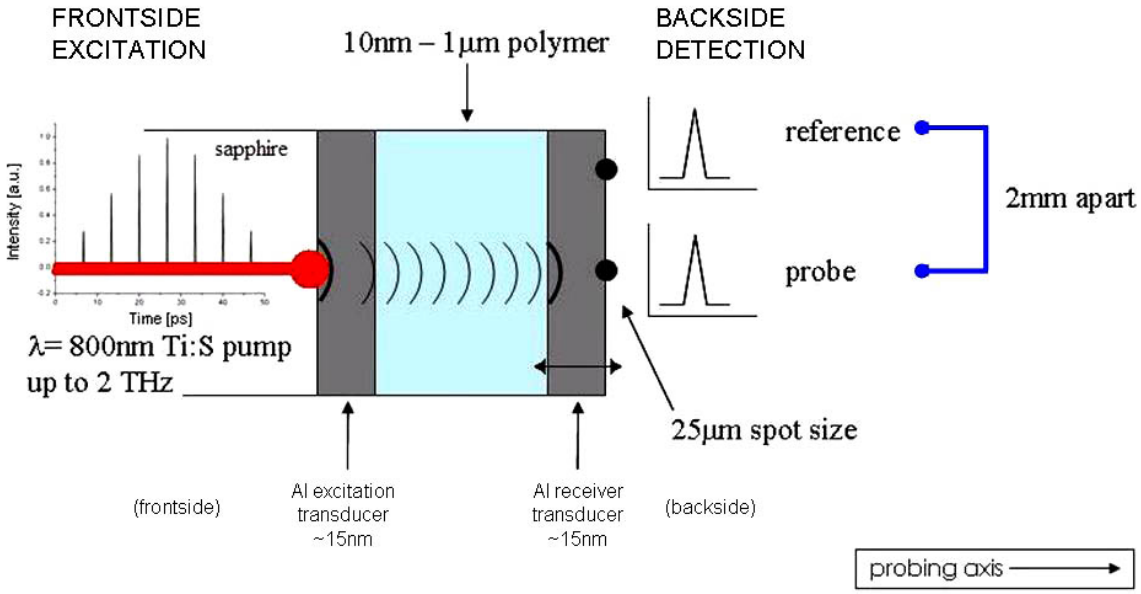

Figure 3-6: Depicted here is the multilayered sample target array, showing interaction with pump and probe beams. The experiment employs *frontside excitation* and *backside detection*.

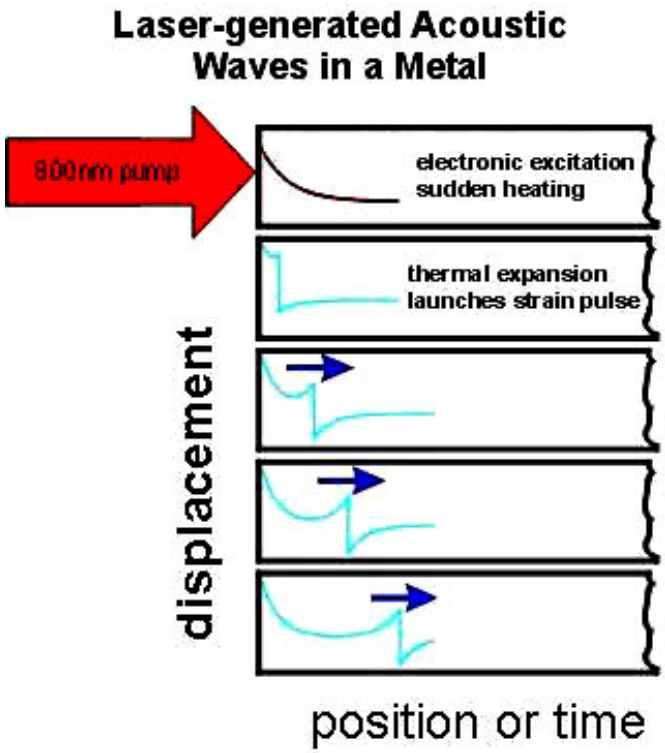

Figure 3-7: Step-by-step progression of an acoustic strain pulse propagating through an aluminum thin film (Nelson Group).

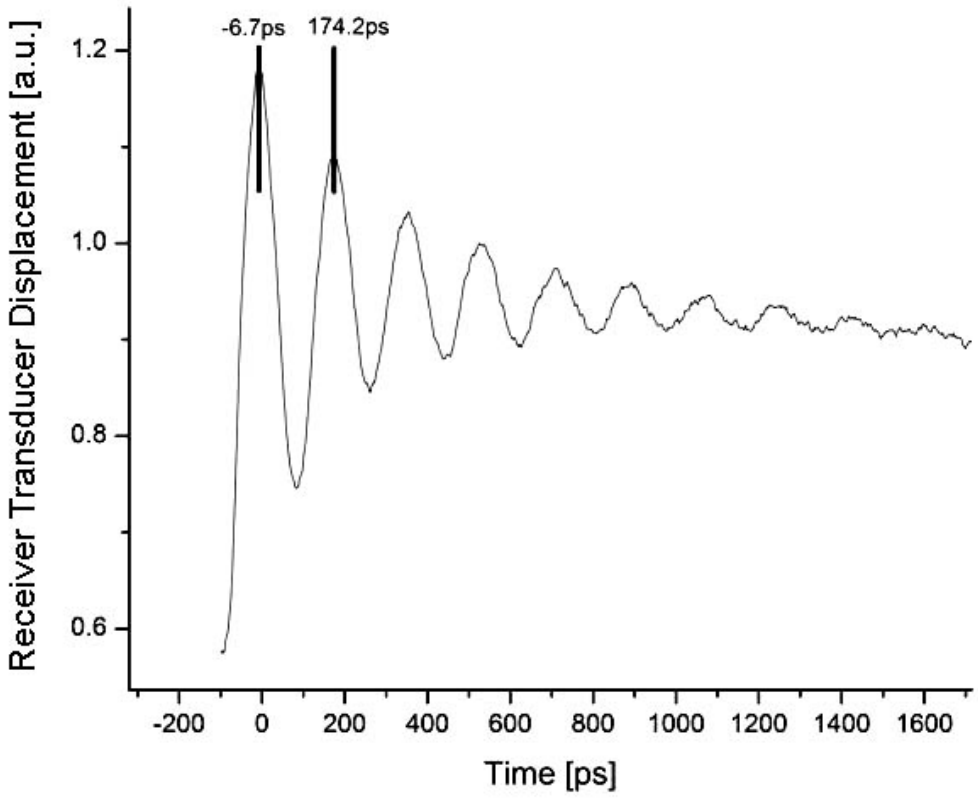

Figure 3-8: Shown is a plot of the typical receiver transducer displacement observed during a broadband investigation of a polymer sample sandwich.

pump light by the aluminum down to its skin depth ($\approx 23\,\mathrm{nm}$). The light excites electronic transitions in the aluminum atoms, which result in *hot electrons*. This thermal energy is coupled into phonon modes of the aluminum lattice as per electron-phonon coupling constants, electronic specific heats, and phonon frequency. Consequently, there is a temperature rise in the aluminum ($\Delta T \approx 100\,\mathrm{K}$). The adjacent sapphire substrate has a much higher thermal conductivity than the polymer, and its volume is about five orders of magnitude larger than that of the polymer. This ensures that all the heat diffuses nearly instantaneously into the sapphire, leaving the polymer nearly isothermal[2]. It is therefore assumed that there is no temperature rise in the polymer film.

From the excitation transducer, the phonon is transmitted across the Al|polymer interface into the polymer film (refer to Section 2.1 for a discussion on propagation across interfaces). The thermal expansion of aluminum transducer is directly responsible for generating the acoustic signal. Accordingly, the transducer needs to have sufficient time to cool down before the next wavepacket arrives. This is why the laser repetition rate is kept at $75\,\mathrm{kHz}$, allowing for $13.3\,\mu\mathrm{s}$ in between wavepackets for the Al to reach thermal equilibrium.

The acoustic energy then travels through the polymer and displaces the receiver transducer with direction and magnitude proportional to the incident strain pulse. The amplitude of the strain pulse is determined by the optical power of the pump laser beam (see Section 4.1). This local perturbation of the receiver transducer is detected interferometrically from the backside by the *reference beam* and *probe beam* (Figure 3-6). Because the two arms of this interferometer travel the same path on the benchtop, noise due to air density fluctuation and table vibrations are minimized. The interferometer should be enclosed by curtains since ambient air currents can affect the signal. This is particularly important during cryogenic experiments since

[2]Experiments using glass cover slips instead of sapphire substrates were unsuccessful because of thermal buildup issues.

there can be suboptimal SNR to begin with[3]. The reference beam is offset by about two millimeters. The ensures that diverging (i.e. shear) acoustic energy cannot reach the reference beam during the picosecond timescale over which the experiment takes place. Light for the interferometer is picked off the pump beam near the laser output (i.e. before pulse-shaping) and frequency-doubled to 398 nm. Both the probe and reference beams are reflected back (i.e. toward the right in the figure) by the receiver transducer. Because of the interferometer configuration this particular setup is said to be operating in *reflection mode*. The probe is collinear with the incoming excitation beam that hits the assembly on the front-side. The pump and the probe beams must be focused such that they cross at the right time and in the same plane as the sample. This is done by observing optical diffraction patterns and using a pinhole to verify spatial alignment. When the reference and probe beams are recombined, an observable diffraction pattern is created. A photodiode and a lock-in amplifier detect and display the *signal*[4], which indicates receiver transducer displacement as a function of time.

This signal varies temporally since the propagating strain pulse causes variable receiver transducer displacement. This signal is the directly observed parameter for both the narrowband and broadband investigations. It is a function of the coupling of incident acoustic energy with the polymer sample. To observe the temporal evolution of the signal another delay line is used. The signal is recorded at every point while the stage is translated. The speed with which the stage moves and the spatial range it covers determine the resolution and temporal window of the scan (this in turn determines how long it actually takes to finish the scan). A plot of the typical signal observed for a sandwich structure is shown in Figure 3-8. The delay line is

[3]In cryogenic experiments, there is steady liquid helium flow into the sample cryostat to maintain a constant temperature. The flow of the helium itself can affect the interferometrically detected signal because of transient density fluctuations. Accordingly, special care is required in alignment, and SNR should be closely monitored.

[4]The signal will refer to the observed receiver transducer displacement (or intensity) vs. time.

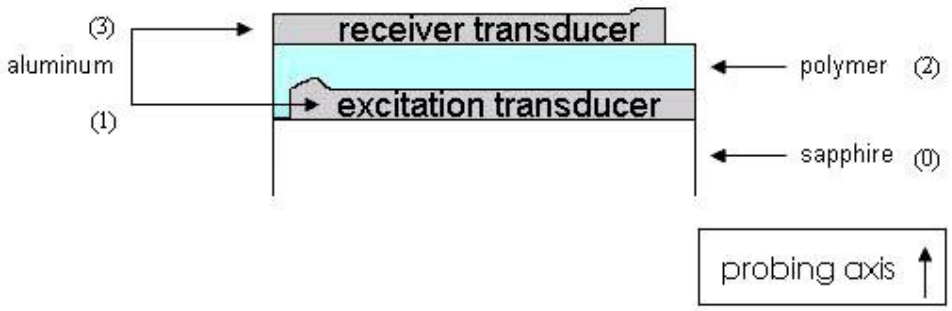

Figure 3-9: The sample assembly includes a single crystal sapphire substrate (0), an aluminum excitation transducer (1), a polymer thin film (2), and an aluminum receiver transducer (3). The aluminum films are incomplete at the edges because of clamps used to hold the assembly in place during deposition. The sapphire substrate is about 6 mm thick. The numbers indicate the order in which the layers are deposited.

moved to a point at which the signal intensity is relatively high (in this case, to $t = -6.7\,\text{ps}$). This corresponds to the point of maximum displacement of the receiver transducer (i.e. maximum strain). Essentially, the strain pulse is pushing out the receiver transducer, as indicated by increasing signal intensity up to $t = -6.7\,\text{ps}$. After reaching the maximum strain, the signal begins to decrease as the receiver transducer returns to its original position. This entire set of oscillations (i.e. the whole signal) occurs with every incoming wavepacket, which arrives with a frequency of 75 kHz (the repetition rate of the laser). While the delay stage is at $t = -6.7\,\text{ps}$, the phase mask is translated perpendicular to the beam path to optimize the signal intensity. The phase mask is the main optic comprising the interferometer, and its operation is described in Section 4.1. The sample position also affects the signal intensity and must be adjusted accordingly. The mirrors and lenses also require appropriate placement. This must be optimized prior to measurement and whenever the sample is changed. An in-depth discussion of the interferometer design is given by Glorieux [16].

3.3 Sample Assembly Preparation

The sample assembly is a multilayered sandwich structure, as shown in Figure 3-9. The sandwich is supported by a sapphire substrate. Sapphire is used because it is an effective heat sink for the heated aluminum excitation transducer. It is also transparent in the visible and does not absorb much pump light. Sapphire is very rigid as well, effectively reflecting the entire strain pulse back into the aluminum. The target polymer film thickness should be determined based upon (1) the frequency of the incident acoustic pulse and (2) the thickness of the receiver transducer. If the polymer film is too thick, then signal is poor because acoustic energy is damped too strongly as the wavepacket traverses the sandwich. Essentially, the $e^{-\alpha x}$ term in Equation 2.5 becomes smaller with increasing thickness (x). Recall also that attenuation increases for higher frequencies ($\alpha \sim \omega^2$), making the signal even less. Thicker samples are thus ill-suited for frequency-dependent narrowband studies and should be used only for broadband investigation. However, thin samples also have limitations. Low frequency signals become convoluted when the round trip time is similar to the period of the acoustic echoes generated by the receiver transducer. The ringing of the transducer then clouds the true acoustic response of the polymer. This can be resolved by changing the thickness of either the polymer layer or the receiver transducer.

3.3.1 Transducer Fabrication

The first layer is the excitation transducer, an aluminum film deposited using a CVC Thermal Evaporator under a vacuum of 10^{-6} torr. An alternative method is electron beam deposition. Because it offered only comparable film surface quality (i.e. roughness) as indicated by atomic force microscopy (AFM) and was considerably less convenient, it was not pursued. The target thickness of the aluminum excitation layer is 15 nm, a value calculated theoretically and empirically found to be optimal.

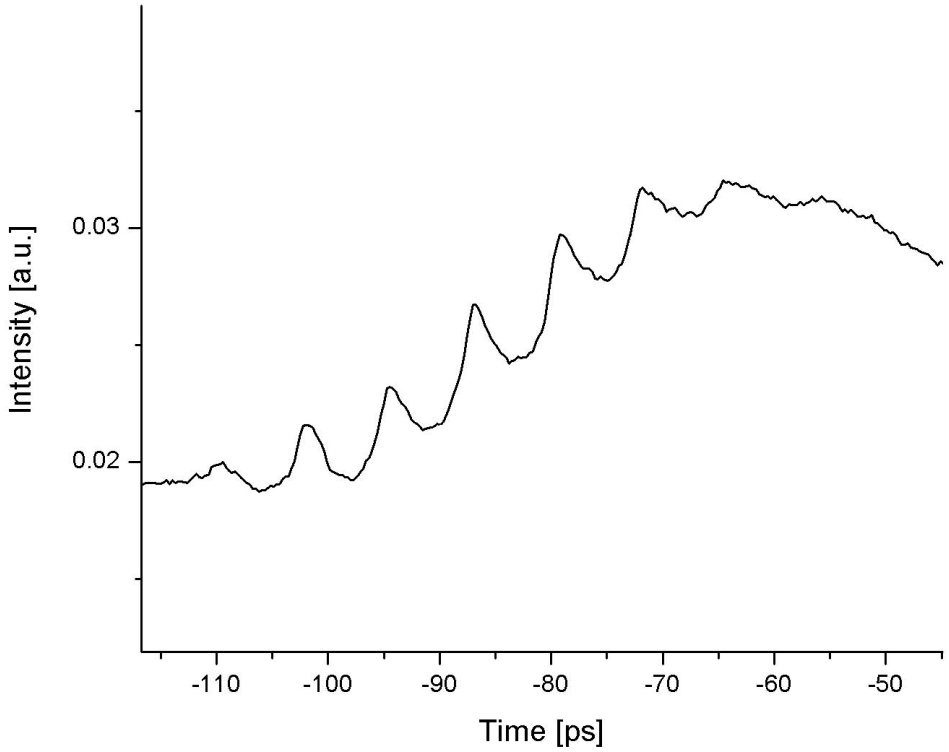

Figure 3-10: The strong periodic response observed when a 22.9 nm aluminum film is driven at its resonance frequency of 140 GHz.

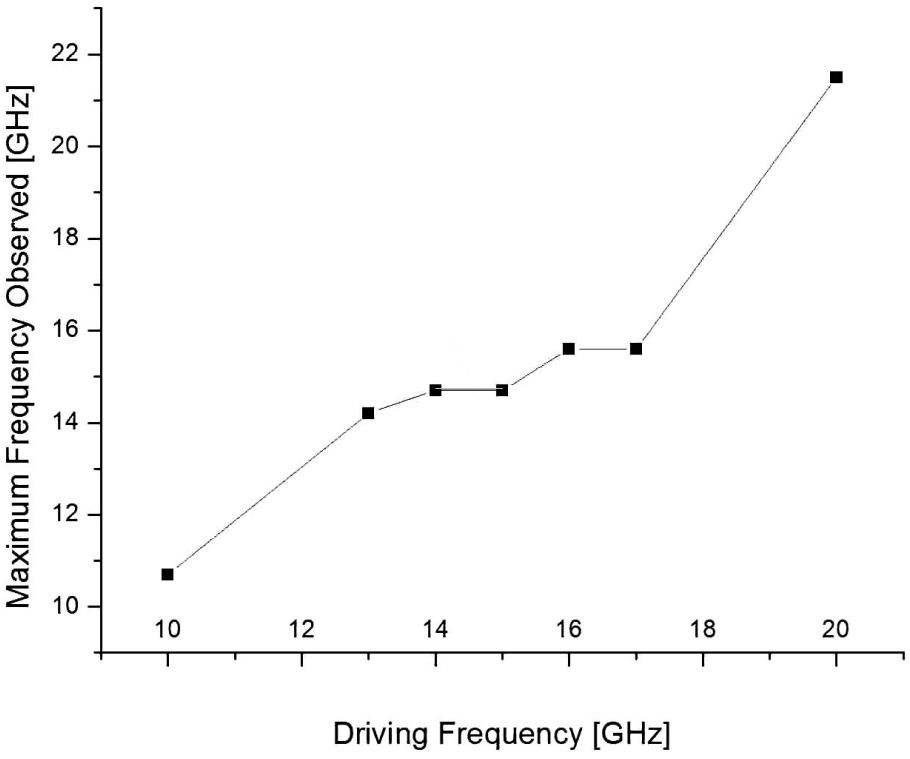

Figure 3-11: When this multilayered sandwich is driven anywhere near its resonance frequency, the highest spectral intensity is observed at the resonance frequency ($\omega_{resonance} \approx 15\,\mathrm{GHz}$).

One consideration is that the aluminum layer should be thick enough that it absorbs sufficient pump light. The absorption is determined by the optical penetration depth or absorption length ($\approx 23\,\text{nm}$ at $\lambda = 800\,\text{nm}$ [6]). A thicker transducer will continue absorbing more pump light until a thickness equal to the penetration depth is reached. However, a thicker film is not able to expand as rapidly as a thin one, thus limiting the acoustic bandwidth. The bandwidth is the maximum phonon frequency generated by the transducer. While a thinner film would increase the upper frequency limit, the signal intensity would diminish.

The thickness of the metal transducer film can be verified using several characterization methods. A quartz crystal resonator on the deposition apparatus was found to be unreliable since the angle at which the detector faces influences the portion of the variable vapor distribution observed[5]. This was circumvented by including a bare silicon wafer chip of known native oxide thickness with the sapphire window to be coated. The thickness of the resultant Al film on the Si wafer was measured via ellipsometer with a $\pm 0.1\,\text{nm}$ accuracy.

Another method of determining the thickness of a bare transducer (i.e. aluminum monolayer) on sapphire is by probing resonance behavior. The physical premise of resonance-based thickness determination is that the probing wavelength is on the order of the feature size, which in this case is the film thickness. Recall that when $qd \approx 1$ there is strong wave interaction with features of size d within the medium. The acoustic wave in this case interacts strongly with entire thickness of the film because there are no other heterogeneities. There is a characteristic thickness-dependent frequency at which the incoming pulse train coherently and constructively interferes with the generated acoustic echoes. As shown by the periodic stream of oscillations in Figure 3-10, driving the film at its resonance frequency induces a strong constructive

[5]In general, this can be a reliable method if the quartz crystal is in close proximity to the deposition substrate. However, the particular apparatus used at the MIT Exploratory Materials Laboratory did not permit this configuration.

response. The driving frequency is iteratively chosen until these peaks are as clearly defined as possible. A pair of five minute scans is all that is required for resonance-based thickness determination. From the resonance frequency, the thickness (d) can be determined to Angstrom-level accuracy using the expression:

$$d = \frac{c_{acoustic}}{2\omega_{resonance}} \tag{3.1}$$

where $\omega_{resonance}$ is the resonance frequency. For example, the pulse frequency that generates the signal observed in Figure 3-10 is 140 GHz, corresponding to an acoustically determined thickness of 22.9 nm (assuming c_{Al}=6420 m/s [31]). This is in excellent agreement with the ellipsometrically determined thickness of 23.10 nm as well as that measured by mechanical stylus profilometry. In this particular case, each frequency increment of 1 GHz corresponds to a change in calculated thickness of ≈ 0.2 nm, thus defining the resolution of the method. Whatever variation observed is predominantly attributed to the assumed acoustic velocity of the aluminum film, which is known to be different for the bulk and thin film geometries. Depending of the crystal texture axis of the polycrystalline aluminum deposited, the speed of sound may vary anywhere from 6284 m/s to 6473 m/s [18].

Figure 3-11 shows that the strongest frequency component observed for a different sample is the resonance frequency. Even when the assembly is driven anywhere from 13 GHz to 17 GHz, a few GHz in either direction from its resonance frequency of 15 GHz, the characteristic resonance frequency is the dominant response (i.e. the frequency with the maximum observed spectral intensity). This shows how strong and reliable the acoustic resonance response in a material really is. Accordingly, resonance behavior is a rapid, non-destructive, and an extremely accurate method of determining transducer film thickness.

Table 3.2: Specifications of the polymers used in the experiment.

Polymer	**Source**	$\overline{M}_{\mathrm{w}}$ $\left[\frac{\mathrm{g}}{\mathrm{mol}}\right]$	**PDI**
a-PS	Sigma-Aldrich	575,000	1.06
a-PMMA	Polymer Laboratories	518,900	1.03

Table 3.3: An overview of the spin-coating parameters used to achieve the various polymer film thicknesses along with a summary of the thickness compositions of the sandwich structure. The sandwich structure is depicted in Figure 3-9.

Polymer	**Solution Concentration [wt.%]**	**Spin Rate [RPM]**	**Excitation Transducer [nm]**	**Polymer Film [nm]**	**Receiver Transducer [nm]**
a-PS	0.5	3000	11.5	22.5	23.9
a-PMMA	0.5	3000	23.1	19	13.8
a-PMMA	0.5	2000	25.7	32	23.7
a-PMMA	1.0	2000	25.7	77	23.7
a-PMMA	3.0	2000	8.3	215	14.2

3.3.2 Polymer Thin Film Fabrication

Specifications of the polymers used in the experiment are given in Table 3.2. Morath and Maris found no differences in acoustic attenuation for a-PMMA of two different molecular weights ($\overline{M}_{\mathrm{w}}$=496,000 g/mol and 950,000 g/mol). Accordingly, it is assumed that the molecular weights chosen do not influence the results of the current study. Polydispersity index (PDI) is the ratio of the weight-averaged molecular weight ($\overline{M}_{\mathrm{w}} = \frac{\Sigma M_i N_i}{\Sigma N_i}$) to the number-averaged molecular weight ($\overline{M}_{\mathrm{n}} = \frac{\Sigma N_i M_i^2}{\Sigma N_i M_i}$). Here, N_i is the number of individual polymer molecules of molecular weight M_i in the bulk sample [2].

Either a-PS or a-PMMA was spin-coated onto the aluminum-coated sapphire substrate (sapphire|Al| ← polymer). A summary of the thicknesses of the samples used in this investigation, along with spin-coating parameters, are presented in Table 3.3. The polymer film thickness is a function of the solvent used, the concentration of the polymer solution, and the rotational speed of the spin-coater. For PS and PMMA, the

solvent of choice is found to be toluene because it readily dissolves both polymers and has a high boiling point (111 °C [30]), so it does not volatilize too rapidly. The spin time for all the samples was one minute, with thirty seconds allowed for deceleration to a complete stop. To remove the solvent, the films are baked at 90 °C, below the boiling point of toluene. This is to make sure that residual toluene in the film does not boil. Otherwise, bubbles would form in the polymer. To increase thickness uniformity, the films can be annealed around the T_g of the polymer, but this was not found to be necessary after investigation of surface roughness by AFM. The spin-coating apparatus used can make a significant difference in thickness uniformity. Films were initially coated using the Specialty Coating Systems G3P-8 Spincoat. This particular model required a constant nitrogen purge in the spinning chamber. The result was very large film thickness variation along the radius due to the air currents caused by the nitrogen flow. To resolve this, a spin coater from Laurel Technologies, the WS400-A 6NPP Lite, was employed since it operates without needing external air flow.

Thickness uniformity and accurate measurement of the polymer film thickness are extremely important in this experiment since either thickness or acoustic velocity are required to effectively interpret the time-resolved signal. Profilometry and ellipsometry can be used to measure the polymer film thickness, just as they are used for measuring the aluminum film thickness. By scratching the polymer film with a razor blade and taking a mechanical stylus profilometry scan, the thickness profile can be measured. Profilometry is best suited for a polymer monolayer on a hard substrate, such as Si or sapphire. This technique, while reasonably accurate (± 1 nm), is not preferred since it locally damages the film. Ellipsometry can also be used to evaluate the thickness of a polymer film on a substrate such as Si, but becomes very difficult for transparent substrates such as sapphire. The modeling required to fit thickness has been known to be increasingly inaccurate for polymer films below ≈ 40 nm thick

[31]. While time-of-flight (i.e. resonance) works well for single films as shown for Al in Section 3.3.1, the impedance mismatch issues at the film interfaces in a sandwich structure complicate reflection and transmission of the acoustic wave. For this reason, a computational propagation model is used. The model keeps track of the contributions to the total signal of partial reflections and partial transmissions of the strain pulse occurring at each of the boundaries within the multilayered structure. To determine the thickness, the theoretical response is fit to the observed response. The details of the model are discussed in Section 4.2.

3.3.3 Sample Considerations

Thin polymer films can exhibit a glass transition dependent upon film geometry (e.g. free-standing films, substrate-supported, or sandwiched between sub- and superstrates). Studies by Sills *et al.* indicate that for polystyrene films thicker than about 250 nm supported by a silicon substrate, the contributions from regions near the surface are minimal. The shear-modulated scanning force microscopy they perform probes the bulk response. For thinner films, there is a region of reduced mobility near the interface between the polymer and the substrate [41]. The thickness dependence of T_α and T_β is discussed in Section 2.4.3.

The treatment of the aluminum layers adjacent to the polymer is discussed by Fukao *et al.* [15]. The sandwich structure they use is similar to the one used for this thesis. The only difference is that they use a glass substrate instead of sapphire (i.e. glass|Al|polymer|Al|air). It is presumed that the mechanical constraint offered by glass and sapphire is comparable. The bottom Al layer is a rigid support since it lies between the polymer and the glass substrate. However, the top Al layer must be treated differently. In one of their dielectric relaxation measurements, they heat the entire structure to 415 K. At this temperature, some deformation is evident in the top Al layer under an optical microscope. Fukao speculates that this is caused

by the stresses imposed from the thermal expansion of the underlying polymer layer. The author does not mention the thickness of the Al layer. It may be possible that such deformation would only happen for very thin Al. If it is known below what critical thickness this effect is observed, then the problem can be obviated by coating a thicker receiver transducer. Moreover, if the polymer films were not of uniform thickness to begin with, then the Al coating would be rough even before heating.

For the Deathstar experiment, these "wrinkles" would not matter even if they were to exist. The lock-in amplifier is reset once the sample is equilibrated at the target temperature. Thus, even if there were some thickness change caused by the heating, the interferometric probes would be recalibrated to observe the newly defined (and static) state of the receiver transducer. In a sense, the lock-in amplifier takes into account changes in the sandwich structure. Of course, if the deformation were to vary temporally during the course of the scan (i.e. it were not static), then it would affect the signal. Since the entire scan is completed while the sample is at thermal equilibrium in an insulated cryostat, there should be no dynamic change in surface texture. Accordingly, the signal observed is then solely from pump light induced displacement, and it is not affected by the roughness of the receiver transducer.

Comparison of ellipsometry and dielectric measurements by Fukao and Miyamoto indicate that the PS glass transition temperature is the same with and without the top Al layer [13]. The PS film thicknesses they study range from 6 nm to 489 nm. This implies that the top Al layer does not affect polymer dynamics, an important point since the current investigation effectively uses the same sandwich structure.

Chapter 4

Acoustic Characterization of PS and PMMA

The Deathstar GHz spectroscopic technique has previously been used to study amorphous silica [4], but the current study is the first to examine polymers. Initial investigations set out largely to be proof-of-concept, showing that the technique is applicable to polymers. The experimental parameters for successfully probing polymeric materials were previously unknown. Experiments have focused upon measuring the acoustic velocity and phonon attenuation in two simply polymers. PS and PMMA were selected because they are typical (and simple) glassy amorphous polymers. Both materials have been extensively studied by several dynamic mechanical methods and various spectroscopies. Accordingly, much is already known about their absorption of mechanical energy as a function of frequency and temperature. As outlined in Chapter Two, dynamic mechanical and spectroscopic techniques probe velocity and attenuation in several different frequency regimes. Sometimes there is overlap with the frequencies accessed by the Deathstar GHz spectroscopy.

The frequency-dependent attenuation provides great insight about how energy is lost into a material. The goal of the current investigation is to be able to accurately

measure the acoustic attenuation $\alpha(\omega$=55 GHz to 160 GHz). It is a longer term goal to relate the attenuation at high frequencies to a material-specific energy dissipation mechanism(s). Knowing the molecular reasons for damping will allow for materials design to exploit these loss mechanisms. Potential applications include soldier armor and blast protection for vehicles and buildings. PS and PMMA, along with the entire class of amorphous polymers, could serve as platforms for energy loss in more complex nanocomposite systems. Thus, attempting to better understand the loss dynamics of homopolymers is a natural starting point for further study.

This chapter discusses the strain rates reached in the experiment, along with a basic phonon propagation model. This model is used in the broadband investigation to measure the temperature dependence of the acoustic velocity. Finally, the narrowband study is presented. This includes the calculation of phonon attenuation as a function of frequency.

4.1 Strain Rate Calculation

The strain rate is a measure of how fast a sample is deformed. In general, materials behave differently depending on by how much and how quickly they are deformed. The strain rate is not related to the acoustic frequency the way strain rate is related to oscillation frequency in dynamic mechanical testing. The acoustic or phonon frequency discussed throughout is that of the narrowband pulse train. Tunable narrowband phonons are what comprise the high frequency wavepacket. The time between the pulses is the inverse of the acoustic frequency.

A broadband experiment is done for the strain rate calculation. Recall that the broadband signal is a single pulse, which displaces the transducer in one continuous motion. The amount of this displacement and how fast it happens, determines the strain rate.

The engineering strain for uniform deformation over an initial gauge length (l_0) is the ratio of the extension or displacement (Δl) divided by the initial gauge length of the sample:

$$\epsilon = \frac{l_f - l_o}{l_0} = \frac{\Delta l}{l_0} \tag{4.1}$$

The strain rate is given by:

$$\dot{\epsilon} = \frac{d\epsilon}{dt} = \frac{d}{dt}\left(\frac{l_f - l_0}{l_0}\right) = \frac{1}{l_0}\frac{dl}{dt} \tag{4.2}$$

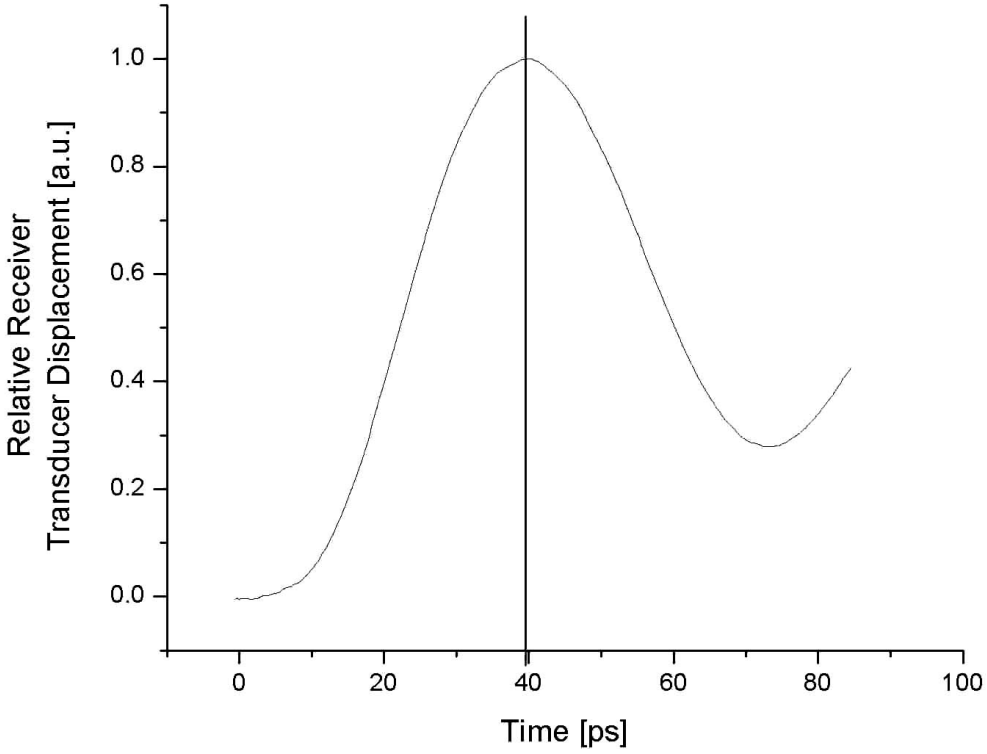

Figure 4-1: The broadband response of a 19 nm PMMA sample. Only the first echo is shown here (see Figure 4-5). The strain is determined by calibrating the relative receiver transducer displacement. The strain rate is then calculated based upon the time taken to reach maximum displacement (≈ 40 ps).

In our experiment, l_0 is simply the polymer film thickness. It is the deformation (i.e. displacement) that needs to somehow be measured absolutely. This deformation

is monitored by the displacement of the receiver transducer (recall from Figure 3-6 that this is the upper aluminum layer). The only probe of this movement is the interferometer, whose function is briefly described in Section 3.2.2. Glorieux developed the interferometer and discusses its intricacies and the details of what the lock-in amplifier is actually measuring [16]. The physical displacement of the receiver transducer occurs when a strain pulse is propagated through the sandwich structure. Since the interferometer observes only the receiver transducer, this is where the effect of the strain pulse is observed. The only variable that controls the amount of this displacement is the intensity of the incident pump beam. The higher the pump power, the greater the magnitude of the strain pulse and the larger the transducer displacement.

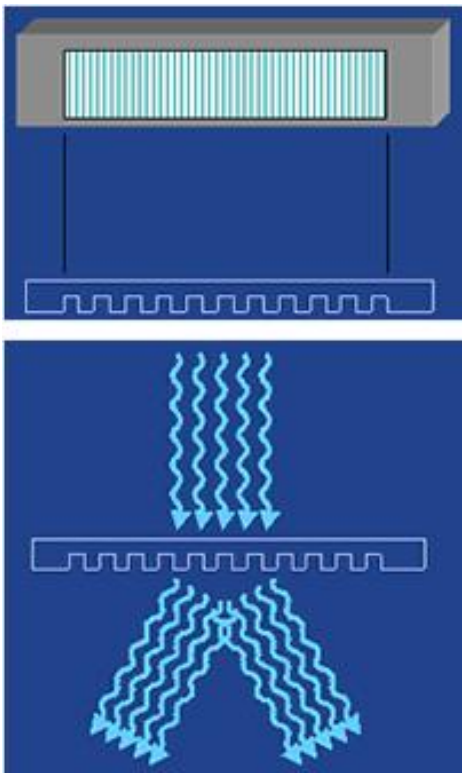

Figure 4-2: A phase mask is a period grating of grooves etched into silica (top). An incoming light beam is diffracted into two outgoing beams (bottom).

The optical path delay between the probe and reference beams is ξ and has units of length. Signal intensity is measured on the lock-in amplifier and is maximum ($V_{\max}$)

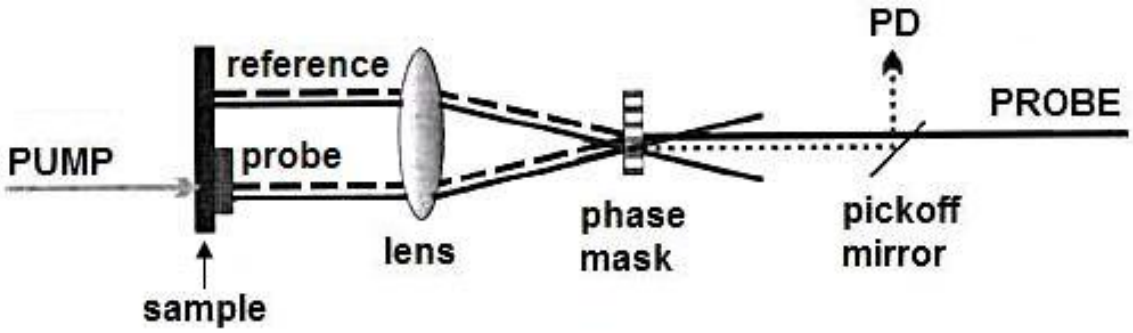

Figure 4-3: The probe and reference arms of the interferometer are generated and recombined at the phase mask [16].

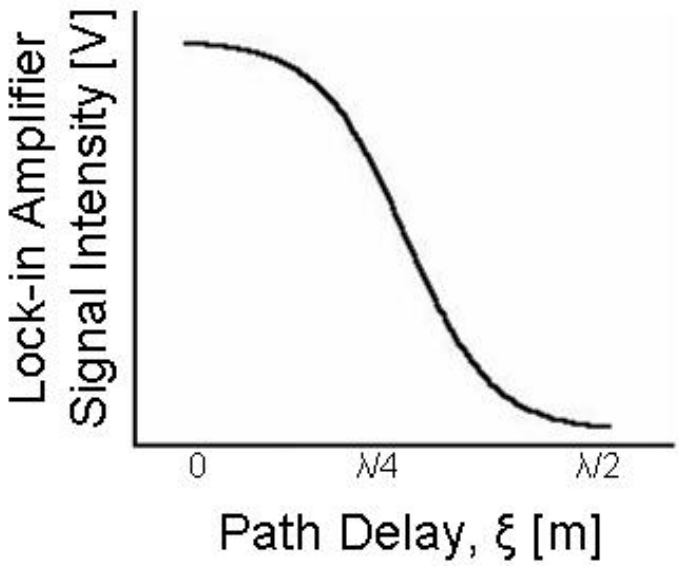

Figure 4-4: The variation of signal intensity with optical path delay between the probe and reference arms is shown to indicate that interferometer sensitivity (i.e. the slope of the curve shown) is greatest half-way between the maximum and minimum signal intensity.

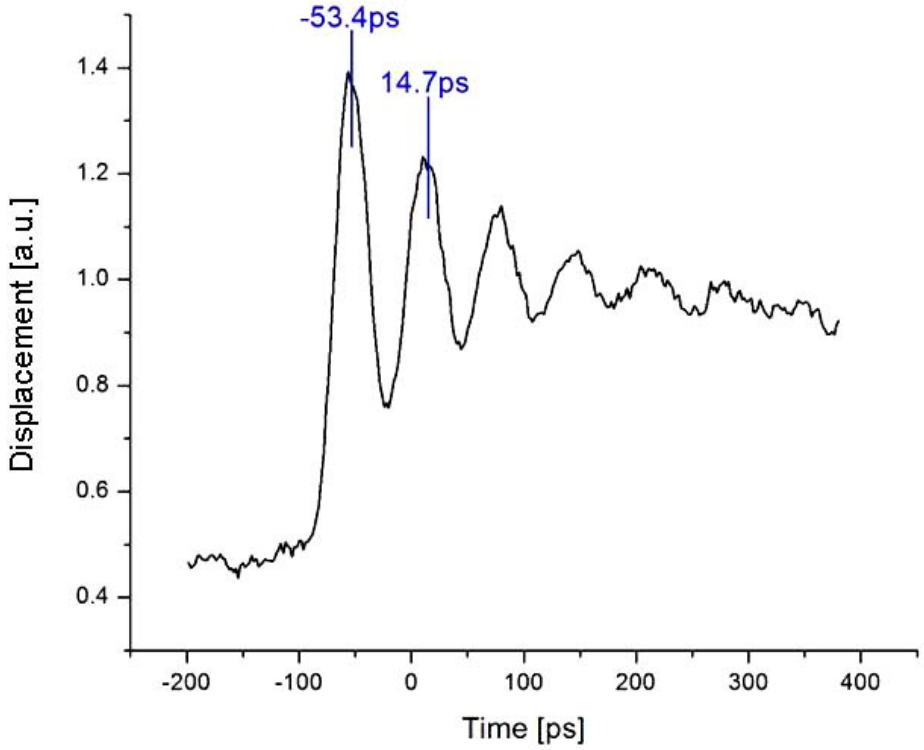

Figure 4-5: The broadband response of a 19 nm PMMA sample. The wide temporal window shows several echoes within the sandwich structure. The peak-to-peak time is used to calculate the resonance frequency shown in Figure 4-6. The pump power is 10 mW. The displacement is that of the receiver transducer and the time is relative (i.e. $t = 0$ is arbitrary).

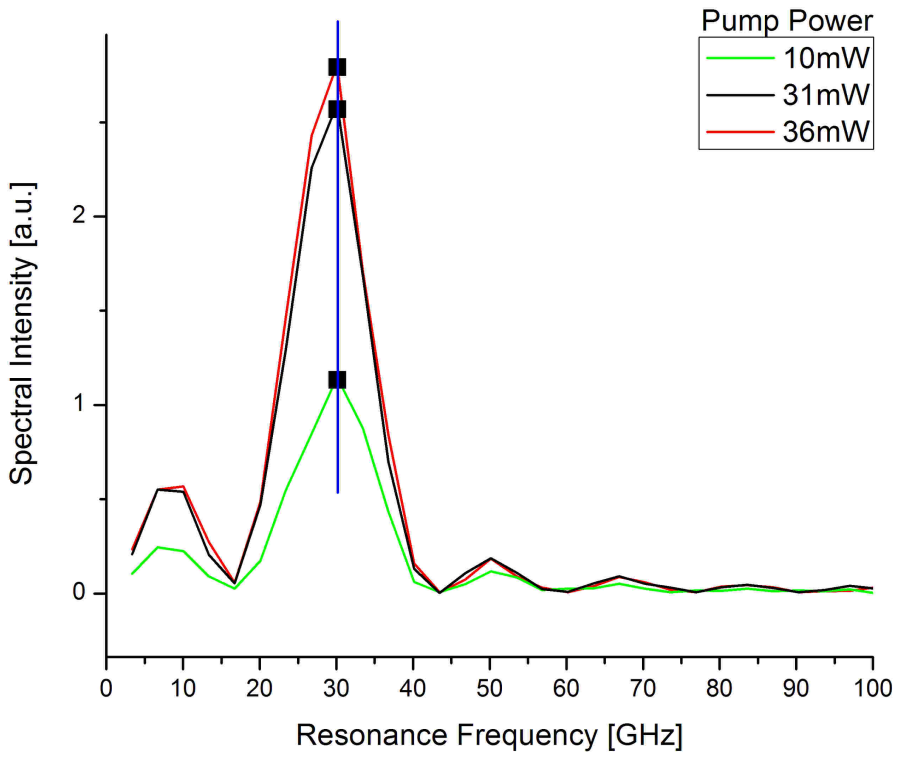

Figure 4-6: The pump power dictates the magnitude of the strain in the sample. The resonance frequency is 30.1 GHz regardless of the pump power for this 19 nm thick PMMA sample assembly at 298 K.

when the reference and probe beams are in phase and constructively interfere (i.e. ξ is 0, λ, 2λ ...). $V_{\min}$ occurs when the reference and probe beams are out of phase and destructively interfere (i.e. ξ is $\lambda/2$, $3\lambda/2$ ...). Recall that the wavelength of the probe beam is 398 nm. The optical path delay then determines whether the two arms of the interferometer are in or out of phase. The phase is modulated by the phase mask, which is a surface relief grating etched in fused silica. Incoming light is diffracted into two outgoing beams as shown in Figure 4-2. Such a phase mask is placed in the path of the beam labeled *Probe*, which gets split into two beams–the probe and the reference (see Figure 4-3). The two arms of the interferometer are focused to different spots on the sample, as described in Section 3.2.2. They are reflected off the sample and once again pass through the phase mask. On this return trip, the beams diffract through the grating. This diffraction is observed by a photodetector. The phase difference between the reference and probe beams changes as the phase mask is translated perpendicular to the path of the light. This is because the two arms travel through more or less silica, thus changing the path delay. The lock-in amplifier sensitivity can be thought of as the amount of change in the measured intensity in relation to the change in optical path delay between the two interferometer arms. The signal measured by the lock-in is the direct observable in both the broadband and narrowband investigations. Figure 4-4 depicts how the signal intensity varies with path delay. Sensitivity is the slope of this curve, $\frac{dV_{\text{sig}}}{d\xi}$ and is maximized when the signal level is half-way between $V_{\max}$ and $V_{\min}$. This is summarized in the following expression:

$$\left|\frac{dV_{\text{sig}}}{d\xi}\right|_{\max} = (V_{\max} - V_{\min})\,\frac{\pi}{\lambda} \tag{4.3}$$

To calculate the sensitivity, only the maximum and minimum values of signal intensity are required. The entire strain calibration was done for the 266.2 nm PS sample. The maximum lock-in reading was 26 nA while the minimum value was 1.2 nA. Using the sensitivity formula (Equation 4.3), $\left|\frac{dV_{\text{sig}}}{d\xi}\right|_{\max} = 0.2\,\frac{\text{nA}}{\text{nm}}$. The signal intensity at maxi-

mum sensitivity is 180 pA. The displacement of the receiver transducer is calculated as shown:

$$\frac{180\,\text{pA}}{0.2\,\frac{\text{nA}}{\text{nm}}} = 0.9\,\text{nm} \pm 10\% \tag{4.4}$$

This corresponds to a mechanical strain of $\epsilon = \frac{0.9\,\text{nm}}{266.2\,\text{nm}} \approx 0.003$. The displacement occurs over 170 ps, which gives a strain rate of roughly $2\times10^7\,\text{s}^{-1}$. The same calibration is done for the 22.5 nm PS film, where $\epsilon = 0.01$ and $\dot{\epsilon} = 3\times10^7\,\text{s}^{-1}$. The displacement of the receiver transducer is assumed to be largely caused by expansion of the polymer film within the sandwich structure. The reason for this is that for a given stress, the material with the lowest Young's modulus will strain the most since $\epsilon = \sigma/E$. The Young's moduli of sapphire, aluminum, and polystyrene at room temperature are 335 GPa, 70 GPa, and 5.5 GPa, respectively [22]. Since the Young's modulus of PS is significantly lower that those of aluminum and sapphire, the majority of the observed strain is actually caused by the PS.

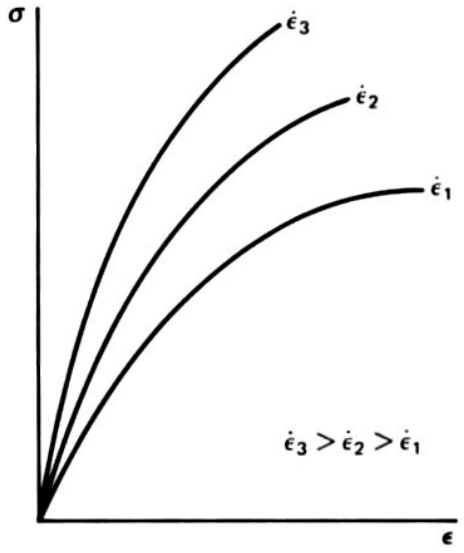

Figure 4-7: The Young's modulus is the proportionality constant between the imposed stress (σ) and the resulting strain (ϵ). The modulus (i.e. slope of the curve) increases with increasing strain rate ($\dot{\epsilon}_i$) [22].

It is well known that a strain rate dependence is observed for the Young's modulus

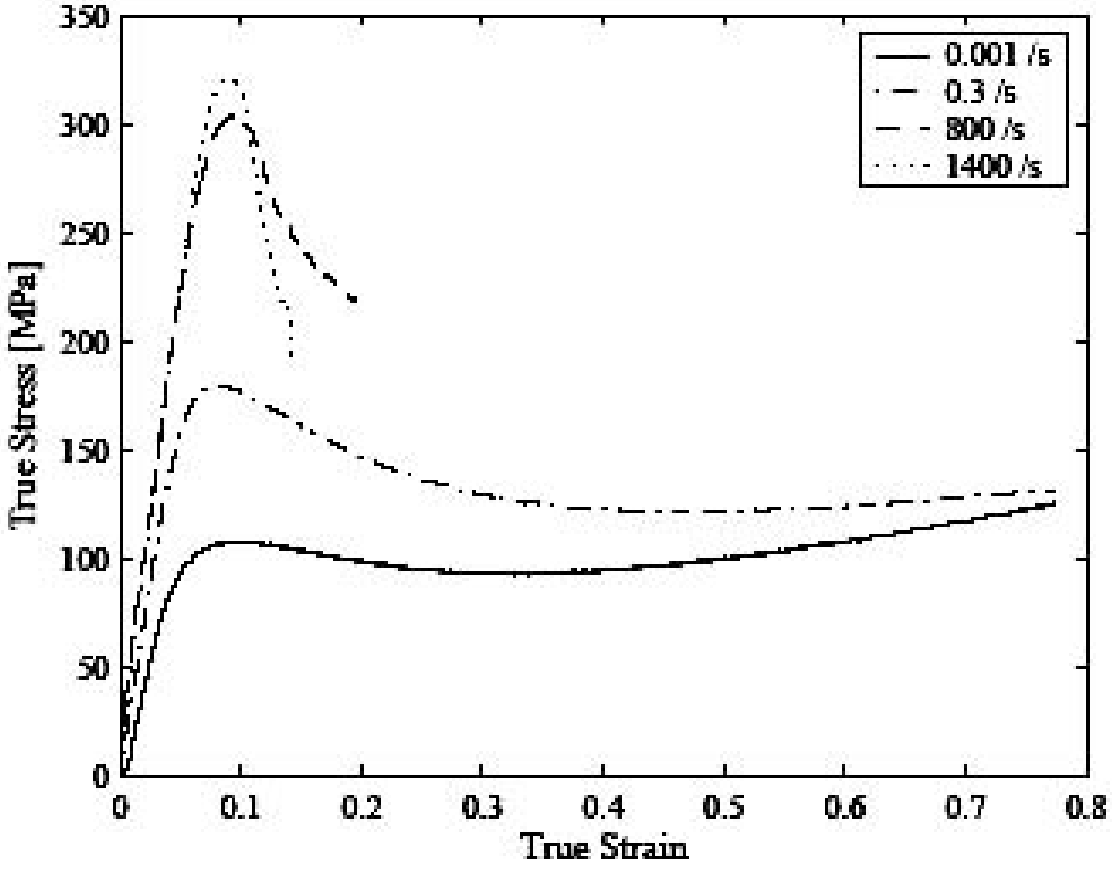

Figure 4-8: The true stress-true strain behavior in uniaxial compression for PMMA as characterized by split-Hopkinson bar testing. The slopes of the curves in the initial linear elastic region (i.e. where the Young's modulus is measured) decrease as strain rate is increased over seven orders of magnitude. This shows that the proportionality between stress and strain varies less at higher strain rates [33].

of amorphous polymers at strain rates from 10^{-4} to $10^{4}\,s^{-1}$ [33]. Increasing the strain rate typically results in an increase in modulus (see Figure 4-7). As explained in Section 2.1, the modulus is proportional to the acoustic velocity. Accordingly, an investigation was done to see if a strain rate dependence of acoustic velocity exists at the strain rates induced by the Deathstar GHz spectroscopy. The strain in the sample and the strain rate can easily be controlled by incrementally changing the pump power incident upon the excitation transducer. Typical values of optical power for the pump (measured at the sample) range from 5 mW to 60 mW. To see the effect on the response for the 19 nm PMMA film, pump power was varied from 10 mW to 37 mW. The lower limit of the pump power is dictated by the minimum amount of intensity needed for sufficient SNR. The upper limit is determined by the damage threshold of the excitation transducer. Too high of a pump power will ablate the Al excitation transducer, making the sample unusable at that spot. The total amount of strain could be increased if a thicker transducer were used, since the total amount of thermal expansion in the Al would be greater. However, this greater Al film thickness would be slower in expanding, thus decreasing the overall strain rate. Since signal intensity varies from scan to scan, it is always normalized and reported in arbitrary units. The only way to note the absolute strain is to recalibrate each time the pump power is changed, as described above. Although the magnitude of the strain increases with pump power, the acoustic velocity is inferred from the resonance frequency observed. Recall from Section 3.3.1 that the resonance behavior implies how long it takes for the phonon to make a round trip within the structure. This is indicated by the peak-to-peak time in the original signal (see Figure 4-5). Here, the oscillation period is nominally 68.1 ps (from -53.4 ps to 14.7 ps) for two round trips. The time for one round trip is half of this value or about 34 ps. The inverse of the period is the frequency, which here is about 30 GHz. This is the resonance frequency of the structure calculated by picking off the peak positions by eye. A better method for

arriving at the resonance frequency is by taking the Fast Fourier Transform (FFT) of the original signal[1]. This gives the peak-to-peak frequency and the power at that particular frequency. The Fourier spectrum for three different pump powers is shown in Figure 4-6. While the power of the FFT spectrum increases steadily with pump power, the peak position is at exactly the same frequency for each. This means that the resonance frequency is 30.1 GHz irrespective of the pump power. The original data was separately zero-padded to improve the resolution of the transform, but there was still no change in peak position. It is then concluded that no pump power dependence of acoustic velocity exists from 10 mW to 37 mW. It is possible that the acoustic velocity (and accordingly, the Young's modulus) may be independent of strain rate at such high strain rates. Such a limit could be the result of all molecular motions within the polymer already being restricted at these strain rates. Therefore, further increasing the strain rate will neither make energy propagate through the medium any faster nor will it make the material response any stiffer. Such a situation is hinted at by examining the stress-strain behavior of PMMA over a range of strain rates. Mulliken measures the variation of true stress with true strain using the split-Hopkinson bar for several strain rates. He observes a diminishing increase in Young's modulus (the slope of the stress-strain curve) as the strain rate is increased over seven orders of magnitude (from $10^{-3}\,\mathrm{s}^{-1}$ to $10^{4}\,\mathrm{s}^{-1}$) [33]. Although further investigation is necessary before drawing such a conclusion, it seems as though this diminishing trend would continue as strain rates were increased, eventually leading to proportionality between stress and strain that is independent of strain rate.

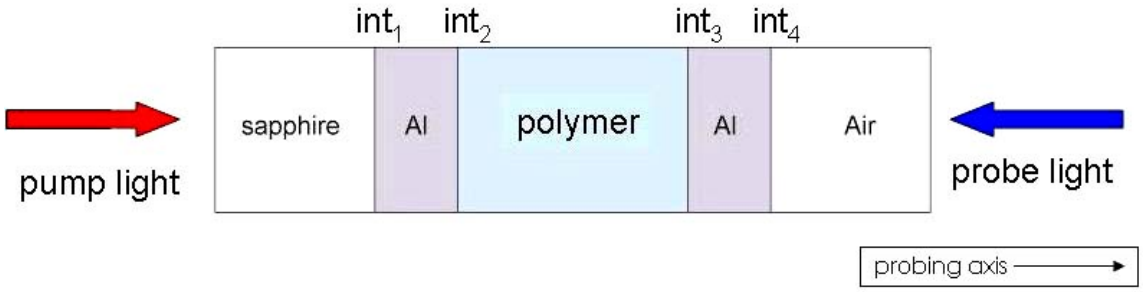

Figure 4-9: The phonon propagation model calculates the reflection and transmission coefficients at each interface (int_i). The coefficients are then used to determined amplitudes of partial reflection and partial transmission as the acoustic wave propagates through the structure.

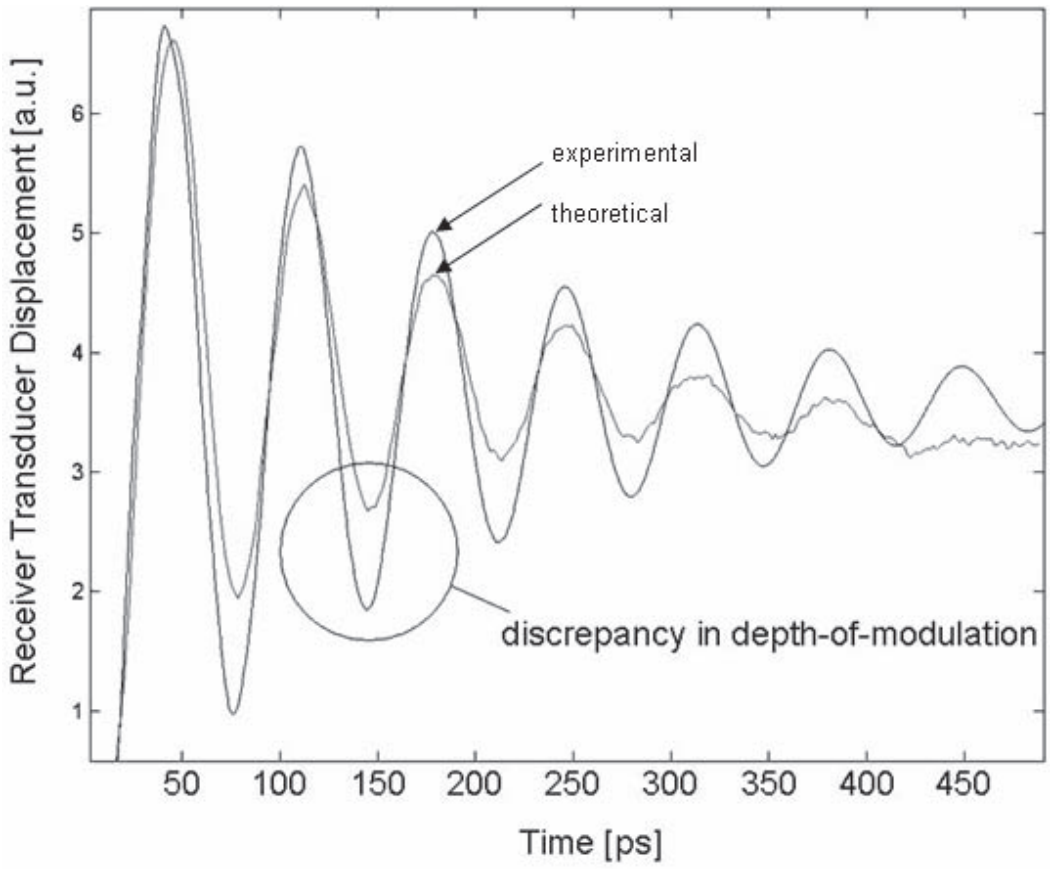

Figure 4-10: A phonon propagation model is used to generate the theoretical broadband signal. The excitation and receiver transducers are 23.1 and 13.8 nm thick, respectively. The PMMA film is 19 nm thick, assuming an acoustic velocity of 2680 m/s [7]. The experimentally observed broadband signal is shown for comparison.

4.2 Propagation Model

A phonon propagation model for the sandwich structure was developed by Jaime D. Choi. The model is based upon acoustic impedance mismatch theory. The complete derivation for the multilayer case is given by Slayton [42]. A program was written in MATLAB to perform the transfer matrix method computations. Inputs refer to values entered into the program by the user.

The multilayer system that is modeled is shown in Figure 4-9. The five layers included are the sapphire substrate, Al excitation transducer, polymer film, Al receiver transducer, and air. The entire calculation is done in the frequency domain to account for phonon dispersion[2]. However, the phonon dispersion relations for the polymers have not yet been incorporated for this preliminary study. The incident optical waveform (i.e. either broadband or narrowband input signal) is determined by the pulse duration and pulse train frequency of the incoming wavepacket, which the user inputs into the model. An acoustic wave with an amplitude $u_{\text{excitation}}(\omega)$ is assumed to originate at interface int_1[3]. As the wave propagates through the structure, it experiences partial reflection and partial transmission at each of the interfaces. This is described by the reflection coefficients at the boundaries (see Section 2.1). Accordingly, the model must include the necessary material parameters, $c_{acoustic}$ and ρ, for each material. The thickness of each layer is also required. The model assumes there is no absorption or scattering at the interfaces, only reflection and transmission. After passing through the entire multilayer structure, some amount of the original acoustic wave intensity displaces the receiver transducer so that it pushes against the

[1]The Fourier Transform is an algorithm use to analyze the frequency content of a continuous signal. It decomposes the original signal into its sine components. The result is a plot of amplitude or power of the resolved components as a function of their frequency.

[2]Recall that phonon dispersion describes $\omega(\mathbf{K})$. The derivative $\left(\frac{\partial\omega}{\partial\mathbf{K}}\right)$ gives $c_{acoustic}(\omega)$.

[3]The model assumes that the acoustic strain pulse dictated by the incident optical waveform originates at the Al|polymer interface. In the experiment, the strain pulse is induced by the rapid thermal expansion of the aluminum excitation layer.

air. Transforming the amplitude of this displacement back to the time domain gives the theoretical temporal signal, $u_{\text{signal}}(t)$. There is some acoustic intensity irrecoverably lost into the air and sapphire due to partial transmission across the Al|sapphire and Al|air interfaces, respectively. This is why the amount of receiver transducer displacement decreases with each oscillation. Figure 4-10 is an example of how the theoretically calculated and experimentally observed signals compare. This particular PMMA thin film was nominally measured to be 14.5 nm by ellipsometry. The propagation model more accurately gives the thickness to be 19 nm.

There are two noteworthy discrepancies between the calculated and observed curves. The first is the difference in the depth-of-modulation. The depth-of-modulation describes the extent to which the valleys dip before beginning to rise again. One such point is circled in Figure 4-10. While some of the assumptions made in the model may explain this, there are also experimental realities that are not taken into account. The model assumes ideal reflection and transmission at the interfaces. The amplitudes of the oscillations shown result from the calculated reflection coefficients at each interface. These reflection coefficients would be different if there were interfacial defects in the sample assembly. The most likely cause of such a difference in depth-of-modulation is local film delamination. If adhesion between layers of the sandwich structure is compromised, then there could be an air gap. This would change elastic wave propagation from layer to layer. The second source of difference between the theoretical and experimental curves is the assumption of a dispersionless velocity. The acoustic velocity is actually a complex quantity that is dependent upon frequency. To account for this, the phonon dispersion relations need to be incorporated into the model. This can be done using the Kramers-Kronig relations, along with the frequency-dependent damping. Finally, while it is true that most of the acoustic energy is either reflected or transmitted, there is some amount of absorption and scattering. When the frequency dependence of the attenuation is better understood,

this can be added into the model as well.

Most of the material properties used in the model are very accurate. The material densities are known well, as are the acoustic velocities of sapphire and aluminum. The thicknesses of the aluminum layers are measured accurately by ellipsometry. Subsequently, the propagation model can be used to calculate the thickness of the polymer film given its room temperature acoustic velocity. It is assumed here that the room temperature acoustic velocity (based on literature values for E and ρ) is accurate [7]. The ellipsometrically measured polymer film thickness is used as a nominal first approximation. The experimental signal must also be observed at room temperature as a reference. The polymer film thickness input into the model is iteratively changed by the user until the theoretical signal matches the observed signal. When the two signals coincide, the user knows that the polymer thickness is accurate given the assumed acoustic velocity.

4.3 Broadband Investigation

Broadband studies have been done to determine the temperature dependence of the acoustic velocity in the polymer thin films. There are two important points for clarification: (1) how acoustic velocity changes as a function of temperature and (2) how acoustic velocity for a thin film compares to the bulk.

The room temperature longitudinal acoustic velocity for PS is calculated using Equation 2.6, assuming literature values for Young's modulus and bulk density [7]:

$$c_{acoustic}^{PS}(T = 295\,\mathrm{K}) = \sqrt{\frac{E}{\rho}} = \sqrt{\frac{5.65\,\mathrm{GPa}}{1056\,\frac{\mathrm{kg}}{\mathrm{m}^3}}} = 2313\,\mathrm{m/s} \tag{4.5}$$

The thickness of the PS film is 18.2 nm, as roughly measured by ellipsometry. It is found that the thickness of polymer films is consistently underestimated by ellipsometry, sometimes by a factor of as much as 1.5. The reason for this is that the Cauchy

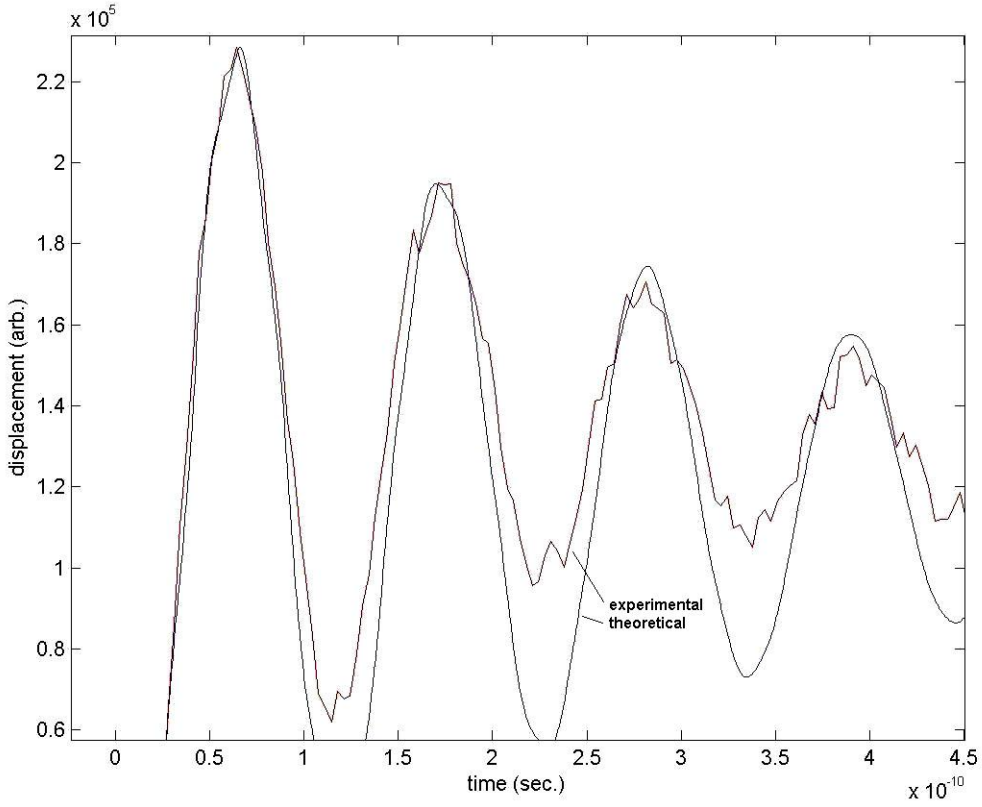

Figure 4-11: A phonon propagation model is used to generate the theoretical signal. The excitation and receiver transducers are 11.5 nm and 23.85 nm thick, respectively. The PS film thickness is determined to be 22.5 nm, assuming an acoustic velocity of 2313 m/s [7]. The observed signal is shown for comparison.

model used to fit the optical constants of the polymer sometimes does not match well[4]. In this particular case, however, the fit was reasonably good, underestimating the thickness by only 19%. Nevertheless, the ellipsometrically measured thickness is used only as the starting input for the propagation program (described in Section 4.2). Figure 4-11 shows how the theoretical and experimental signals compare. The propagation model assumes the bulk velocity (2313 m/s [7]). The nominal PS film thickness (18.2 nm) is input into the program. The relative positions of the theoretical and observed peaks are noted. The thickness input into the model is then adjusted systematically until the two curves coincide as best as possible. This renders an accurate thickness of 22.5 nm as compared to 18.2 nm measured ellipsometrically. Since there is reasonable agreement between the values measured acoustically and ellipsometrically, it can be concluded that the assumed room temperature bulk velocity of PS is accurate even for films below approximately 25 nm thick.

Once the thickness is accurately evaluated, the model can be used to determine the acoustic velocity as a function of temperature. The broadband response is probed at temperatures starting at 295 K and going down to 10 K. The signal intensity for each scan is normalized by dividing the amplitude at each point in the signal by the maximum signal amplitude. This accounts for random baseline intensity variations. The acoustic velocity used in the propagation model is iteratively varied until the theoretical signal matches the observed signal for each temperature. The thickness of the film is assumed to remain constant at 22.5 nm. This is justified since PS contracts by only 1.42% when cooling from 293 K→4.2 K. This results in a total thickness change of only 0.3 nm [25]. The actual starting temperature (the *room temperature*) is generally between 293 K to 298 K. Because the sample is within a

[4]The optical constants of a material refer to $\boldsymbol{n}(\lambda)$ and $\boldsymbol{k}(\lambda)$, which comprise the complex wavelength dependent index of refraction: $\boldsymbol{n}$'=$\boldsymbol{n}(\lambda)$+i$\boldsymbol{k}(\lambda)$. The optical constants of aluminum are known well, making ellipsometry very accurate for measuring the thickness of the transducers. However, $\boldsymbol{n}(\lambda)$ and $\boldsymbol{k}(\lambda)$ must be fit for each organic compound separately, starting from a generic Cauchy model.

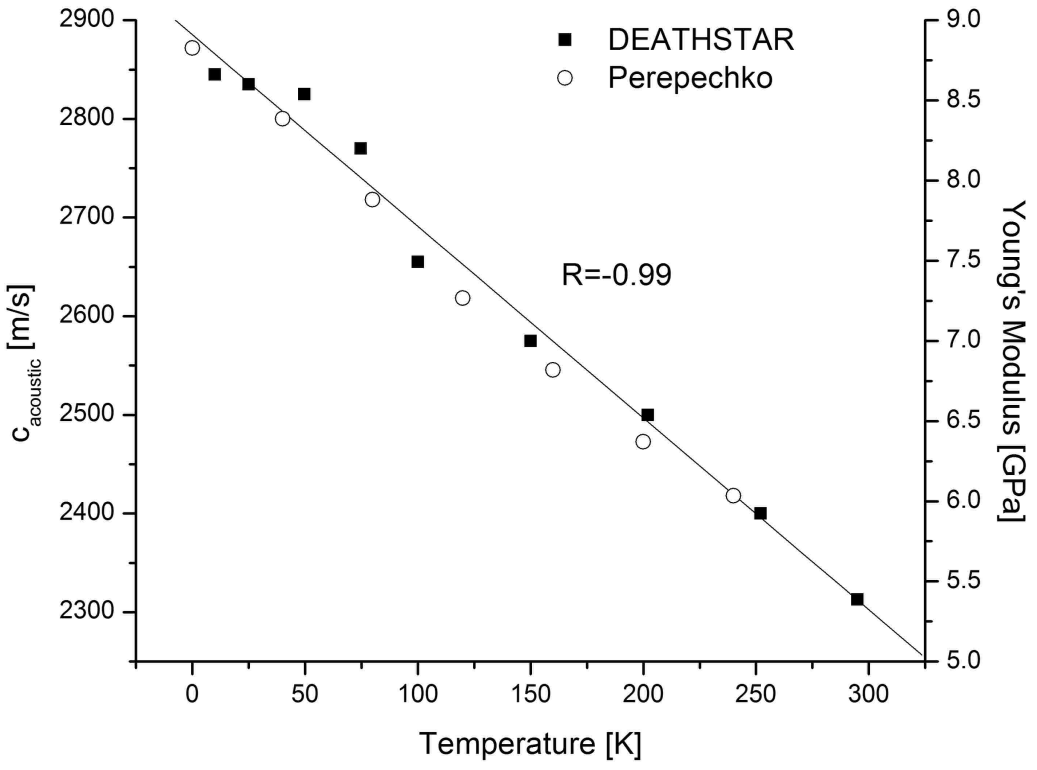

Figure 4-12: The phonon propagation model is used to help determine the experimentally observed longitudinal acoustic velocity in PS as a function of temperature. The linear regression is fit to the Deathstar Data (■). The phonon frequency is 9.37 GHz and the PS film is 22.5 nm thick. The Young's Modulus is calculated using ρ=1.06 g/cc and the indicated velocity. Data from Perepechko is shown for comparison (○) [35].

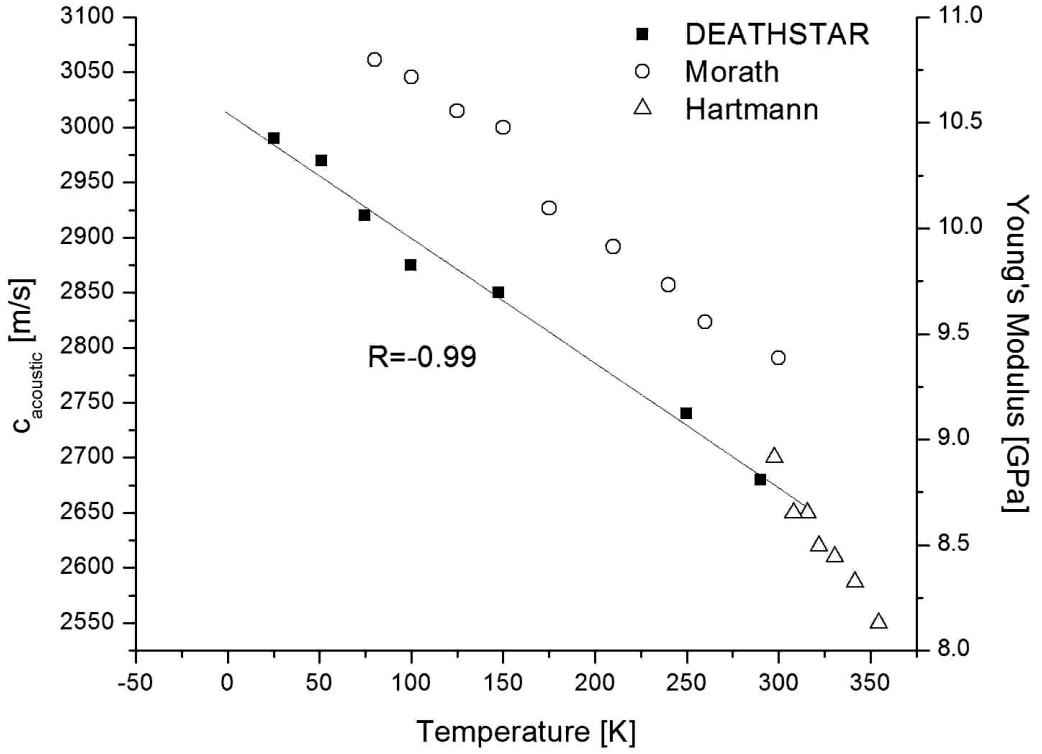

Figure 4-13: The phonon propagation model is used to help determine the experimentally observed longitudinal acoustic velocity in PMMA as a function of temperature. The linear regression is fit to the Deathstar Data (■). The phonon frequency is 14.3 GHz and the PMMA film is 19 nm thick. The Young's Modulus is calculated using ρ=1.19 g/cc and the velocity shown on the left axis. Shown for comparison are the picosecond ultrasonic results of Morath and Maris [31] and the ultrasonic immersion results of Hartmann and Jarzynski [20].

cryostat, exposed to liquid helium flow and a resistive heater, the same steady-state temperature is not always reached. The experiment begins whenever a temperature can be held constant; this may be at 298 ± 5 K. Of course, the exact temperature is recorded to ± 0.1 K accuracy using a thermocouple.

The experimentally observed temperature dependence of the acoustic velocity in PS is shown in Figure 4-12. Numerous experimental investigations show a linear relationship between the speed of sound and temperature. The range of velocities (from 2313 m/s at 295 K to 2845 m/s at 10 K) and linear dependence observed is in excellent agreement with values (from 2410 m/s at 240 K to 2875 m/s at nearly 0 K) measured by Perepechko [35]. He uses an ultrasonic pulse-phase method and his results are shown with the velocities measured by the Deathstar GHz spectroscopy. The close agreement observed implies that the probing frequency does not significantly affect the acoustic velocity. Perepechko's apparatus probes at 5 MHz while the Deathstar probes at 9.37 GHz in this case. More knowledge of the phonon dispersion relations at these wavevectors is required for further interpretation as to why there is such close agreement despite a difference in probing frequencies of three orders of magnitude. The probing frequency in the Deathstar GHz spectroscopy depends upon the thicknesses of the layers comprising the sandwich. Thinner polymer films will result in higher probing frequencies.

The temperature dependence of longitudinal acoustic velocity measured in the same way for PMMA is shown in Figure 4-13. The observation frequency for the 19 nm thick PMMA sample is 14.3 GHz and the temperature dependence found is -1.9$\frac{\mathrm{m}}{\mathrm{s \cdot K}}$. For comparison, the acoustic velocity measured using picosecond ultrasonics at 130 GHz by Morath and Maris is shown for a 60 nm thick PMMA film supported by a sapphire substrate. The temperature dependence (i.e. slope) they note in the same temperature range is similar to what the Deathstar GHz spectroscopy implies. However, the actual velocities noted by Morath and Maris are roughly 10% higher

at each temperature than what we observe. Since they used the acoustic round trip time and note errors in measuring the thickness of their films, this is probably responsible for the error in velocities they measure. Also shown are the ultrasonic results of Hartmann and Jarzynski, who measure the longitudinal sound speed for bulk PMMA from 298 K to 353 K. The immersion technique they use renders a temperature dependence of -2.5$\frac{\mathrm{m}}{\mathrm{s \cdot K}}$.

Besides confirming the linear temperature dependence of acoustic velocity, there is excellent agreement between thin film and bulk acoustic velocity values for both PS and PMMA. This refutes results from the GHz range picosecond acoustic measurements taken by Lee *et al.* that indicate a 300% increase in acoustic velocity for polymer films of similar thicknesses supported by silicon substrates (see Section 2.4.1). They also report the following two conflicting room temperature acoustic velocities for two PMMA films of the same thickness (23 nm) using the same technique: 6800 ± 800 m/s and 7800 ± 800 m/s [29]. The Deathstar measurements taken for the 19 nm thick PMMA film clearly do not show such anomalous thin film acoustic wave velocities.

The importance of studying the temperature dependence of the acoustic velocity is the direct relationship with the Young's modulus. From the agreement of the results shown, it can be said that bulk values of longitudinal acoustic velocity are in agreement with those observed for thin films. It is also clear that longitudinal acoustic velocity shows a linear dependence upon temperature from 10 K to 300 K.

4.4 Narrowband Investigation

The narrowband investigation involves the propagation of a high frequency wavepacket of phonons through the sample. The signal observed is still the receiver transducer displacement as a function of time (this is called a single *scan*). A scan is taken for

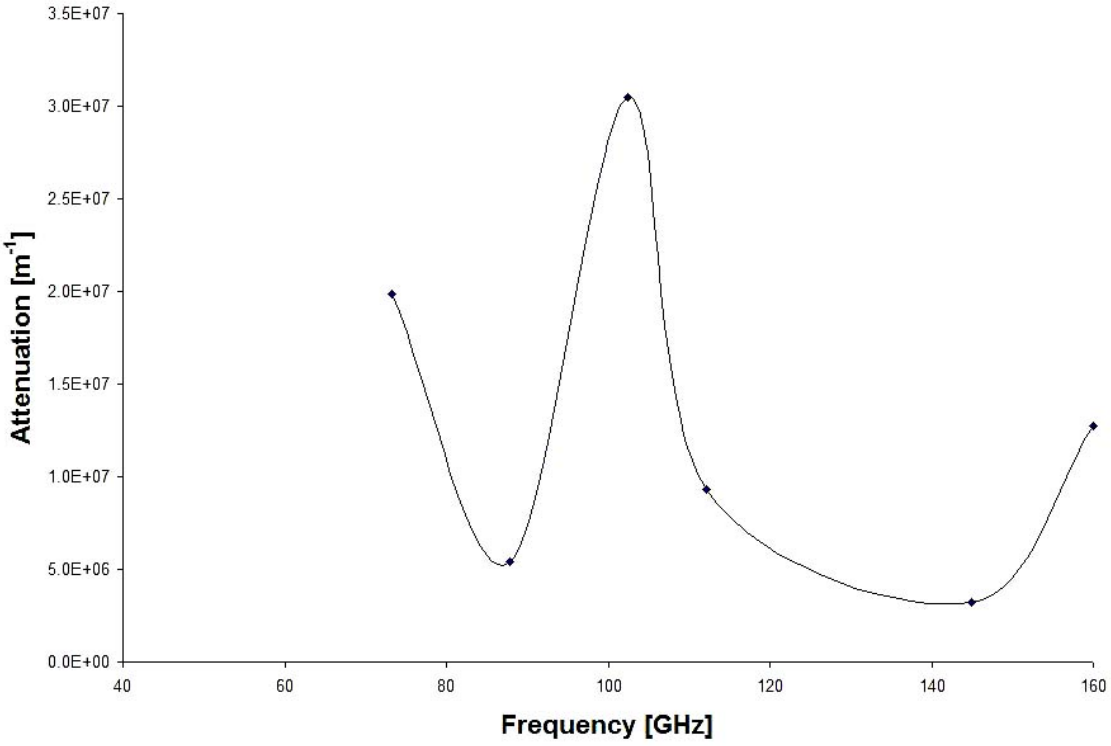

Figure 4-14: Frequency dependence of longitudinal phonon attenuation in PMMA at 295 K. The damping peak occurs at ≈ 100 GHz.

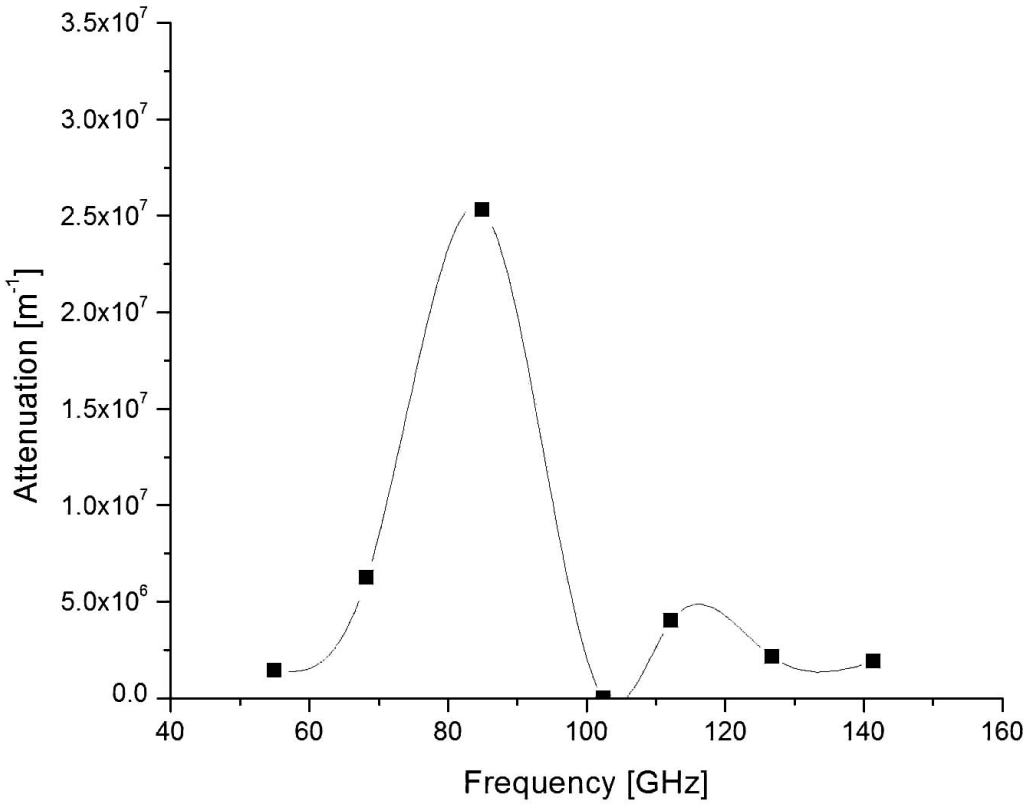

Figure 4-15: Longitudinal phonon attenuation in PMMA at 425 K (above $T_g^{\mathrm{PMMA}} = 378\,\mathrm{K}$ [8]). The damping peak occurs at $\approx 87\,\mathrm{GHz}$.

two different film thicknesses of the same polymer, at the same frequency, and at the same temperature. Changes in the signal then are solely due to the acoustic wave traveling through a different amount of material. Observing how much less signal is transmitted through the thicker film than the thinner one allows the absolute attenuation coefficient (or damping) to be calculated. Whereas, Morath and Maris make several assumptions and approximations in calculating $\alpha(\omega)$. To their observed signal they fit a cosine function multiplied by a decaying exponential to account for the long ringing time in their transducer. Since the technique they use has frontside excitation and frontside detection, there is a convolution of the transducer excitation with the acoustic response they are trying to probe. Moreover, from the original data they subtract the contribution of the rising thermal background. Since the polymer is the only layer adjacent to the aluminum film (recall Figure 2-16), heat diffuses *through* the polymer and into the sapphire substrate. Essentially, the measurement is being taken while the temperature of the polymer is changing. This could easily affect the subsequent attenuation calculation. After these subtractions from the original data, they calculate the damping by comparing the acoustic data to numerical simulations where it is assumed that there is no attenuation. They compare the ratio of the amplitude of the initial ringing of the transducer ($A_{sim}^{(0)}$ and $A_{exp}^{(0)}$, for the simulated and experimental cases, respectively) to that of the first acoustic echo ($A_{sim}^{(1)}$ and $A_{exp}^{(1)}$ for the simulated and experimental cases, respectively). The following expression shows their calculation of the attenuation:

$$\alpha(\omega_0) = \frac{1}{d_s} \ln \left[\frac{A_{sim}^{(1)}/A_{sim}^{(0)}}{A_{exp}^{(1)}/A_{exp}^{(0)}} \right] \tag{4.6}$$

By comparison, the Deathstar GHz spectroscopy is an absolute measurement since no assumptions are made about the material properties at all. For a given driving

frequency ω_i, the damping is determined in the Deathstar GHz spectroscopy by:

$$\alpha(\omega_i) = \frac{1}{d_{\text{thick}} - d_{\text{thin}}} \ln \frac{I_{\text{thin}}(\omega_i)}{I_{\text{thick}}(\omega_i)} \tag{4.7}$$

The only inputs are the film thicknesses (actually, only the thickness difference) and the ratio of the observed intensities. These intensities are calculated by taking the FFT of the original scan. The temporal window of the original data required is quite short ($\approx 40\,\text{ps}$) since only the single trip of a high frequency wavepacket through the sample assembly is needed to displace the receiver transducer. The FFT gives the spectral intensity (or power) as a function of frequency. The spectral intensity at the driving frequency is then easily read off the graph. The attenuation can be determined in this way for several driving frequencies.

Initially the described narrowband study was attempted with a 22.5 nm thick PS film. However, the damping in PS prevented high frequency phonons from being detected, and sufficient SNR could not be achieved. The literature indicates that damping is lower for PMMA than it is for PS ($\alpha_{\text{PMMA}}(100\,\text{GHz}) \approx 1 \times 10^7\,\text{m}^{-1}$ as opposed to $\alpha_{\text{PS}}(100\,\text{GHz}) \approx 1 \times 10^{7.5}\,\text{m}^{-1}$) [31]. The experiment might be successful if it were repeated with thinner PS samples. It is also known that in polystyrene, the β peak merges into the α peak above $\approx 40\,\text{GHz}$ [21]. This means that these processes are indistinguishable at higher frequencies, further complicating interpretation for this proof-of-concept study.

Accordingly, PMMA was selected for further investigation. The frequency dependence of attenuation at room temperature in PMMA is shown in Figure 4-14. The PMMA samples used for this narrowband study were 32 nm and 77 nm thick. The values measured for attenuation are of the same order as those measured by Morath and Maris for PMMA over the same range of frequencies ($\alpha(\omega) \approx 10^7\,\text{m}^{-1}$). This validates the experimental setup and approached used in this thesis. Initial mea-

surements indicate that attenuation does not change monotonically with frequency. Rather, there appears to be a peak in the room temperature data at roughly 100 GHz. It is not known what specific process might be causing such a change in damping. However, it does indicate that there is in increased coupling of acoustic energy into the material at that particular frequency. Recall that the condition $\omega\tau_c \approx 1$ is being met. This means that for $\omega = 100\,\text{GHz}$, the relaxation time of the observed dynamic process is τ_c =10 ps. Since no previous study has probed polymers under these unique conditions, the physical origin of the attenuation is not readily transparent. Recall that in Figure 2-7, a peak in the damping rate of salol is clearly defined as the temperature is lowered. Peaks in plots of damping or damping rate as a function of temperature or frequency are indicative of dynamic phenomena. Accordingly, it is possible that some change in mode of molecular motion is being probed in PMMA.

The previous attenuation measurement was done at room temperature (295 K), where the PMMA is a glassy solid. However, dynamics can change drastically when the polymer is heated above its T_g. To see if the Deathstar GHz spectroscopy is able to probe such a difference, an identical set of scans were taken at 425 K. This exceeds $T_g^{\text{a-PMMA}}$ by 47 K, ensuring that the polymer is in its rubbery phase [8]. The high temperature attenuation as a function of frequency shows a similarly sized peak, but it is shifted to a lower frequency (Figure 4-15). A loss peak for a given relaxation process will shift to *higher* frequencies as the sample is heated (considering the case where the material does not undergo a phase change). However in this case, the significant jump in temperature causes a phase change from glassy to rubbery. Accordingly, it is unlikely that the same physical processes are being probed. Additional experiments are underway to clarify this.

In comparison to the methods for determining attenuation described in Chapter Two, the Deathstar GHz spectroscopy is more robust. Since no material assumptions are made and the signal intensities are directly observed, there can be more confi-

dence in the attenuation calculations. More data points need to be taken at tighter frequency intervals and for more film thicknesses before drawing any conclusions. Additionally, measurements should be done in a closer range around T_g. The Deathstar GHz spectroscopy is shown to successfully determine acoustic attenuation, but more experiments are needed to fully develop the acoustic spectrum.

Chapter 5

Conclusions

There is a demonstrable need to characterize the high frequency loss mechanisms in amorphous polymers. These transparent plastics are commonly used for transparent armor applications for individual soldiers. They could also find use in building materials, shields, and windows. Being able to effectively measure energy propagation and energy dissipation at GHz frequencies helps to understand relaxation phenomena in polymers. The eventual goal is to determine the origins of these relaxation phenomena and what physical variables control them. An understanding of the intimate relationship between material structure, processing, and function is required. Eventually, materials will be custom-tailored so that lossy processes coincide with imposed stimuli such as ballistic and blast threats. An accurate and relevant method of material characterization is explored to this end.

When polymeric materials are examined with macroscopic techniques, they appear homogenous. Unlike crystals that have long range order, polymers such as PS and PMMA can be amorphous. Only with a high frequency (i.e. short wavelength) technique can structural anomalies and nanoscale features be observed. When probing at shorter lengthscales, even the amorphous homopolymer becomes a structurally diverse and interesting sample. All of a sudden chains ends present pockets of free

volume and corresponding density fluctuations. Entanglements between and within chains also affect the mechanics of the polymer.

On the other hand, as the observation timescales become faster, these seemingly static materials can display a rich collection of dynamic processes. Chemical substituents attached to the carbon backbone such as methyl groups and phenyl rings are constantly rotating and flipping along with other side-chain molecular motions. In order to characterize either these structural or dynamic material features, a technique that accesses appropriate wavevectors, frequencies, and strain rates is required.

To this end a high frequency acoustic technique has been explored to study polymer structure and dynamics. The Deathstar GHz spectroscopy is shown to be a characterization tool capable of quantifying energy propagation through a material and energy dissipation mechanisms. Initial investigations have been able to accurately measure longitudinal acoustic velocity as a function of temperature and phonon attenuation as a function of frequency. The technique is robust in comparison to other spectroscopies in the calculation of both of these parameters. It is also capable of probing linear elastic response at high strain rates. Moreover, since only a small amount of material is needed for testing, the technique is well-suited for studying polymers that are synthesized in limited quantities.

5.1 Longitudinal Acoustic Velocity Measurements

There is a direct relationship between acoustic velocity and elastic modulus. A material with a high modulus appears stiff to an acoustic wave and thus propagates the wave faster than a material with a low modulus. The longitudinal acoustic velocity has been measured as a function of temperature from 10 K to 300 K for PS and PMMA. The results obtained are in excellent agreement with ultrasonic measurements for these same polymers in the bulk. There is a strong linear dependence of

acoustic velocity on temperature. However, the velocities measured do not agree with similar picosecond acoustic techniques that report three-fold increases in velocity for thin films. Deathstar measurements show that room temperature acoustic velocity is the same for thin films and the bulk. Moreover, the change in velocity as temperature is lowered from room temperature to absolute zero is 10-20%. Acoustic velocity decreases linearly over this range. The close agreement between the propagation model and the experimental results lends credibility to the observed trends.

Additional broadband measurements should be done at smaller temperature intervals to probe for kinks in the temperature dependent velocity. This would better define the bounds of underlying relaxation processes, if there are any. The change in position of these kinks with probing frequency would help in understanding their molecular origins. Samples of different thicknesses can be used to this end. This would also increase the statistical validity of the experiment.

5.2 Absolute Acoustic Attenuation Measurements

Besides evaluating energy propagation, energy dissipation is also readily characterized by the Deathstar GHz technique. Damping within a material can be due to several mechanisms, and characterizing the frequency dependent attenuation can help better understand the dynamic processes responsible for energy absorption. Moreover, since the mean free path is simply the inverse of the acoustic attenuation, the size scale of absorbing and scattering heterogeneities can easily be determined from the damping. The phonon attenuation of PMMA has been measured as a function of frequency from 55 GHz to 160 GHz. This range of frequencies is not readily accessible by other techniques and could be host to interesting material dynamics. Moreover, the approach used is arguably more reliable than others since no material assumptions are made. Any two PMMA films of different thickness can be used for the calculation

of the absolute attenuation coefficient. This measurement can be made quickly at several different frequencies. The upper and lower frequency limits are determined by the thickness of the samples. Since damping is directly proportional to frequency, thinner samples can be used to probe material response at higher frequencies.

Measurements can be repeated for different pairs of PMMA films to not only confirm the attenuation values, but also the frequency dependence. Literature shows that attenuation increases as a function of frequency, but there is little agreement on the dependence. That is, $\alpha(\omega) \sim \omega^p$, but the values observed for p range from 2.5 to 6 [31]. The Deathstar GHz spectroscopy can help make progress in determining this dependence. Thinner films of PS can be studied to circumvent the high damping issue. The addition of temperature as a variable in the attenuation measurements opens another dimension in the material characterization map. A master curve can potentially be developed, which outlines the lossy processes occurring in amorphous polymers as a function of both frequency and temperature. At higher temperatures, slower relaxation processes might become evident. At lower temperatures, most dynamics would be frozen out. The remaining attenuation could then be largely attributed to structural inhomogeneities. Complex structures can be systematically studied in this way. This would also be an incredibly valuable tool in predicting bulk material response for nanocomposites.

5.3 Future Work and Potential Applications

The amorphous polymers initially studied are homogenous and isotropic. Subsequent investigations with PS and PMMA could include molecular weight effects since the relative concentration of free ends decreases as the molecular weight is increased. The influence of thermal history could be studied by varying the annealing schedule. Polymers such as polyisoprene could be studied to explore the effect of cross-linking.

Rotational isomerism in polymers could also be probed since the potential barrier for torsional excitation is characteristically different for *cis* and *trans* isomers.

The properties of such amorphous polymers do not vary with direction. However, directionality may be introduced in heterogeneous polymer systems (e.g. crystalline polymers, blends, and block copolymers) by exposure to external stimuli during processing. Extruded and roll-cast films show anisotropy in the direction of the flow field. Some materials can be aligned by imposing electric fields as well. Draw fibers often exhibit anisotropy, with different elastic constants perpendicular and parallel to the drawing direction.

Investigating biphasic materials and nanocomposites introduces limitless compositional variability. Block copolymers also present the opportunity to explore the effect of structural anisotropy. The effect of domain sizes and minority phase concentration in phase-separation block copolymers can be studied. Orientation of domains is routine in materials processing laboratories. Multilayer stacks of alternating glassy and rubbery phases are effective photonic crystals, but could also be characterized acoustically. The acoustic impedance mismatch resulting from varying the layer thicknesses and total number of layers could affect absorption and sound propagation, uncovering analogous phononic crystals.

Recently developed phononic bandgap structures by the Thomas Group could also by studied using the Deathstar GHz spectroscopy. These structures are comprised of an epoxy matrix with a three-dimensionally periodic lattice of air holes. The acoustic properties would presumably vary with probing direction.

Another variable that can be changed is the concentration of toughening fillers in composite matrix materials. Carbon nanotubes, iron nanorods, and similar hard phases have been shown to dramatically change mechanical properties, even when used in very small volume fractions. To isolate the response of structural features from dynamic responses, the sample can be cooled down using liquid helium. This

ensures that only resonance interactions with nanoscale heterogeneities would be observed. Hence, the Deathstar GHz acoustic technique could probe particle size distributions by measuring the broadness of resonance peaks. It could detect particle dispersion within the matrix by rastering spatially across the sample. Characterization of particle dispersion is currently limited to the qualitative evaluation of TEM images.

Processing defects such as void formation during the drawing of fibers and the extrusion of films could be evaluated by measuring both attenuation and acoustic velocity. This is because air voids scatter sound, and the velocity is directly related to the density. Being able to characterize both of these parameters would be a useful diagnostic.

Acoustic microscopy has been previously limited to micron resolution, but the Deathstar GHz technique could show hundredfold improvement. Such a technique would be a direct analogue to light microscopy, but more telling since resulting images reflect the acoustic impedance mismatch within the material. Thus, subsurface features are probed, which could not be observed using conventional optical and electron microscopy.

Another interesting experiment might be to evaluate the effect of multidirectional strain pulses. The current investigation launches a longitudinal acoustic wave through the plane of the multilayer structure. How might this propagation be affected if an additional acoustic wave were traveling *in* the plane of the sample at the same time? It could be that the combined signals interfere destructively to form some sort of strain shield.

The Deathstar GHz spectroscopy may also be used for damage analysis in ballistic materials. By comparing the acoustic spectrum before and after a penetration or blast event, plastic deformation can be assessed. It would be useful to learn what kind of permanent damage is caused by such loading conditions.

Exploring the effects of all of these parameters upon longitudinal acoustic velocity and acoustic attenuation is made possible by using the Deathstar GHz acoustic technique.

Bibliography

[1] A. Akheizer. *Zhur. Eksper. i Teoret. Fiz.*, 8(12):1319, 1938.

[2] R.G.C. Arridge. *Mechanics of Polymers*. Clarendon Press, Oxford, 1975.

[3] U. Buchenau, C. Schönfeld, and D. Richter. Neutron scattering study of the vibration-relaxation crossover in amorphous polycarbonates. *Physical Review Letters*, 73(17):2344–2347, 1994.

[4] J.D. Choi. *Generation of Ultrahigh Frequency Acoustic Waves for the Characterization of Complex Materials*. PhD dissertation, Massachusetts Institute of Technology, Department of Chemistry, February 2005.

[5] E.D.H. Davies. A critical study of the Hopkinson pressure bar. *Philosophical Transactions A*, 240:375–457, 1948.

[6] E.D. Palik (Ed.). *Handbook of Optical Constants of Solids III*. Academic Press, San Diego, 1998.

[7] J.E. Mark (Ed.). *Physical Properties of Polymers Handbook*. AIP Press, Woodbury, NY, 1996.

[8] H. Elias. *Macromolecules: Structure and Properties*. Plenum Press, New York, 2nd edition, 1984.

[9] J.A. Forrest, K. Dalnoki-Veress, and J.R. Dutcher. Brillouin light scattering studies of the mechanical properties of thin freely standing polystyrene films. *Physics Review E*, 58(5):6109–6114, 1998.

[10] K. Fukao. Dynamics in thin polymer films by dielectric spectroscopy. *European Physical Journal E*, 12(1):119–125, 2003.

[11] K. Fukao and Y. Miyamoto. Glass transition temperature and dynamics of α-process in thin polymer films. *Europhysics Letters*, 46(5):649–654, 1999.

[12] K. Fukao and Y. Miyamoto. Dielectric and dilatometric studies of glass transitions in thin polymer films. *Journal de Physique IV (Proceedings)*, 10(7):243–246, 2000.

[13] K. Fukao and Y. Miyamoto. Glass transitions and dynamics in thin polymer films: dielectric relaxation of thin films of polystyrene. *Physics Review E*, 61(2):1743–1755, 2000.

[14] K. Fukao and Y. Miyamoto. *European Physical Journal E*, 12(1):119–125, 2003.

[15] K. Fukao, S. Uno, Y. Miyamoto, A. Hoshino, and H. Miyaji. Dynamics of α and β processes in thin polymer films: Poly(vinyl acetate) and poly(methyl methacrylate). *Physical Review E*, 64(5):051807, 2001.

[16] C. Glorieux, J.D. Beers, E.H. Brentford, K. Van de Restyle, and K.A. Nelson. Phase mask based interferometer: Operation principle, performance, and application to thermoplastic phenomena. *Review of Scientific Instruments*, 75(9):2906–2920, 2004.

[17] J.E. Graebner, B. Golding, and L.C. Allen. Phonon localization in glasses. *Physics Review B*, 34(8):5696–5701, 1986.

[18] I.S. Grigoriev and E.Z. Meilikhov. *Handbook of Physical Quantities*. CRC Press, New York, 1997.

[19] R.A. Haldon and R. Sinha. Multiple transitions in polyalkyl methacrylates. *Journal of Applied Physics*, 39(3):1890–1899, 1968.

[20] B. Hartmann and J. Jarzynski. Immersion apparatus for ultrasonic measurements in polymers. *Journal of the Acoustical Society of America*, 56(5):1469–1477, 1974.

[21] R.N. Haward and R.J. Young (Eds.). *The Physics of Glassy Polymers*. Chapman & Hall, New York, 2nd edition, 1997.

[22] R.W. Hertzberg. *Deformation and Fracture Mechanics of Engineering Materials*. John Wiley and Sons, New York, 4th edition, 1996.

[23] C.Y. Hsieh, S. Nagarajan, and R.H. Zee. Infrared thermographic analysis of polymer composites during ballistic impact. *Review of Scientific Instruments*, 63:2296–2304, 1992.

[24] D.A. Jackson, H.T.A. Pentecost, and J.G. Powles. Hypersonic absorption in amorphous polymers by light scattering. *Molecular Physics*, 23(2):425–432, 1972.

[25] M. Jäckel, F. von Schoolbook, U. Eschar, and A. Gladden. Low-temperature thermal properties of amorphous polycarbonate and polystyrene. *Proceedings of the International Cryogenic Engineering Conference*, 16:2023–2026, 1996.

[26] E. Kato. Brillouin scattering in polymethyl methacrylate from 4 to 300 K: Temperature dependence of the Grüneisen constant and thermal properties. *Journal of Chemical Physics*, 73(3):1020–1025, 1980.

[27] L.E. Kinsler. *Fundamentals of Acoustics*. John Wiley and Sons, New York, 2nd edition, 1962.

[28] Charles Kittel. *Introduction to Solid State Physics*. John Wiley and Sons, New York, 7th edition, 1996.

[29] Y. Lee, K.C. Bretz, F.W. Wise, and W. Sachse. Picosecond acoustic measurements of longitudinal wave velocity of submicron polymer films. *Applied Physics Letters*, 69(12):1692–1694, 1996.

[30] D.R. Lide. *CRC Handbook of Chemistry and Physics*. CRC Press, New York, 84th edition, 2003.

[31] C.J. Morath and H.J. Maris. Phonon attenuation in amorphous solids studied by picosecond ultrasonics. *Physical Review B*, 54(1):203–213, 1996.

[32] C.J. Morath, G. Tas, T.C. Zhu, and H.J. Maris. Phonon attenuation in glasses studied by picosecond ultrasonics. *Physica B*, 219-220:296–298, 1996.

[33] A.D. Mulliken. Low to high strain rate deformation of amorphous polymers: Experiments and modeling. MS thesis, Massachusetts Institute of Technology, Department of Mechanical Engineering, June 2004.

[34] R. Nava, D. Pereira, and L. Amorer. Glasslike ultrasonic properties of Dominican amber above helium temperatures. *Journal of Applied Physics*, 69(1):99–102, 1991.

[35] I. Perepechko. *Low-Temperature Properties of Polymers*. Pergamon Press, New York.

[36] J.A. Rogers, A.A. Maznev, M.J. Banet, and K.A. Nelson. Optical generation and characterization of acoustic waves in thin films: Fundamentals and applications. *Annual Review of Materials Science*, 30:117–157, 2000.

[37] J.P. Runt and J.J. Fitzgerald (Eds.). *Dielectric Spectroscopy of Polymeric Materials: Fundamentals and Applications*. American Chemical Society, Washington, DC, 1997.

[38] G.P. Scherg, R. Gartner, P. Berberick, and H. Kinder. *Phonon Scattering in Condensed Matter VII*. Springer, Berlin.

[39] M. Schmidt, R. Vacher, J. Pelous, and S. Hunklinger. *Journal of Physics (Paris) Colloquia*, 43(C9-501), 1982.

[40] I.W. Shepherd. Inelastic laser light scattering from synthetic and biological polymers. *Reports on Progress in Physics*, 38(5):565–620, 1975.

[41] S. Sills, R.M. Overney, W. Chau, V.Y. Lee, R.D. Miller, and J. Frommer. Interfacial glass transition profiles in ultrathin, spin cast polymer films. *Journal of Chemical Physics*, 120(11):5334–5338, 2004.

[42] R.M. Slayton, A.A. Maznev, and K.A. Nelson. Transient grating measurements of film thickness in multilayer metal films. *Journal of Applied Physics*, 90(9):4392–4402, 2001.

[43] G. Swallowe and S. Lee. A study of the mechanical properties of PMMA and PS at strain rates of 10^{-4} to 10^{3} over the temperature range 293-363 K. *Journal De Physique IV*, (110):33–38, 2003.

[44] Y. Wada and K. Yamamoto. Temperature dependence of velocity and attenuation of ultrasonic waves in high polymers. *Journal of the Physical Society of Japan*, 11:887–892, 1956.

[45] I.M. Ward and D.W. Hadley. *An Introduction to the Mechanical Properties of Solid Polymers*. John Wiley and Sons, New York, 3rd edition, 1993.

[46] T.O. Woodruff and H. Friedreich. Absorption of sound in insulators. *Physical Review*, 123(5):1553–1559, 1961.

[47] Y. Yang and K.A. Nelson. Impulsive stimulated light scattered from glass-forming liquids. II. Salol relaxation dynamics, nonergodicity parameter, and testing of mode coupling theory. *Journal of Chemical Physics*, 103(18):7732–7739, 1995.

[48] T.C. Zhu, H.J. Maris, and J. Tauc. Attenuation of longitudinal-acoustic phonons in amorphous SiO_2 at frequencies up to 440 GHz. *Physical Review B*, 44(9):4281–4289, 1991.